Design and Dynamics of Jet and Swirl Injectors

Vladimir Bazarov*
Moscow Aviation Institute, Moscow, Russia

and

Vigor Yang[†] and Puneesh Puri[‡]
Pennsylvania State University, University Park, Pennsylvania

Nomenclature

A = geometric characteristic parameter of swirl injector, $A \equiv \bar{R}_{in}/\bar{A}_{in}$; area
a = nondimensional parameter of swirl injector, defined in Eq. (75)
b = nondimensional parameter of swirl injector, defined in Eq. (71)
C = coefficient of nozzle opening, $C \equiv \bar{R}_{in}$
$C*$ = characteristic velocity
c = specific heat
D = diameter of injector element
d = diameter of substance (drop, spray)
f = functional symbol; frequency
h = liquid film thickness
Im = imaginary part of complex variable
K = momentum-loss coefficient; O/F ratio
k = ratio of specific heats, C_p/C_v
l = length of injector element
M = Mach number
m = mass
$\dot{m}$ = mass flow rate

n = number of passages
p = pressure
Δp = pressure drop
Q = volumetric flow rate
$q\,(\lambda)$ = gasdynamic function; tangent of nozzle surface inclination to injector axis
R = gas constant; radius of injector element
Re = Reynolds number
r = radius of jet element; radial location of liquid film
S = surface
Sh = Strouhal number
T = temperature, K
t = time; spacing between injectors
U = velocity
V = volume
$x,\,y,\,z$ = coordinates
α = tilt angle of inlet passage; spreading angle of liquid spray
β = tilt angle of wall
Δ = increment
δ = wall thickness, clearance
ε = coefficient of jet contraction
η = pressure-loss coefficient; efficiency; acoustic admittance function
$\aleph$ = polytropic exponent
λ = velocity coefficient; drag coefficient; wavelength
μ = mass flow coefficient
μ_d = dynamic viscosity
ν = kinematic viscosity
Π = response or transfer function
ξ = hydraulic-loss coefficient; fluctuation of liquid film thickness
π = nozzle expansion ratio
ρ = density
σ = surface tension
τ = time interval
Φ = phase angle of individual process
φ = coefficient of passage fullness, i.e., fractional area occupied by liquid in nozzle
Ψ = phase angle of element in the assembly
Ω = amplitude of liquid surface wave
ω = radian frequency

Subscripts

a = axial
c = combustion chamber
eq = equivalent
e = nozzle exit
exp = experimental
ext = external

f = propellant feed system
fl = flow
fr = friction
g = gas
gg = gas generator
gl = gas-liquid
id = ideal
i = injector
in = inlet
j = jet
k = head end of vortex chamber
l = liquid
m = liquid vortex
mix = mixing
N, n = nozzle
out = outlet
r = radial
s = vortex chamber
sp = spray
sw = swirl
T = inlet passage
t = tangential spacing between injectors
th = nozzle throat
u = circumferential
w = wall, wave
v = saturated vapor
vc = vortex chamber
Σ = total
0 = initial conditions
1 = exit conditions
∞ = infinite value

Superscripts

$-$ = dimensionless parameter
$\prime$ = pulsation component

I. Introduction

MIXTURE formation is one of the most important processes in liquid rocket combustion devices because it determines combustion efficiency, stability, and heat transfer characteristics. This process is implemented through the use of propellant injectors, which not only accomplish their main missions of propellant atomization and combustible mixture formation, but also represent elements of an engine as a complex dynamic system operating under various conditions. Any change in engine operating conditions (such as startup, thrust variation, and shutdown) or flow paths in the feed line and combustion chamber (such as turbulence and pulsations) may lead to a drastically different injector behavior.

The operating conditions of propellant injectors are complicated, and as such the types of injectors and injector assemblies as a whole are numerous. The selection and design of a specific injector depends on the situations of concern and must fulfill the following basic requirements:

1) To provide high combustion efficiency, injectors should ensure high-quality propellant mixing with uniform distributions of mixture ratio and flow intensity over the combustion chamber as much as possible. Minimum consumption of energy is required for propellant atomization and mixing.

2) To protect combustor walls against excessive thermal loading, injectors should provide nonuniform distributions of mixture ratio and flow intensity in regions of concern.

3) To suppress combustion instability in the chamber and to achieve staged combustion, injectors should achieve prescribed distributions of atomization dispersivity, mixture ratio, and flow intensity in the mixture-formation zone. For gas injectors, provisions should be made to remove acoustic energy from the chamber.

4) To suppress flow instabilities, the acoustic conductivity of an injector should be minimized, with a smallest possible response to disturbances arising from variations of the flow rate and other parameters.

5) For more complicated situations such as pulse-triggered instability and thrust transients, injectors must feature prescribed dynamic characteristics within preset limits with fixed steady-state characteristics.

6) For a liquid rocket engine (LRE) operating in a pulse mode, additional requirements of minimizing the volume of injector cavity must be fulfilled. For LRE with a wide range of thrust variation, prescribed mixture-formation parameters should cover the entire operating envelope.

To meet these requirements, injectors should provide pre-specified liquid-sheet thickness, spray-cone angle in the range of 36–120 deg, and dynamic characteristics. In addition, the fabrication procedure should be simplified to achieve reliable designs. Because many of these requirements vary for LRE of different types, a great number of injector types have been developed and implemented. The selection for a specific application is a result of a compromise between the preceding requirements and to a great extent depends on technological expertise, design tradition, and development experience.

A. Classification of Injectors and Methods of Mixture Formation

Liquid propellant injectors and methods of mixture formation can be classified on the following basis:

1) applications: low-thrust engines, gas generators, medium-thrust engines, and boost engines of launchers;

2) propellants: earth-storable, hypergolic, and cryogenic propellants;

3) pressure drop: high-pressure and low-pressure drops across injectors;

4) design features: dimensions and configurations of flow passages; and

5) propellant mixing: external and internal mixing.

To disperse liquid into droplets and distribute them over the mixture-formation zone, various kinds of energies can be used. The choice, however, is

limited for injectors. The classification of propellant injectors from the standpoint of the type of energy used for propellant atomization and mixture formation is discussed here.

1) The most often used concept for an LRE injector is the conversion of potential energy of the liquid in the form of pressure drop across the injector into kinetic energy of a liquid jet, which subsequently produces a spray of droplets. This atomization principle is used for jet, film, and swirl injectors. The energy efficiency of such injectors, however, is rather low. A major part of the energy is consumed in increasing the droplet velocity, rather than overcoming the surface tension. The pressure drop for a commercial LRE typically ranges between 0.29 and 3.75 MPa. The upper limit is determined by chamber stability considerations instead of the required atomization quality.

2) In the case of gas-liquid injectors, the kinetic energy of the gas flow is used to generate wavy motions at the liquid-gas interface, separate wave crests from the liquid core, and to accelerate drops. The pressure drop across the gas passage for achieving required atomization quality is significantly lower than that of liquid injectors. It is mainly determined by the requirements of operation stability and uniformity of propellant distribution between injectors. In the case of increased requirements of atomization quality, for example, in low-thrust engines, gas-liquid injectors are used for liquid propellant atomization with the help of additional high-pressure gas.

3) Thermal energy is often used to heat the liquid being atomized, in order to change its surface tension and viscosity, and in the limiting case (e.g., hydrazine) to evaporate and decompose the liquid to provide gaseous-phase mixing. In most LREs, the heating and evaporation of liquid propellants take place in cooling jackets or in heat exchangers. Only in hydrazine thermal-decomposition reactions, atomizers with developed surface of thermal contact with the liquid are used for initiating reactions.

4) Acoustic energy is used in acoustic and ultrasonic injectors. The resultant flow oscillations promote the formation of surface waves in the liquid stream, which then disintegrates into droplets with a low energy consumption rate.

5) Mechanical energy is used in injectors with reciprocating atomizers or rotors. The former has been employed only in experimental low-thrust engines (up to 1 N) using piezoelectric or magnetostriction vibrators. The latter has found application in low-thrust jet engines and in some designs of liquid propellant rocket engines.[1]

6) Electric energy has been used to activate piezoelectric and magnetostrictive vibrators for injectors of low-thrust engines operating in the pulse mode. In the latter case, the electric energy is directly converted into the potential energy of liquid. In addition, there have been proposals to use electric discharges in non-conducting liquids to obtain pressure pulses, so-called electrohydraulic effect. These methods have not found practical applications in commercial LREs.

7) Combined atomization methods using several different kinds of energy.

Different conversion techniques can be used simultaneously to intensify atomization, such as combined utilization of the potential energy of liquid and kinetic energy of atomizing gas. Application of vibrational energy during pneumatic and hydraulic atomization produces the most significant effect. This combination allows considerable savings of the energy spent for atomization.

B. Liquid Injectors

1. Jet and Slit Injectors

The jet injector is the simplest device for converting the potential energy of liquid in the form of pressures drop to the kinetic energy of a jet. The injector also represents a local contraction connecting the propellant manifold to the atomization zone. The ideal-liquid exhaust velocity U_{id} is determined by Bernoulli's equation:

$$U_{id} = \sqrt{\frac{2}{\rho}\Delta P_i} \tag{1}$$

where ΔP_i is the pressure drop across the injector, and ρ is the liquid density. The effect of viscous loss is usually taken into account by using either empirical coefficients or expressions derived from the boundary-layer theory. The liquid flow rate is determined by the following equation:

$$m_{i.id} = \mu_n A_N \sqrt{2\rho\Delta P_i} \tag{2}$$

where A_N is the injector cross-sectional area. The discharge coefficient μ_N mainly depends on the injector shape.

The slit injector has a flow passage formed by either flat or concentric surfaces. The hydraulics of slit injectors are well understood and reliable design methods are available.[2] The atomization mechanism of a liquid stream involves disintegration into drops due to the loss of flow stability under the effects of aerodynamic forces on the liquid surface.[3]

The jet and slit injectors are exclusively used for bipropellant applications, with their sprays formed by the intersection of liquid streams. Figure 1 shows an injector with five intersecting jets (four oxidizer jets and one fuel jet). It
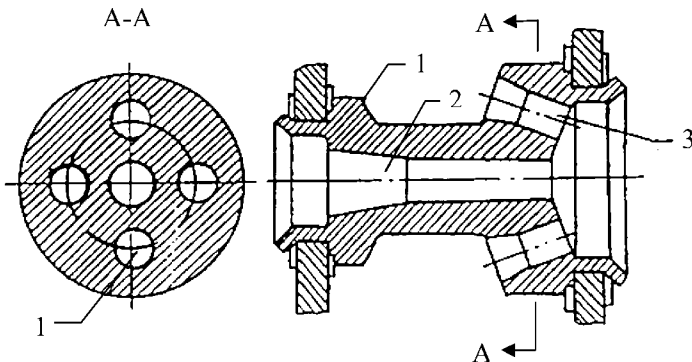

Fig. 1   Bipropellant spray injector with intersecting fuel and oxidizer jets; 1-casing, 2-fuel passage, 3-oxidizer passage.

contains a casing (1) brazed into the assembly bottom, an axial hole (2), and four axially symmetric holes (3) for the other propellant tilted towards its axis. The number of holes (3) may vary from two to four. In case two holes are employed, no axial hole is needed, and one of the holes (3) should be connected to the manifold of the other propellant. This situation is referred to as a doublet injector.[4] As the propellants flow out, a thin flat bipropellant lobe providing high-quality mixing and sufficiently fine dispersion of propellants is formed, as illustrated in Fig. 2. Injectors of the "triplet" type (with two lateral holes for one of the propellant) have the same scheme of liquid-propellant atomization and mixing. In other cases, a sharp bipropellant spray cone with rather coarse atomization is formed at the place of jet intersection.

The advantages of injectors with intersecting jets are:

1) simplicity of design and reliability of hydraulic analysis;
2) satisfactory atomization quality and uniform propellant mixing for doublet and triplet injectors; and
3) short flow residence time in the injector and short ignition delay.

The disadvantages of jet injectors are:

1) stingy requirements imposed on the fabrication technology. A small deviation in dimensions may considerably change the atomization and mixing quality;
2) significant non-reproducibility of the resultant spray property;
3) considerable differences of propellant-mixing pattern between flow tests for model liquids and real propellants in case of hypergolic propellants. This is attributed to the liquid sheet repulsion and deterioration of the mixing conditions, caused by gaseous products produced in liquid-phase reactions between the intersecting propellant flows;
4) the spray fan formed in the propellant-flow intersection region is extremely sensitive to local flow fluctuations, especially in the transverse direction. Injector assemblies consisting of doublet injectors are very susceptible to high-frequency transverse instabilities.
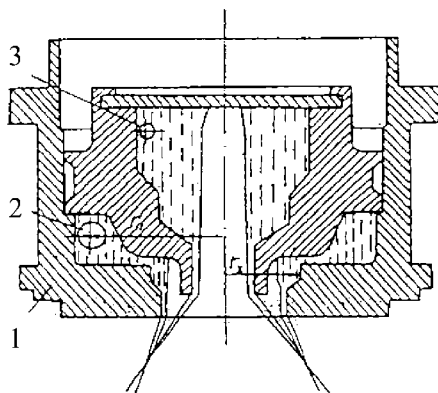

Fig. 2   Formation of fine dispersion of propellants in a doublet swirl injector; 1-casing, 2-fuel channel, 3-oxidizer channel.

To reduce the effect of fabrication errors, slit injectors with flat holes producing intersecting sheets are made by spark erosion machining. For example, the platelet manufacturing technology was used for the impinge jet multi-injector assembly for the Space Shuttle Orbit Maneuver System (OMS),[5] as shown in Fig. 3. Although the vacuum bonding of thin sheets of metal results in injector passages of stepwise form with enhanced hydraulic losses, the propellant mixing efficiency is considerably improved, especially for hypergolic propellants. Injectors with three or five jets forming a narrow long spray (see Fig. 1) were placed on the injector assembly as a means to increase the combustion zone length and thus to decrease its response to pressure fluctuations.

Application of injectors with intersecting jets has practically ceased for high- and medium-thrust engines with staged-combustion cycles, except for gas generators in which high-frequency instabilities were not nearly so critical due to the lower power intensity and longer operation processes. Injectors with intersecting coaxial sheets have found applications in so-called pintle injectors[6] for throttable LRE, as shown in Fig. 4. The disadvantages common to all of the designs of combined slit injectors with variable passage cross sections are stingy requirements on manufacturing accuracy. The generally permitted misalignment ~ 0.03 mm is too large for this injector. For example, in the case of nominal liquid-sheet thickness of 1 mm for a 10-fold decrease of thrust, the misalignment amounts to $\pm 30\%$ of the average width of the injector passage cross section. The ensuing deviation in the mixture ratio reduces the engine efficiency. The presence of a movable element in the immediate vicinity of the heat release zone poses another serious challenge in ensuring reliable operation of injector assemblies, and consequently restricts the design to single-injector assemblies.

2. Swirl Injectors

Swirl injectors are predominantly used in Russian LRE gas generators and in combustion chambers with pressurized feed systems or gas-generator cycles.
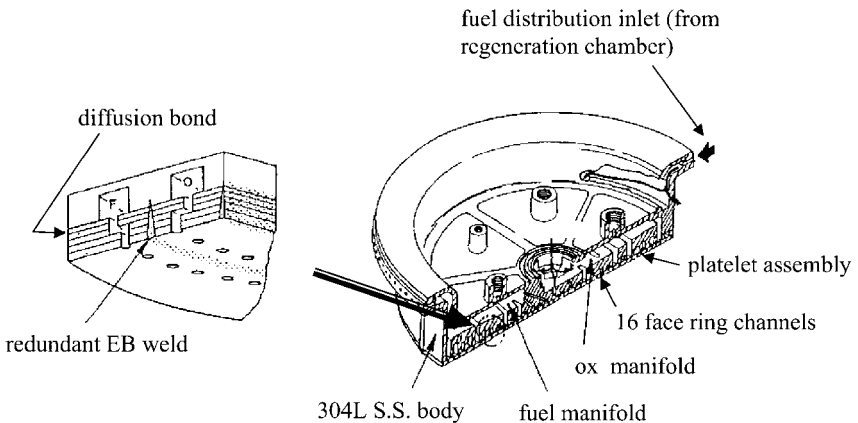

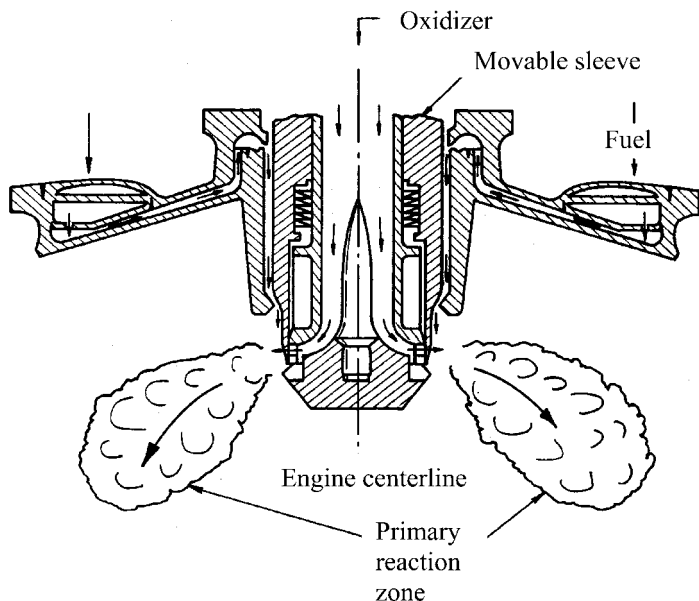Fig. 3   Space Shuttle OMS engine injector.

Fig. 4   Pintle injectors of throttable LRE.[6]

Monopropellant swirl injectors of screw-conveyer or tangential-channel type were used in early LRE, as shown in Fig. 5. The former employs a screw conveyer as swirler and are predominantly used in gas generators with moderate combustion temperatures. Each injector has a casing (1) brazed into the bottom of the assembly. The casing has a nozzle (2) and an axisymmetric cavity (3) connected to the liquid manifold through tangential passages (4). The bottom (5) is flared out and welded in the casing (1) forming a vortex chamber (6). In recent injector designs, the bottom (5) is made profiled to optimize the shape of the passage cross section of the vortex chamber (6). In screw-conveyer injectors (Fig. 5a), a screw-conveyer swirler (7) whose external passages (8) serve as tangential passages (4) is fitted into the casing (1).

Important geometric parameters determining swirl-injector characteristics are:

1) nozzle radius R_n;
2) cross-sectional area of the inlet flow passage A_{in};
3) swirling arm, i.e., the distance from the axis of the tangential passage to the injector axis, R_{in}.

These parameters form a dimensionless number known as the geometric characteristic parameter of a swirl injector:

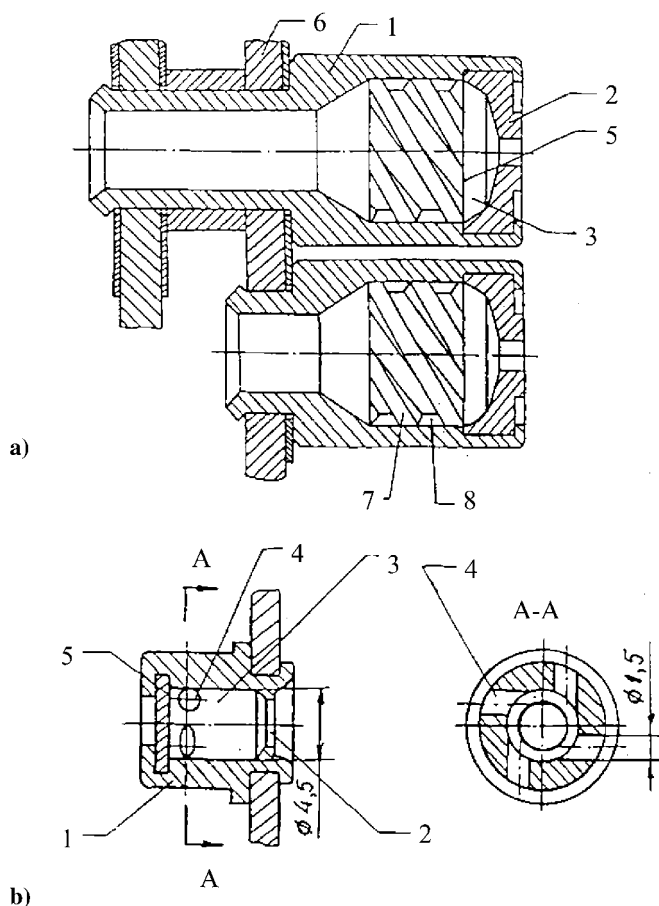$$A = \frac{A_n}{A_{in}} \cdot \frac{R_{in}}{R_n} \qquad (3)$$

Fig. 5 Monopropellant swirl injectors with a) screw conveyer and b) tangential passages.

It determines the injector flow coefficient μ, the nozzle filling coefficient φ, the spray cone angle at the cylindrical nozzle exit, and other output parameters. A table of expressions for calculating these parameters is given in Ref. 7. In addition, there are some secondary parameters, which are of importance in determining the liquid flow residence time and viscous losses in injectors. These include:

1) the diameter and length of the vortex chamber;
2) the nozzle length and the convergence angle of the vortex-chamber wall adjacent to the nozzle.

When fed through the tangential (4) or screw passages (8), the liquid is set in rotary motion in the chamber (3), and forms a liquid vortex with a free internal surface whose radius smoothly changes from the minimum at the bottom

(5) $r_{mk} = R_N \sqrt{a}$ to $r_{mN} = R_N \sqrt{1 - \varphi}$ in the nozzle, where the flow area ratio $\varphi = A_L/A_N$ is the liquid-occupied fraction of the injector nozzle section, and $a = 2(1 - \varphi)^2/(2 - \varphi)$. At the nozzle exit, the spreading angle of the liquid sheet slightly increases due to the conversion of the centrifugal pressure produced by the rotating liquid sheet to the axial velocity component, i.e., the Skobelkin effect.[2] The pressure on the liquid surface is equal to the pressure in the combustion chamber. For an ideal fluid, the velocity at the liquid surface can be written as

$$U = \sqrt{U_a^2 + U_u^2 + U_r^2} = \text{const} = \sqrt{\frac{2}{\rho} \Delta P_i} \tag{4}$$

where ΔP_i is the pressure drop across the entire injector. Any change in the velocity components U_i is unequivocally associated with a change in the surface radius r_m. The liquid flows out of the nozzle exit as a thin sheet whose thickness and spreading angle are independent of the pressure drop in a wide range of its variations, and the initial section has the shape of a single-cavity hyperboloid. The thickness of the sheet decreases farther downstream. It loses its stability and disintegrates into droplets according to the mechanism described in Ref. 3. It should be noted that under typical chamber conditions of a modern LRE, the liquid sheet from a swirl injector does not have enough time to get thin and to lose its stability since the aerodynamic effects of the surrounding high-pressure turbulent flow tends to disintegrate the liquid sheet more effectively. Thus, one has to analyze atomization for the startup and steady operating conditions of the same injector using two different methods.

The following features of swirl injectors, which determine their predominant applications in Russian LREs, are noteworthy:

1) For the same pressure drop and liquid flow rate, the average median diameter of droplets is 2.2 to 2.5-fold smaller than that of jet injectors. This advantage prevails for high flow rates and decreases when the counter pressure (i.e., the sum of the combustion chamber pressure and the centrifugal pressure created by liquid swirling motion) grows.

2) Compared with jet injectors, swirl injectors are not so sensitive to manufacturing errors such as deviation from prescribed diameter and surface misalignment.

3) The flow passage areas of swirl injectors are much larger than those of jet injectors with the same flow rates, and consequently they are less susceptible to choking or cavitation.

4) The pressure drop across a swirl injector is shared between the tangential channels ΔP_T and the vortex chamber ΔP_{vc}. Under steady-state conditions, the relation between ΔP_T and ΔP_{vc} can be easily defined, with the latter much higher than the former in most operational injectors. During the engine startup, when the vortex chamber is initially empty, the entire pressure drop is applied to the tangential channels and the liquid velocity is much higher than its steady-state value. The vortex chamber begins to be filled with high-speed rotating liquid. The ensuing increases in the centrifugal pressure and viscous losses then decrease the pressure drop across the inlet passage and subsequently the

mass flow rate prior to ignition. This self-tuning capability with variable flow resistance under transient conditions improves the engine startup operation.

Swirl injectors also feature wide spray-cone angles (in the range of 36 and 140 deg) and sharp non-uniformity of flow distribution. The liquid is practically absent near the injector axis. These features can be considered as a disadvantage when flow non-uniformity is detrimental for the process, for example, irrigation of catalyst grains for hydrazine decomposition. They are, however, advantageous for most applications in LRE since hot combustion products are recirculated to the injection region to stabilize the flame. The formation of a thin uniform liquid sheet also protects the injector face plate against excessive heat transfer from the high-temperature region.

Extensive effort has been applied to develop theories of swirl-injector hydraulics in Russia since as early as the 18th century (e.g., Leonard Euler, a member of the St. Petersburg Academy of Sciences). Among them, the principle of maximum flow rate postulated by N. Abramovich[8] in 1944 (Diploma of Discovery No. 49) is most noteworthy, which essentially laid the foundation of modern development of swirl injectors. The work was supplemented by the studies of L. A. Klyachko[2] and A. M. Prakhov,[3] as well as empirical data of Y. I. Khavkin[9] and many other scientists. It now gives reasonably reliable calculation results. Investigation of the dynamics of swirl injectors[7,10] has made it possible to design injectors with prescribed dynamic properties and use them as a means of suppressing various mechanisms of high-frequency instabilities. Work was conducted to study injectors with flow modulation capabilities[11] for modulating spray cone angles and flow rates with prescribed degrees of atomization.

The disadvantages of swirl injectors are:

1) the internal-cavity volume is significantly larger than that of a jet injector and has a longer startup transient time, which restricts their application in low-thrust LREs with pulse operations;

2) complex configuration and heavy weight.

The types of swirl injectors used in LREs are diversified because of specific requirements for different applications.

3.   *Monopropellant Swirl Injectors*

Monopropellant injectors (see Fig. 5) were widely used in open-loop engines. As a rule, they are arranged in assemblies in the chess-board or honeycomb patterns with alternating fuel and oxidizer injectors. In welded and brazed assemblies, oxidizer injectors with elongated casings are attached to the assembly bottoms and thus serve as structural elements. They often have two- to four-run screw-conveyer swirlers with cylindrical configurations. Conic screw-conveyer injectors, which are technologically less effective and widely used in jet engines, are seldom used in LREs. They are used only in low-flow injectors to minimize the vortex-chamber volume and to eliminate nonswirling liquid leaking through the gap between the screw conveyer and casing.

Contemporary monopropellant swirl injectors have tangential passages. As a rule, the number of passages is three or four. A smaller number of passages

increases the nonuniformity of flow distribution along the spray cone circle. Two passages are used only in highly closed injectors or in very long injectors. One passage is used for special purposes, when flow nonuniformity is required along the circumference, such as in near-wall regions. At present, monopropellant swirl injectors are mainly used in gas generators to provide efficient propellant delivery or as near-wall injectors in combustion chambers. Their relatively low combustion efficiency ($\sim$97%) and high sensitivity of fuel and oxidizer mixing increases the susceptibility to combustion-driven flow oscillations.

4. Bipropellant Swirl Injectors

Since the mid-1960s, bipropellant swirl injectors have been used most often in Russian LREs of various types and applications. Figure 6a shows a typical design of such injector elements. It has a hollow casing (1) with a nozzle (2). The hollow insert (3) with the nozzle (4) and flared-out bottom (5) are brazed into
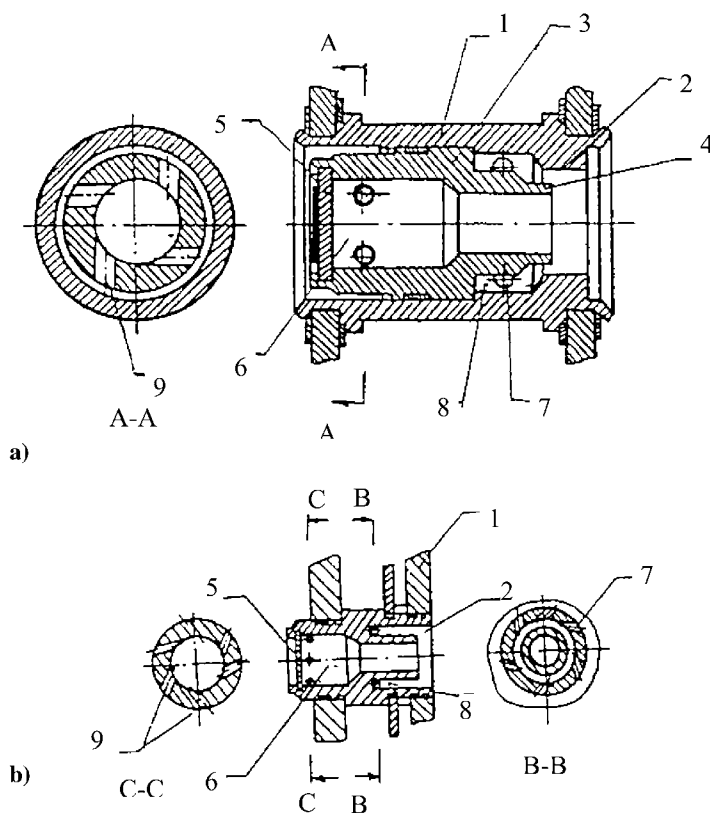

Fig. 6   Two different designs of bipropellant swirl injectors; 1-casing; 2-casing nozzle; 3-insert; 4-insert nozzle; 5-bottom; 6-central vortex chamber; 7–9 tangential passages; 8-peripheral vortex chamber.

it. The bottom and the insert form the vortex chamber (6), which is connected to the propellant-delivery manifold through tangential passages (9). The insert (3) and casing (1) form a peripheral vortex chamber (8) for the other propellant connected to its delivery manifold through tangential passages (7).

A more advanced and compact design of bipropellant injectors is given in Fig. 6b. It is beam welded to the fire face. For hypergolic propellants, the edge of the nozzle (4) is usually buried in the nozzle (2) of the peripheral injector by 0.7–2.2 mm. The specific dimension depends on the propellant type and injector geometry. Oxidizer injectors can be used as peripheral injectors (so-called direct scheme). Such an arrangement is more preferential from the standpoint of mixing hydrodynamics since it will produce sheets of the same or approximately the same thickness. In more recent engines, however, the reverse scheme with fuel delivery through the peripheral stage has found applications, due to the ease of arrangement with the cooling jacket and the fire bottom of the injector assembly. Injectors of the direct scheme have either propellant mixing outside the injector (in this case, the spreading angle of the external spray should be less than its counterpart of the internal spray), or mixing at the external-nozzle edge. Injectors of the reverse scheme, whose peripheral fuel stage have a considerably wider spray cone angle than that of the internal oxidizer injector, may have propellant mixing at the nozzle edge alone. Internal mixing of hypergolic propellants should be avoided in such injectors since they are not safe against ingress of one of the propellants to the cavity of the other one. Cryogenic propellants of the oxygen-kerosene type can be mixed directly in the vortex chamber of the peripheral oxygen stage, in which the swirling liquid-oxygen layer provides the cooling of the injector walls.

5. *Combined Jet-Swirl Injectors*

To increase the length of the combustion zone and to decrease the combustion response to chamber flow fluctuations, combined jet and swirl injectors have been widely used since the 1950s. Figure 7 shows sectors of the injector assemblies equipped by such injector elements. Each or some of the screw swirlers inside the vortex chambers are drilled to form a passage for a liquid jet inside the surrounding conical spray. A combination of impinging jets and such a type of injector element was used in place of baffles in several Chinese booster LREs (see Fig. 8) to suppress high frequency combustion instabilities. One should be careful with this design because such an injector could be a source of LRE unsteadiness if improperly designed,[12] and may lead to operations in two different manners, even at the same pressure drop. There may be a situation with separate outflows of jet and swirling liquid or with a joint outflow. The central jet could also disappear and the swirling spray could have a narrow spreading angle and become poorly atomized. Figure 9 schematically shows a sector of a combustion chamber injector assembly with alternating bipropellant swirl and impinged jet injectors.

C. Gas-Liquid Injectors

Gas-liquid injectors utilize the kinetic energy of a gas flow for liquid atomization and are mainly used in combustion chambers of closed-loop LREs and in
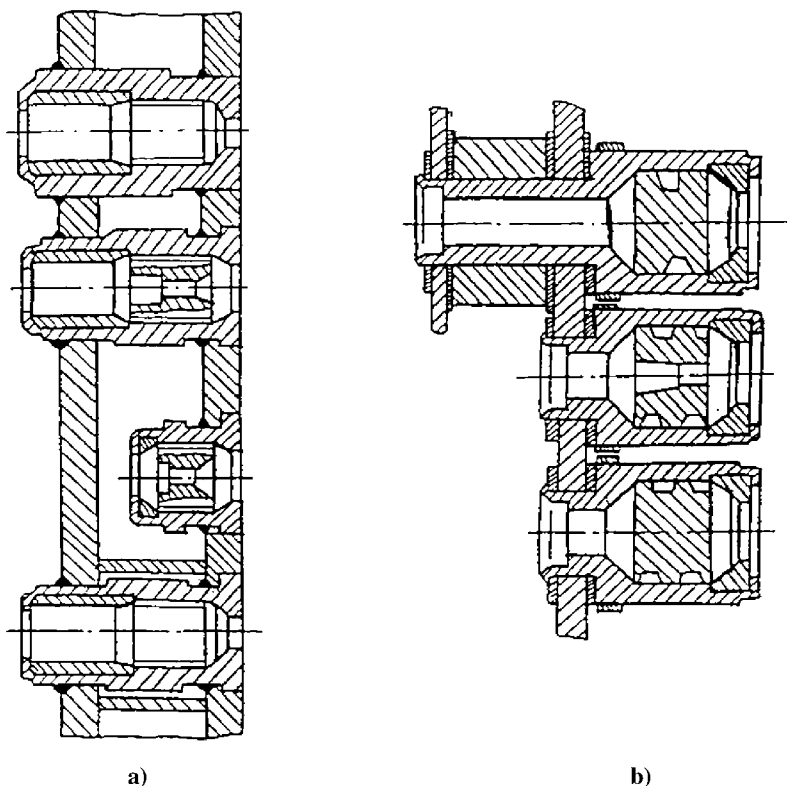
a)   b)

Fig. 7   Injector assemblies with alternating swirl and spray-swirl injectors.

some open-loop LREs having special operating conditions such as large thrust control while using prevaporized, decomposed, or gasified propellant, with preburning of a small amount of the propellant.

Figure 10 shows the main design schemes of gas injectors used in LREs. They can be classified into three basic categories: injectors with peripheral liquid and central gas delivery (a, d); injectors with peripheral gas and central liquid delivery (b, c, and e); and injectors with two-sided atomizing-gas delivery to the liquid sheet being atomized (f).

1. Jet Injectors

The gas-liquid jet injector (Fig. 10a) is one of the designs most commonly used in both hypergolic and hydrocarbon-oxygen LREs. It has a tubular casing (1) with an axial gas passage (2) and holes (3) for liquid propellant delivery. Passages can be arranged along the length of the casing (1) in different ways, depending on the propellants used. Passages (3) are predominantly located in the vicinity of the exhaust edge of the casing (1). The axes of passages (3) were made intersecting with the casing axis at an angle of 45 to 60 deg. Recently, it has become
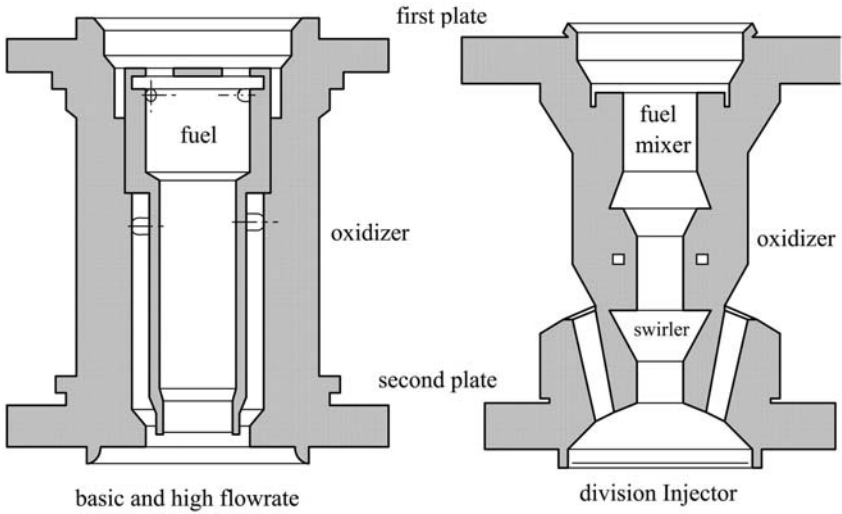
Fig. 8   High flow rate and division injection elements for Chinese YF-1 engine.

preferential to make passages (3) chordal, which increases the uniformity of propellant mixing.

The diameter of passage (2) usually varies between 6 and 18 mm, depending on the engine thrust requirement. The length of passage (2) is chosen to maximize the
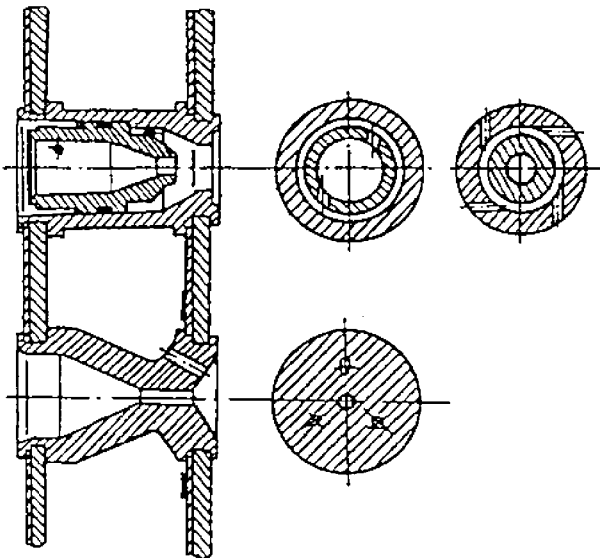

Fig. 9   Combustion chamber injector assembly with adjacent bipropellant jet and swirl injectors.
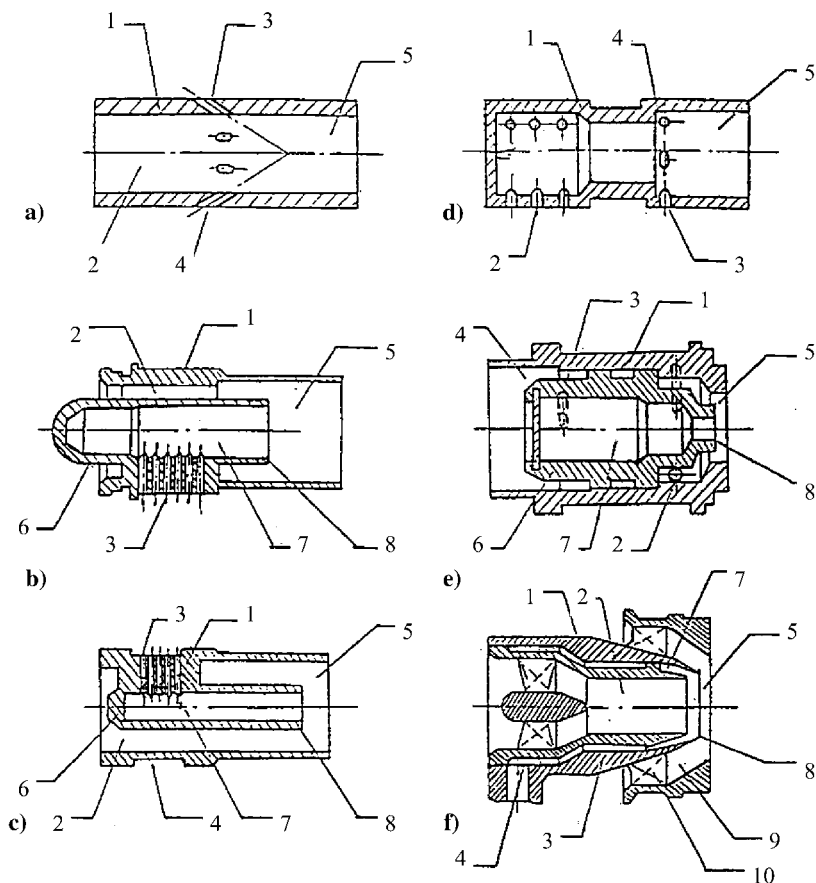
Fig. 10   Pneumatic injectors used in main combustion chambers and gas generators of LRE: a) jet-jet injector; b), c) jet-swirl injector; d), e) swirl-swirl injector; f) slit injector with alternating liquid and gas injection; 1-casing; 2, 9 gas passage; 3-liquid passage; 4-liquid manifold; 5-mixer; 6-bottom; 7-vortex chamber; 8-nozzle; 10-gas swirler.

removal of acoustic energy from the combustion chamber by treating the injector as a half-wave acoustic resonator. Figure 11 shows a gas-liquid spray injector assembly with a swirl fuel injector at the periphery, which protects the fire bottom of the assembly against overheating. Liquid propellant jets injected into the mixer (5) are atomized by the gas flow from passage (2). The combustion process occurs immediately downstream of the injected jets since the flame is stabilized on the walls of casing (1) behind holes (3). Simplicity of design and fabrication and high-quality mixing are the advantages of injectors of the type shown in Fig. 10a. The disadvantage is the relatively high sensitivity to pressure pulsations, which, however, can be compensated by changing the injector geometry to remove acoustic energy at prescribed frequencies from the combustion chamber.
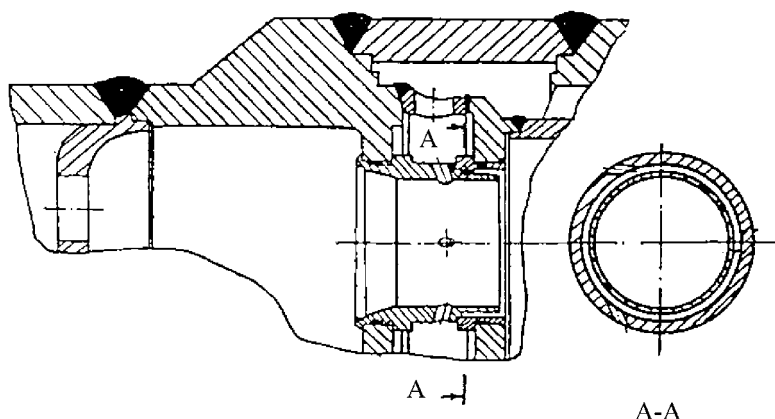
Fig. 11   Injector assembly with gas-liquid jet-jet injector equipped with a peripheral liquid swirl stage.

2. Swirl Injectors

In the aforementioned case, if holes (3) in the casing wall are made tangential, blocked from the entrance face, a swirl injector is formed with peripheral liquid propellant delivery and central delivery of a hot swirl gas flow (Fig. 10d). This design features a contraction between passages (2) and (3) and a shoulder in front of passages (3) to ensure the formation of a swirling liquid sheet on the internal walls of the mixer (5). The gaseous propellant arriving through the tangential passages (2) forms a swirling flow in the internal cavity of casing (1), travels around the liquid sheet running along the walls of the mixer (5), forms surface waves on it, and finally blows away the crests and disperses the liquid into droplets. Such injectors are widely used in high-power LREs with hypergolic propellants. The main advantage is a wide stability margin for operation over a broad range of mass flow rates. This feature may be attributed to the low sensitivity of the atomization and mixing processes stabilized by the mixer wall to pressure fluctuations and flow-velocity variations. Positioning liquid passages (4) at the periphery of the mixer (5) allows cooling of the fire bottom of the assembly by means of a cone-shaped screen formed by the evaporating-liquid sheet.

High-quality atomization achieved by swirling gas and liquid flows allows manufacturing of large injectors with diameters of the mixer (5) in a range of 50–60 mm and flow rates of several kilograms per second. To suppress high-frequency instability in the combustion chamber, unique acoustic properties of injectors such as acoustic impedance of the mixer (5) and acoustic resonance of the gaseous-propellant vortex chamber are used. Important results are obtained when the acoustic properties of the mixer and vortex chamber are combined.

The disadvantage of swirl injectors is the non-uniformity of flow intensity and mixture composition along the spray-cone radius, which does not provide adequate combustion efficiency. Figure 12 shows an example of a full-scale injector with central delivery of swirling gas. The gas resonance cavity minimizing flow
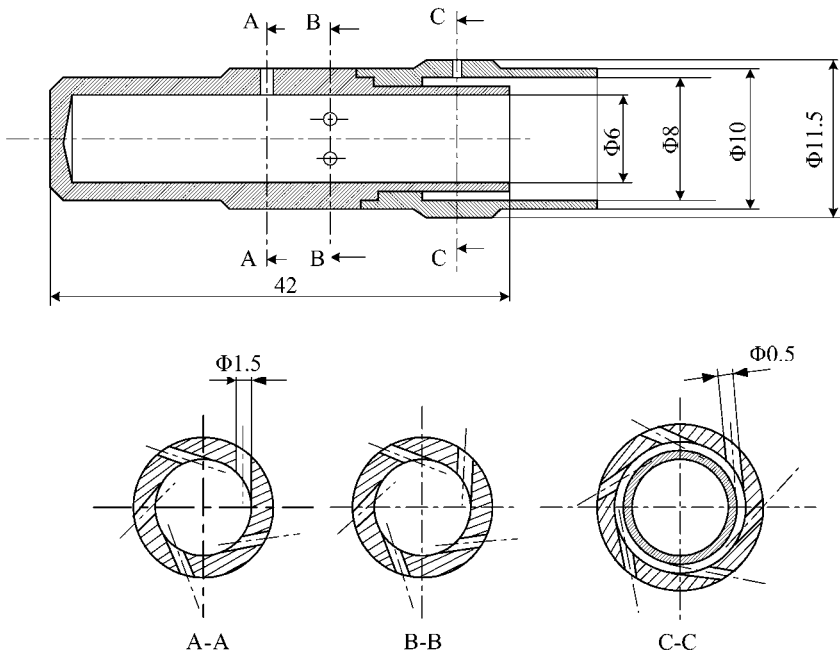
Fig. 12   Injector with central injection of swirling gas and acoustically tuned gas stage.

fluctuations is clearly visible. In low mass flow-rate injector elements with exterior swirling liquid flows, the central gas stage could be made of a non-swirling stepped channel, as shown in Fig. 13.

3.   Coaxial Injectors with Central Liquid Stage

This type of design includes jet, jet-swirl, and swirl-swirl injectors, as shown in Figs. 10b, c, and e. The injector has a tubular casing (1) with passages (2) for gaseous propellant delivery [usually between the pylons having passages (3) for liquid propellant delivery]. The pipe (6) with passage (7) and nozzle (8) is usually buried in the tubular casing (1) and mounted rigidly on the pylons. When the liquid stage (6) is made as a jet injector, passages (3) are radial and passage (7) is elongated. In this case, injectors are used for mixing liquid oxygen and hydrogen-enriched gas. When the central stage is made as a swirl injector, passages (3) are of either the tangential or screw-conveyer type (the latter is mainly used in hydrogen-oxygen gas generators). In this case, a swirling liquid sheet flowing out of the nozzle (8) is in the form of a cone-shaped film interacting with the coaxial gas flow. The quality of propellant atomization and uniformity of mixing are significantly enhanced, which allows manufacturing of larger injectors (with nozzle diameters of 8–12.5 mm) with propellant flow rates of up to 2 kg/s for each injector element. The presence of a hollow liquid vortex inside the passage (7)
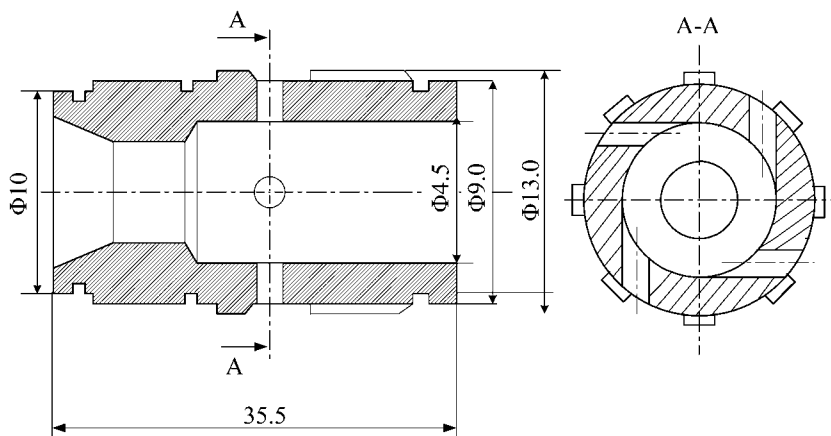
Fig. 13   Oxygen-kerosene injector with tangential injection of liquid oxygen.

makes it possible to use the liquid stage of the injector as a quarter-wave resonator to absorb the acoustic energy in the combustion chamber, for which purpose the passage (2) should be further elongated (see Fig. 10b), and in some cases it is necessary to make additional holes in the walls of the acoustic damper (6) or to equip the liquid stage of the injector with an additional Helmholtz transmission resonator.

The main advantage of such injectors is high-quality atomization and mixing of propellants. Their disadvantage lies in the complexity of manufacturing and adjustment. The possibility of self-oscillations of the liquid sheet in the coaxial gas flow in injectors of this type, which were first noted in Ref. 13, is an additional problem. Testing of full-scale engines revealed the presence of self-oscillations at the frequency of ∼5500 Hz, leading to pressure pulsations in the oxidizer passage with an amplitude of up to 0.9 MPa accompanied by subsequent breakdown of pipe connections with no significant pressure fluctuations in the combustion chamber.

Investigations of these injectors using models and actual propellants made it possible to establish the mechanism of self-oscillations described in Ref. 14 and to develop methods for their suppression. The presence of self-oscillations may sharply intensify propellant atomization and mixing, especially for injectors with low pressure drops. It has been proved both theoretically and experimentally that such induced high-frequency fluctuations are not related to intrinsic oscillations in the combustion chamber and are safe and even beneficial for combustion stability and efficiency. The self-oscillation regime is sometimes displaced into the engine operating regime requiring throttling (below 75% thrust), and injectors are equipped with devices dampening pressure oscillations arising in the combustion chamber.

The principle of the swirl-swirl injector (see Fig. 10e) is similar to that of the liquid-liquid injector shown in Fig. 6a. The only difference lies in the cross-sectional area of the gaseous propellant passage. Because the gaseous propellant comes through tangential passages (2) from the periphery of the casing (1), the

mixer is not made long. This, however, may lead to overheating and burnout of the casing. Additional means of cooling are thus required to prevent overheating of the fire bottom. Similar measures should also be introduced in jet injectors (see Fig. 10a), usually by putting an additional low-flow swirl injector at the periphery of the mixer nozzle (see Fig. 11). The designs of coaxial swirl-swirl injectors are highly diversified. As an example, Figs. 14 and 15 show swirl-swirl injectors of gaseous oxygen-kerosene engines with gaseous oxygen-cooled walls. Figure 16 shows injectors of oxygen-hydrogen gas generators.

4. Slit Injectors

Figure 10f shows an example of the injector design to provide atomization of a liquid sheet (or a vast number of fine jets) with the gas flow on both sides. This design has found applications in both jet engines and LREs. It contains a hollow
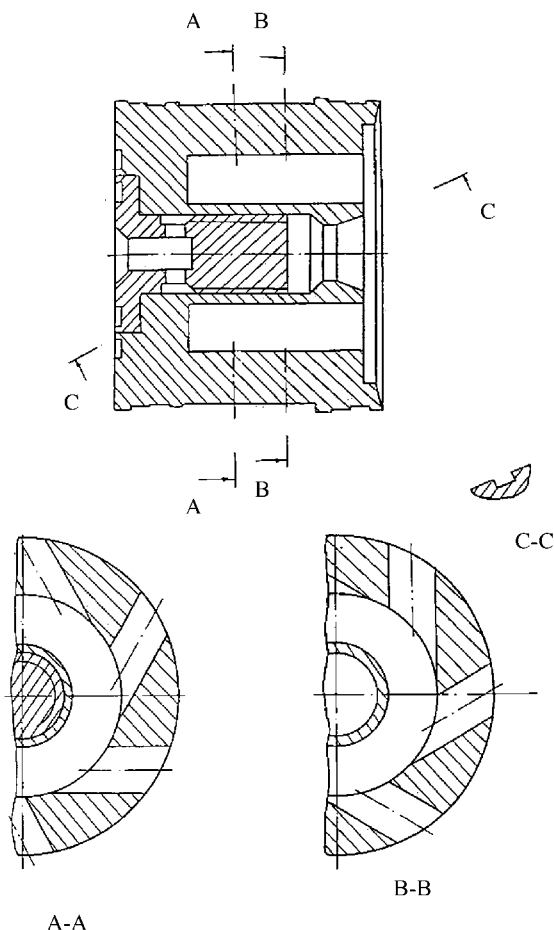

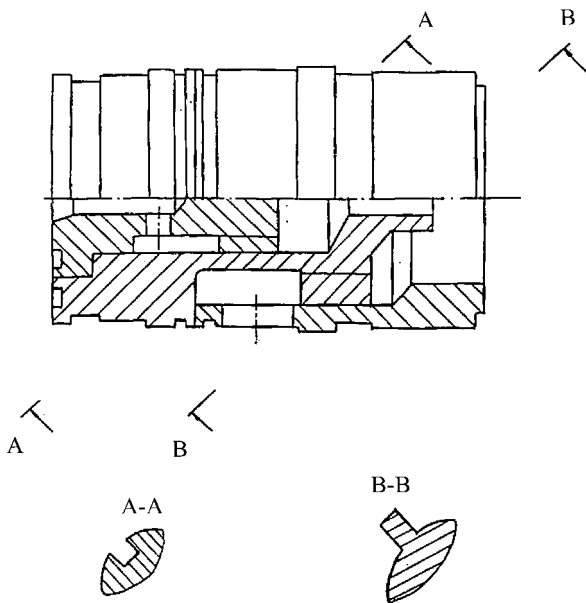Fig. 14   Swirl-swirl injectors of gaseous oxygen and liquid hydrocarbon.

Fig. 15   Modified oxygen-kerosene injector with screw conveyer swirler.

casing (1) with an insert having axial gas passage (2) and slit passage (3) formed
by the insert, and a casing (1) for the liquid propellant. The passage (3) is con-
nected to the feed line (4). The casing (1) is mounted on an external yoke (9)
by means of a gas-flow swirler (10) and forms a vortex chamber (7) for the
liquid, which ends in a nozzle (8). The mixer (5) consists of the nozzle (8) and
yoke (9). The gas-flow swirler (11) or an additional low-flow liquid injector
(not shown in the figure) can be placed into the passage (2). Several alternating
liquid (3) and gas (2) circumferential passages can be made. The advantages of
this design are the most uniform and best-quality propellant atomization and
mixing. As a consequence, one engine with such a design has the combustion
efficiency of around 0.995. The disadvantages include increased production
complexity and cost and insufficient understanding of its dynamic characteristics,
which forbid its application in high-thrust engines.

5. *Jet-Swirl Injectors*

Injector assemblies using jet and swirl elements in the fuel or oxidizer lines are
shown schematically in Fig. 11. Application of a liquid swirl injector in combination
with a jet injector improves the cooling conditions of the fire bottom. The design has
allowed the development of tripropellant injectors (see Fig. 17), which represent in
essence a combination of well-developed designs shown in Figs. 10a and 10b. It
consists of a casing (1) with a cavity (2) and a chamber (3) with a nozzle (4) coaxi-
ally mounted in the casing, which forms a cavity (5) connected to the liquid propel-
lant delivery manifold by tangential or radial passages (6). Passages (7) are formed
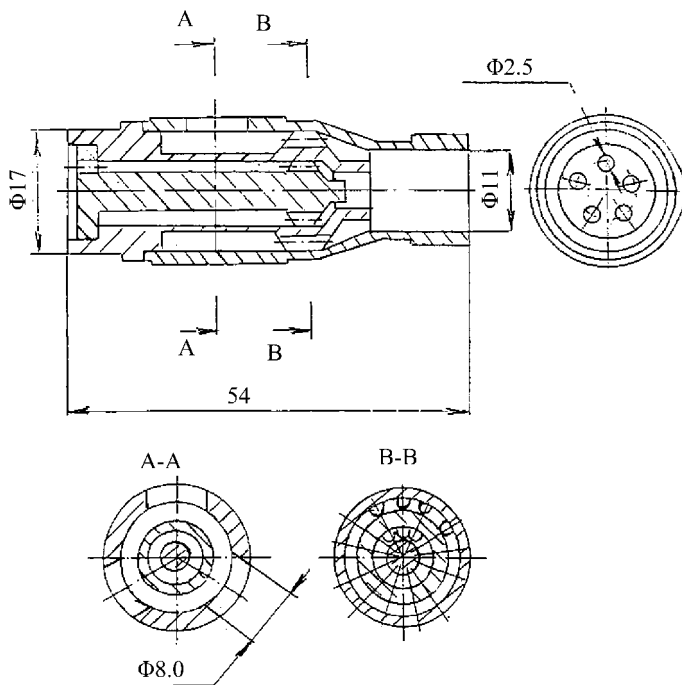
Fig. 16   Injector of oxygen-hydrogen gas generator.

between the chamber (3), the pylons with tangential passages (6) and casing (1). The mixer (8) is formed between the nozzle (4) and the casing (1). Chordal (9) and radial (10) passages for additional propellant delivery are made in the walls of the casing (1). This injector is designed for two applications: reducing and oxidizing generator gases. These versions differ in the dimensions of the passage cross sections alone. In case reducing gas is fed to the injector through passages (7), liquid oxidizer comes to the chamber (3) through passages (6) (similar to the injector in Fig. 10b), and additional fuel (hydrocarbon of the liquefied methane or propane type) is fed through passages (10). In the case of operation according to the scheme with afterburning of the oxidizing generator gas fed via passages (7), less volatile liquid fuel (kerosene) is fed to the chamber (3) through passages (6) and more volatile fuel (hydrogen) via passages (9) and (10). Under this condition, there exists a possibility of throttling of kerosene passage (6) up to its complete disengagement. The injector will operate in the regime characteristic of the injector in Fig. 10b. The results of injector development and testing are given in Refs. 14 and 15.

D.   Intensification of Propellant Atomization and Mixing in Liquid Injectors

The efficiency of liquid injectors is relatively low because much energy is expended for liquid acceleration rather than for atomization. Injectors possessing
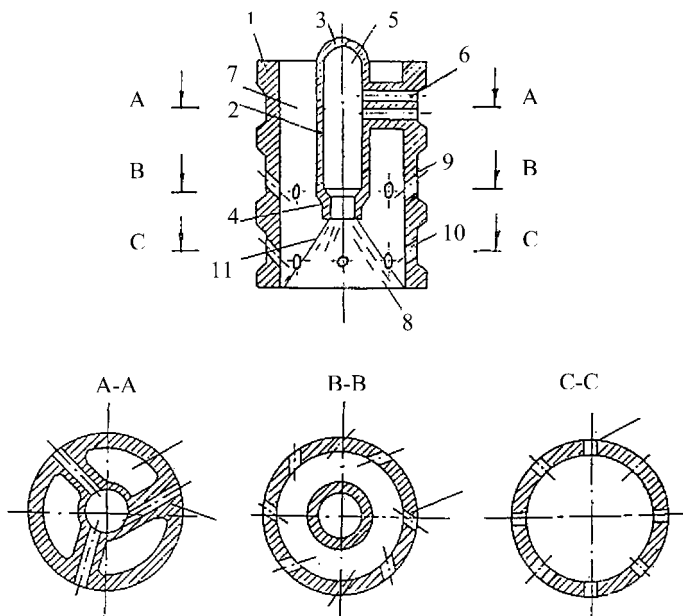
Fig. 17   Design of a tripropellant injector.

higher atomization and mixing characteristics have been developed. The principal means of improving injector efficiency involve reducing viscous losses of the liquid flow and applying nonstationary processes to intensify propellant atomization and mixing. In jet injectors, the former can be accomplished by increasing the quality of the liquid surface and reducing its area (e.g., by shortening injectors). Investigations of viscous-loss mechanisms in swirl injectors have shown the following two contributing processes: interlayer liquid friction in the vortex chamber and friction of the external liquid layers on the walls of the vortex chamber and nozzle. To reduce viscous losses, it is advisable to shorten the lengths of all of the elements, in particular the nozzle, and to reduce the liquid flow velocity by increasing the swirling arm of the liquid, R_{in}. Optimization of the injector shape to meet these requirements has led to the development of short and flat platelet swirl injector assemblies consisting of a stack of plates welded in vacuum with holes, grooves, and saw-cuts to form nozzles, vortex chambers, and passages. Figure 18 shows an injector assembly with stacked plate arrangement having two passages for propellant delivery. The assembly has a casing (1) with an annular manifold (2) to deliver the first-stage flow and disks (3) and (4) fitted in the casing with separation (5), tangential passages (6), vortex chambers (7), and nozzles (8). The casing has an additional manifold (9) for the second-stage propellant, and the disk (4) has additional supply (10) and tangential (11) passages. To decrease the dimensions of the assembly and the distance between the injectors, propellant distribution between them is provided with disks (12) and (13) having grooves (14) and
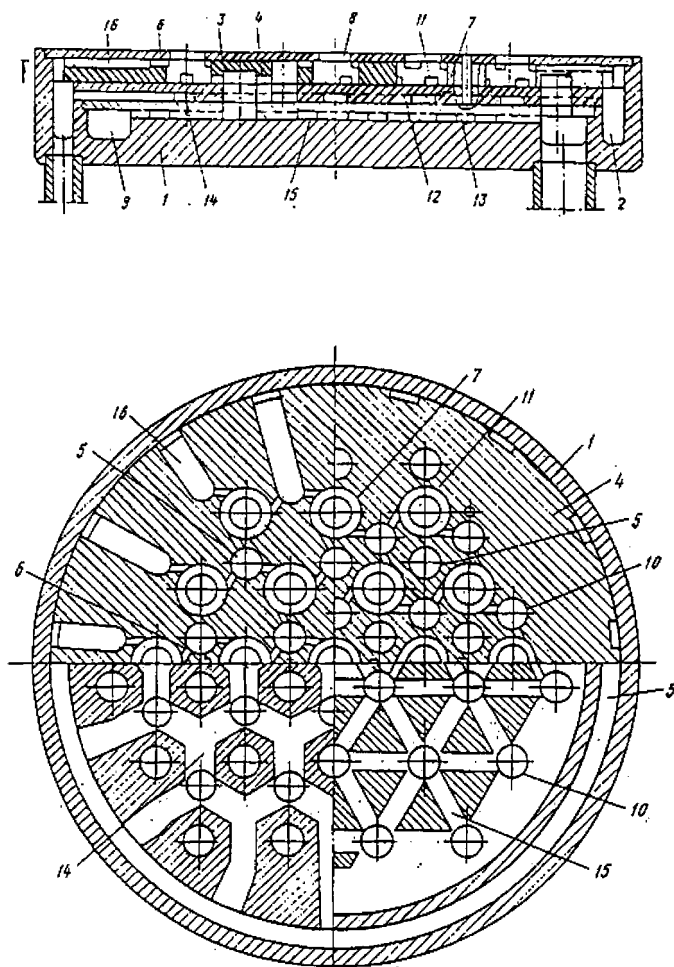
Fig. 18   Design of a stacked bottom injector assembly; 1-casing; 2, 9 propellant manifolds; 3-fire bottom; 4-injector bottom; 5, 10, 14, 16 supply passages; 6, 11-swirl passages; 7-injector vortex chambers; 8-injector nozzles; 12–13 separating disks.

(15) for separation. The fire bottom (3) has grooves (16), which not only deliver part of the propellant to the injectors but also cool it. When accommodated in the casing, disks (3), (4), (12), and (13) are diffusion welded to it in vacuum, after which propellant delivery pipes are welded to the casing.

When fed to the manifolds (2) and (9), the propellant enters tangential passages (6) and (11) through grooves (14), (15), and (16) and delivery passages (5) and (10), gains rotating motion in the vortex chambers (7) and exits from the nozzles (8) in the form of thin circumferential sheets. To decrease viscous losses inside the vortex chamber when using viscous, adhesive or non-Newtonian

liquids such as jells and metal particle suspensions, the vortex chamber and nozzle can be made of a porous material. Figure 19 schematically shows a porous swirl injector in a mandrel for cold-flow tests. The injector has an insert mounted on a branch pipe (1). The insert is made by diffusion-welded porous bottoms (2) and casing (3) fixed by a coupling nut (4). The casing has a heat-resistant coating on the combustion-zone side. The annular manifold formed by the casing and coupling nut (4) can be connected by holes to the branch pipe, as shown in Fig. 18, or to an independent manifold, to deliver low-viscous liquid that penetrates through the porous material of the casing and forms a boundary layer that separates main propellant from the surfaces of vortex chamber and the nozzle of the injector.[16]

   When fed through the branch pipe, the liquid enters the casing cavity through the tangential passages, forms a liquid vortex in the vortex chamber, and leaves the nozzle as a circumferential liquid sheet. Simultaneously, part of the liquid leaks through the porous bottom and casing and reaches the boundary layer flowing around the internal surface of the vortex chamber, thereby decreasing
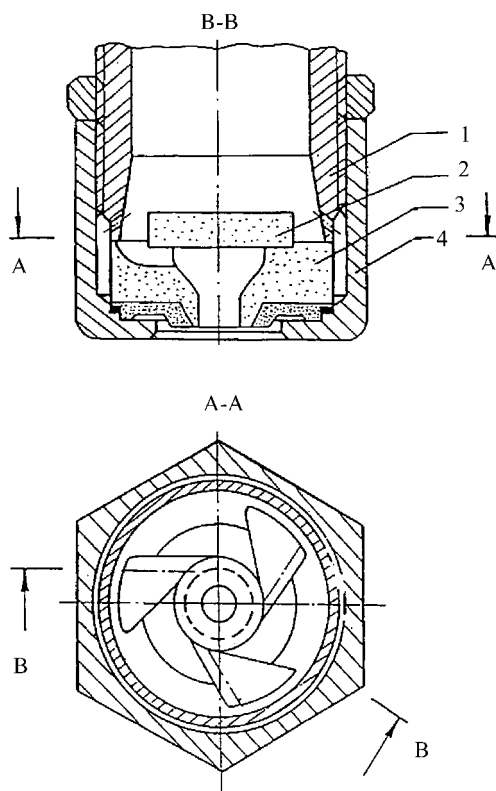

Fig. 19   Swirl injector with porous ceramic-metal swirler; 1-mandrel; 2-bottom; 3-porous casing with tangential grooves; 4-coupling unit.

the gradient of the circumferential velocity and hence the viscous losses. In the case of increased propellant viscosity, a small amount of low-viscosity liquid such as kerosene is fed through the porous walls from an independent source.

In liquid swirl injectors of the classical design, the exhaust process is stable and not accompanied by regular self-oscillations. However, in the presence of some destabilizing factors such as exhaust of a boiling liquid and bubbled media, or with specially profiled vortex chambers, self-oscillations at frequencies from several Hz to several hundred Hz can be produced and used to intensify the process of mixture formation.[17] As for vibrational liquid injectors with magneto-striction or piezoelectric actuators, driven by additional sources of electrical energy, they were used only in experimental designs for research purposes.[18]

E.   Intensification of Propellant Atomization and Mixing in Gas-Liquid Injectors

Because gas-liquid injectors use generator gas produced mainly by one of the propellants, the engine is not in short supply of the atomizing flow. The problem of improving the pneumatic atomization process is not so critical. The limiting factors are length of the combustion zone permitted in chambers of limited dimensions, high flow intensity, maximum flow uniformity and mixture ratio (which is especially important for low-thrust systems), and sensitivity to acoustic instability. In such chambers, methods for intensifying the mixture formation process are:

1) decreasing injector dimensions;
2) increasing surface area wetted by the liquid and flown around by the atomizing gas;
3) emulsification of the liquid, i.e., formation of gaseous bubbles in the liquid flow.

II.   Theory and Design of Liquid Monopropellant Jet Injectors
A.   Flow Characteristics

The mass flow rate of a jet (spray) injector, shown schematically in Fig. 20, can be determined using Bernoulli's theorem:

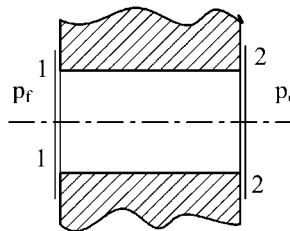$$p_{01} = p_1 + \frac{\rho U_1^2}{2} = p_2 + \frac{\rho U_2^2}{2} + \Delta p_{1-2} \tag{5}$$

Fig. 20   Schematic diagram of jet injector.

where Δp_{1-2} represents the pressure losses in the injector passage and p_{01} the total pressure at the entrance. From mass continuity,

$$\dot{m} = \rho U_1 A_1 = \rho U_2 A_2 \tag{6}$$

The flow area at the injection exit A_2 is usually smaller than the injector cross-sectional area A_n. Thus, $A_2 < A_n$, and $A_2 = \varepsilon A_n$, with ε (≤ 1.0) being the coefficient of jet contraction. For continuous exhaust, $A_2 \equiv A_n$ and $\varepsilon = 1.0$. If the propellant is delivered from a large manifold with $A_1 \gg A_2$, the inlet velocity U_1 can be neglected and $p_1 = p_{01}$. The pressure drop across the injector Δp_i can be obtained from Eq. (5):

$$\Delta p_i = p_f - p_c \equiv p_{01} - p_2 = \frac{\rho U_2^2}{2}(1 + \xi_i) \tag{7}$$

where $\xi_i = \Delta p_{1-2}/(\rho U_2^2/2)$ is the hydraulic-loss coefficient. The subscripts f and c refer to the conditions in the propellant manifold and combustion chamber, respectively. The exit velocity U_2 takes the form

$$U_2 = \frac{1}{\sqrt{1 + \xi_i}} \sqrt{\frac{2\Delta p_i}{\rho}} \tag{8}$$

Substitution of U_2 from this expression into the continuity equation gives the mass flow rate of the injector:

$$\dot{m}_i = \frac{\varepsilon}{\sqrt{1 + \xi_i}} A_n \sqrt{2\rho \Delta p_i} \tag{9}$$

For an ideal liquid flow with $\xi_i = 0$ and $\varepsilon = 1.0$, we have

$$\dot{m}_{i.\mathrm{id}} = A_n \sqrt{2\rho \Delta p_i} \tag{10}$$

Comparison of Eqs. (9) and (10) leads to the expression of the flow coefficient of an injector μ:

$$\frac{\dot{m}_i}{\dot{m}_{i.\mathrm{id}}} = \frac{\varepsilon}{\sqrt{1 + \xi_i}} = \mu \tag{11}$$

Since the hydraulic loss coefficient ξ_i is always positive, the injector flow coefficient μ is less than unity in all cases. In practical designs, ξ_i and ε are determined experimentally, as functions of injector length l_i and cross-sectional area A_n. The mass flow rate can be calculated from Eq. (9) for given pressure drop, fluid density, and injector area.

B. Effect of Injector Configuration

Figure 21 schematically shows the liquid flow in a real injector passage. When entering the injector, the liquid flow separates from the sharp edge at the entrance
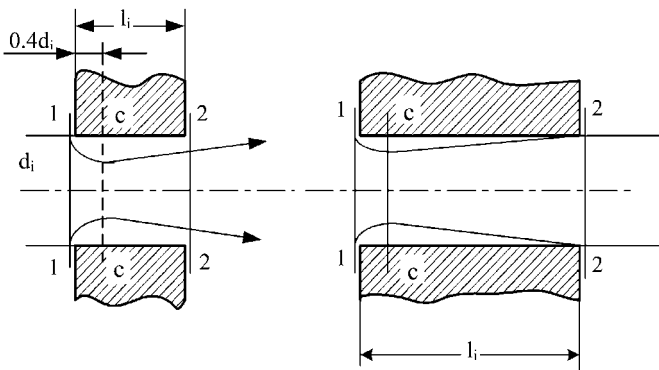
Fig. 21   Schematic diagram of liquid flow in jet injector.

due to the inertia force, and contracts as it proceeds. The largest contraction takes place at a distance of 0.4 d_i from the inlet. The flow then expands and exhausts from the injector. Two different modes of injector operation have been observed:

1) If the passage is short with the aspect ratio of l_i/d_i less than 1.5, the expanding jet is unable to reach the nozzle wall (see Fig. 21a) with the jet contraction coefficient ε less than unity, and an annular space is formed between the jet and the injector wall, which is in communication with the combustion chamber. The exhaust liquid flow is unstable and the mass flow rate is reduced. For this reason, short injectors are seldom used in operational engines.

2) If the injector passage is sufficiently long with l_i/d_i greater than 1.5, the expanding jet reaches the injector wall (see Fig. 21b) and the contraction ratio ε equals to unity. A stagnant zone, however, forms between the flow boundary and injector wall, and a vortex-type liquid flow reaches its steady state there. At high flow velocities, cavitation may occur in the contraction section, and the stagnant zone becomes a cavity. It is clear that each mode of injector operation affects the flow coefficient μ in its own way.

C.   Flow Coefficient

The flow coefficient μ can be determined experimentally based on either the measured mass flow rate or the hydraulic loss coefficient. The total pressure losses $\Delta p_{1-2} = \xi_i \rho U_2^2/2$ for a jet injector can be represented as follows:

$$\Delta p_{1-2} = \Delta p_{1-c} + \Delta p_{c-2} + \Delta p_{fr} = (\xi_{1-c} + \xi_{c-2} + \xi_{fr})\frac{\rho U_2^2}{2} = \xi_i \frac{\rho U_2^2}{2} \qquad (12)$$

where Δp_{1-c} and Δp_{2-c} are the losses in the $1-c$ and $c-2$ sections, respectively, and Δp_{fr} the friction loss on the passage wall. Here,

$$\xi_i = \xi_{1-c} + \xi_{c-2} + \xi_{fr}; \quad \mu = \frac{\varepsilon}{\sqrt{1 + \xi_{1-c} + \xi_{c-2} + \xi_{fr}}} \qquad (13)$$

The coefficient ξ_{1-c} represents the energy loss associated with the vortex generation when the liquid flows into the injector passage. Figure 22 shows the
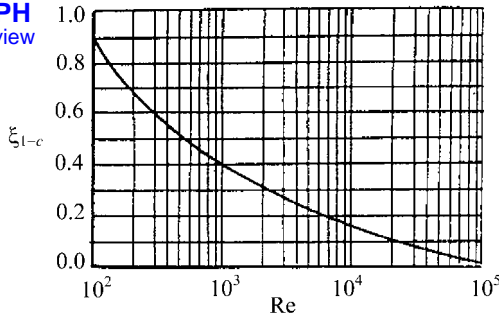
Fig. 22   Effect of Reynolds number on coefficient ξ_{1-c}.

measured ξ_{1-c} vs the Reynolds number ($Re = U_i d_i / \nu$) on a logarithmic scale. It decreases with increasing Reynolds number. The coefficient ξ_{c-2} represents the energy losses associated with the vortices formed when the flow expands after the contraction at the $c - c$ station. The explicit expression for ξ_{c-2} can be derived from the following equations:

Bernoulli's equation

$$p_n + \frac{\rho U_n^2}{2} = p_2 + \frac{\rho U_2^2}{2} + \Delta p_{c-2} \tag{14}$$

where the subscript n denotes the flow properties for an ideal injector without flow contraction.

Momentum conservation

$$(p_2 - p_n)A_2 = \rho U_2 A_2 (U_n - U_2) \tag{15}$$

Mass continuity

$$\rho U_2 A_2 = \rho U_n A_n \tag{16}$$

A simple manipulation of Eqs. (14)–(16) gives the expression for the total-pressure loss:

$$\Delta p_{c-2} = \frac{\rho U_2^2}{2}\left(\frac{U_n}{U_2} - 1\right)^2 \tag{17}$$

which is also known as the Borda-Carnot theorem. It follows from this equation that

$$\xi_{c-2} = \left(\frac{U_n}{U_2} - 1\right)^2 \tag{18}$$

As is shown by experiments, this coefficient depends not only on the degree of flow contraction but also on the Reynolds number in the narrow passage section. However, for $Re > 10^5$, which, in fact, is always the case with LRE injectors, viscosity practically exerts no effect on ξ_{c-2}. It is solely determined by the inlet configuration that affects flow contraction, i.e., $\xi_{c-2} \equiv \xi_{in}$. Figures 23 and 24 show such effects on ξ_{in} for two different designs.[19] As the inlet convergence angle β increases, the value of ξ_{in} initially decreases, reaches a minimum at about 50 deg, and then increases. This optimum value decreases with an increase in the ratio of l_{in}/d_i. Figure 25 shows the ξ_{in} behavior when the injector passage has sharp inlet edges and is tilted with respect to the inlet plane.[19]

The coefficient ξ_{fr} represents the friction losses on the passage wall, and can be expressed as follows:

$$\xi_{fr} = \lambda l_i/d_i \tag{19}$$

where λ is the drag coefficient. For hydraulically smooth pipes in the turbulent regime ($Re > 4 \times 10^3$), λ can be expressed as $\lambda = 0.3164 Re^{-0.25}$. A passage is considered hydraulically smooth if the wall-surface roughness, which depends on the quality of injector production, is less than $0.007d_i$.

The hydraulic-loss coefficient of a jet injector takes the form

$$\xi_i = \xi_{1-c} + \xi_{in} + \lambda l_i/d_i \tag{20}$$

D. Design Procedure

Once the theory behind the operation of jet injectors is established, the following steps can be used to design a jet injector based on the equations derived in the preceding section. These are eight equations and one experimental correlation for 11 variables (i.e., Δp_i, $\dot{m}_i$, l_i, Re, U_i, d_i, λ, ξ_{fr}, μ, ξ_{in}, and ξ_{1-c}). The system can be easily solved using an iterative scheme if two of these parameters such as Δp_i and $\dot{m}_i$ are known:

1) Specify initial data of Δp_i, m_i, l_i, ρ, and ν for the expected injector design.
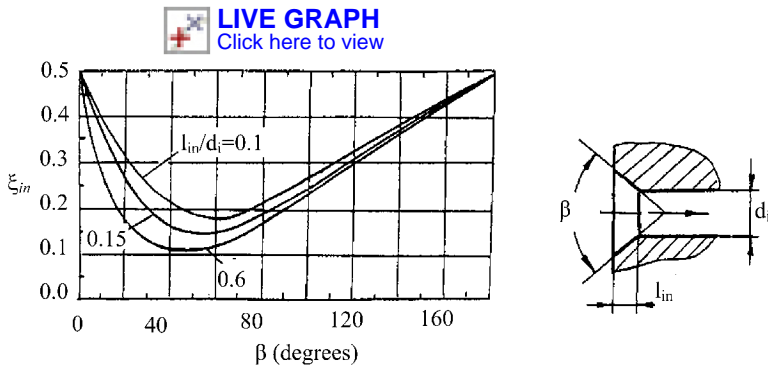2) Initiate the calculation with the flow coefficient $\mu = 1/\sqrt{1 + \xi_{in}}$ as first approximation.

Fig. 23   Effect of inlet-edge contraction on coefficient ξ_{in} in jet injectors.
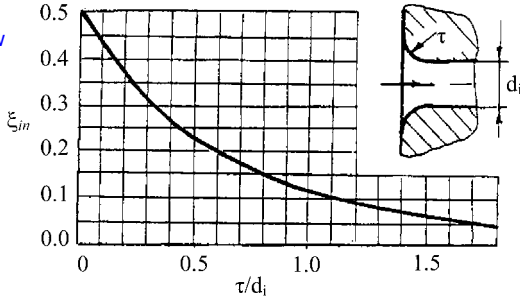
Fig. 24   Effect of inlet-edge rounding on coefficient ξ_{in} in jet injectors.

3) Calculate the diameter of the injector passage, $d_i = 0.95\dot{m}_i^{0.5}(\mu)^{-0.5} \times (\rho\Delta p_i)^{-.25}$.

4) Determine the velocity and Reynolds number based on the values obtained in the previous steps with $U_i = 1.273\dot{m}_i\rho^{-1}(d_i)^{-2}$.

5) Determine λ and ξ_{fr} from their respective relations, $\lambda = 0.3164Re^{-0.25}$ and $\xi_{fr} = \lambda l_i/d_i$.

6) Determine ξ_{1-c} from Fig. 22 and calculate $\xi_i = \xi_{1-c} + \xi_{in} + \xi_{fr}$.

7) Update the flow coefficient with $\mu = 1/\sqrt{1 + \xi_i}$ and repeat steps 3–7 until the calculated coefficient μ converges.

The injector diameter d_i usually falls in the range of 0.8–2.5 mm because a small diameter is susceptible to clogging and a large diameter gives rise to poor atomization quality and increased spray length. If d_i falls outside the aforementioned limits, some changes should be introduced into the mixture formation process and the mass flow rate $\dot{m}_i$ should either be decreased or increased.

The possibility of occurrence of cavitation in the injector passage should be checked. Assuming that $p_2 \equiv p_s$ and $\xi_{c-2} \equiv \xi_{in}$, from Eq. (14) we have

$$p_s - p_n = \frac{\rho U_2^2}{2}\left(\frac{U_n^2}{U_2^2} - 1\right) - \frac{\rho U_2^2}{2}\left(\frac{U_n}{U_2} - 1\right)^2 = 2\sqrt{\xi_{in}}\frac{\rho U_2^2}{2} \qquad (21)$$
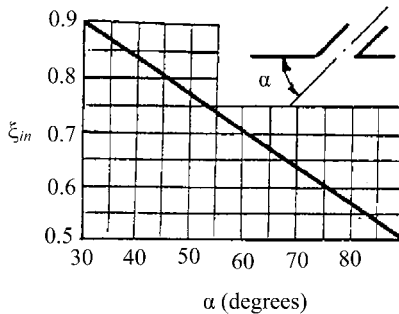
Fig. 25   Effect of tilt angle of injector passage on coefficient ξ_{in}.

Then,

$$\frac{\Delta p_i}{p_s - p_n} = \frac{1 + \xi_{1-c} + \xi_{\text{in}} + \lambda l_i/d_i}{2\sqrt{\xi_{\text{in}}}} = \eta \tag{22}$$

The condition for preventing cavitation becomes

$$p_n = p_s - \frac{\Delta p_i}{\eta} \geq p_v \tag{23}$$

where p_v is the vapor pressure of saturated propellant.

III.   Theory and Design of Gaseous Monopropellant Jet Injectors
A.   Flow Characteristics

The delivery of gaseous combustible mixtures produced in the gas generator into the main combustion chamber is achieved with the aid of jet injectors. The general theory of gas injectors is based on the conservation of mass and energy and the equation of state. The mass flow rate of an injector is expressed as

$$\dot{m}_i = \mu \rho_2 U_2 A_2 \tag{24}$$

where μ is the flow coefficient defined in Eq. (11). The gas density at the injector exit is obtained by assuming an isentropic process through the flow passage:

$$\rho_2 = \rho_{01}\left[\frac{p_2}{p_{01}}\right]^{1/k} \tag{25}$$

The ideal exit velocity U_2 becomes

$$U_2 = \sqrt{2\frac{k}{k-1}RT_{01}\left[1 - \left(\frac{p_c}{p_{01}}\right)^{\frac{k-1}{k}}\right]} \tag{26}$$

where R denotes the gas constant and k the ratio of specific heats. The total pressure of the gas flow p_{01} is the sum of the chamber pressure p_c and the pressure drop across the injector Δp_i, i.e., $p_{01} = p_c + \Delta p_i$. The total temperature T_{01} equals the gas temperature in the manifold. The exit velocity reaches its maximum U_{th}, in the limit of $p_c = 0$. We define the velocity coefficient λ as

$$\lambda_2 = \frac{U_2}{U_{\text{th}}} = \frac{U_2}{\sqrt{2(k/k+1)RT_{01}}} = \sqrt{\frac{k+1}{k-1}\left[1 - \left(\frac{p_c}{p_{01}}\right)^{\frac{k-1}{k}}\right]} \tag{27}$$

Substitution of Eq. (27) into Eq. (24) gives the injector mass flow rate in terms of λ:

$$\dot{m}_i = \mu \frac{(p_c + \Delta p_i)A_n}{C^*} q(\lambda_2) \tag{28}$$

where C^* is the characteristic velocity[20] defined as

$$C^* = \frac{\sqrt{kRT_{01}}}{k\sqrt{[2/(k+1)]^{(k+1)/(k-1)}}} \tag{29}$$

The gasdynamic coefficient function $q(\lambda_2)$ takes the form

$$q(\lambda_2) = \left(\frac{k+1}{2}\right)^{1/(k-1)} \lambda_2 \left(1 - \frac{k-1}{k+1}\lambda_2^2\right)^{1/(k-1)} \tag{30}$$

The flow coefficient μ of a gas injector for incompressible fluids can be written as

$$\mu = \frac{1}{\sqrt{1 + \xi_i}} \tag{31}$$

In evaluating the flow loss coefficient ξ_i, the high permeability of the gas injector assembly should be taken into account. The ratio of the area occupied by the gas flow in the $c - c$ cross section, A_{gas}, to the total injector assembly area, A_{total}, is rather high compared with liquid injector assemblies. This highly packed situation tends to straighten the flow at the injector entrance and reduce the subsequent flow contraction in the injector passage. To account for the effect of neighboring injectors, the following empirical relationship is used:

$$\xi_{c-2} = \xi_{in}(1 - d_i^2/d_1^2) \tag{32}$$

where d_1 is the diameter of the gas flow before entering the injector (i.e., at the $1-1$ cross section). It is taken numerically to be the average distance between the axes of the neighboring injectors. In addition, as a consequence of high-intensity turbulence, viscosity exerts no influence on the local hydraulic losses, i.e., $\xi_{1-c} = 0$. Thus,

$$\xi_i = \xi_{in}(1 - d_i^2/d_1^2) + \lambda l_i/d_i \tag{33}$$

B. Design Procedure

Several parameters are usually specified at the engine system design stage. These include the mass flow rate of the injector assembly and associated flow conditions, diameter of the injector assembly, pressure in the combustion chamber, and pressure drop across injectors. The type of injectors and their surmised number are also provided. The problem can be formalized to determine the injector passage diameter for the prescribed conditions. The numbers of unknown parameters and equations used to close the formulation are the same as those for

liquid injectors. There are, however, three additional unknowns, λ_2, C^*, and $q(\lambda_2)$, which can be solved using Eqs. (27), (29), and (30), respectively.

The injector design proceeds in the following steps:

1) Assume a value for the flow coefficient μ.
2) Calculate $p_{01} = p_c + \Delta p_i$ and determine the velocity coefficient λ_2 from Eq. (27).
3) Calculate $q(\lambda_2)$ using Eq. (30).
4) Calculate C^* from Eq. (29).
5) Determine $A_n = \dot{m}_i C^* / \mu p_{01} q(\lambda_2)$ and $d_i = 1.128\sqrt{[\dot{m}_i C^* / \mu p_{01} q(\lambda_2)]}$.
6) Calculate ξ_i from Eq. (33) and determine $\mu = 1/\sqrt{1 + \xi_i}$.
7) Repeat steps 3–6 until the calculated d_i converges.

If calculations show the lack of space to accommodate the intended number of injectors with the calculated passage diameter d_i on the injector assembly (e.g., the diameter d_i is too large), changes should be made in the engine design by increasing the pressure drop Δp_i since d_i is inversely proportional to Δp_i. If, on the contrary, the injectors with the diameter d_i prove to underutilize the area of the injector assembly (i.e., low permeability of the injector assembly due to small d_i), then a lower value of Δp_i should be implemented. The injector design is considered to be completed when the parameters in Eq. (28) are correlated not only with each other, but also with the engine parameters of the propulsion system and the design of the injector assembly.

IV. Theory and Design of Gas-Liquid Jet Injectors

The main objective of a gas-liquid mixing element is to provide a uniform initial distribution of liquid propellant through the gas flow. This can be achieved by introducing thin liquid jets into the gas flow. Numerous versions of injectors of this type have been designed and fall into the three categories shown schematically in Fig. 26. Slit injectors with gas passages made in the form of concentric slots in the injector bottom represent a derivative of the preceding designs. The principle behind slit injectors and gas-liquid spray injectors is identical. As shown by practice, slit injectors having high permeability are less susceptible to high-frequency instability.

Keeping all of the other factors the same, injectors with external propellant mixing (see Fig. 26a) lead to lower combustion efficiency and therefore have
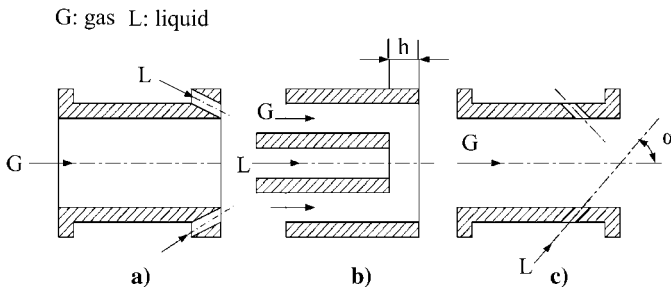

Fig. 26   Major designs of gas-liquid jet-jet injectors.

not found wide applications. Liquid propellant jets can be introduced into the gas flow over a range of injection angle of $\alpha = 0$ to 90 deg. The value of α influences the depth of liquid jet penetration into the gas flow, distribution of droplets, and eventually combustion efficiency. An injector in which the liquid-propellant jet is introduced along the gas-flow axis ($\alpha = 0$ deg) is referred to as coaxial (see Fig. 26b). Injectors of this type have been implemented in liquid oxygen/hydrogen engines, where liquid oxygen is fed through the central passage and gasified hydrogen is delivered through the circumferential passage. The gas-flow velocity should far exceed the liquid-jet velocity to achieve effective atomization. The recess distance between the central post and outer tube also plays an important role in determining the efficiency and stability of injector operation.

As a specific example illustrating the injector design, we consider the following injector geometry and operating conditions (the corresponding nomenclature is given in Fig. 27):

1) injector geometry (taken based on recommendations)

$$d_g = 20\,\text{mm} \quad d_l = 2.2\,\text{mm} \quad \delta = 4\,\text{mm}$$
$$\Delta l = 15\,\text{mm} \quad l_{\text{in}} = 12\,\text{mm} \quad l_i = 45\,\text{mm}$$
$$\alpha = 45\,\text{deg} \quad \beta = 30\,\text{deg} \quad t_i = 30\,\text{mm}$$

2) operating parameters (obtained from the engine design and preliminary analysis of mixture formation)

$$\dot{m}_{i,g} = 2.21\,\text{kg/s}; \dot{m}_{i,l} = 0.516\,\text{kg/s}; p_c = 150 \cdot 10^5\,\text{N/m}^2$$
$$(RT)_g = 180{,}000\,\text{J/kg}; \rho_l = 785\,\text{kg/m}^3$$

The objectives are

1) to construct the liquid jet trajectory in the injector passage;
2) to calculate the flow coefficients of the gas and liquid passages;
3) to evaluate the pressure drops of $\Delta p_{i,g}$ and $\Delta p_{i,l}$, and the pressures of p_g and p_l required to provide the prescribed gas and liquid mass flow rates through the injector.
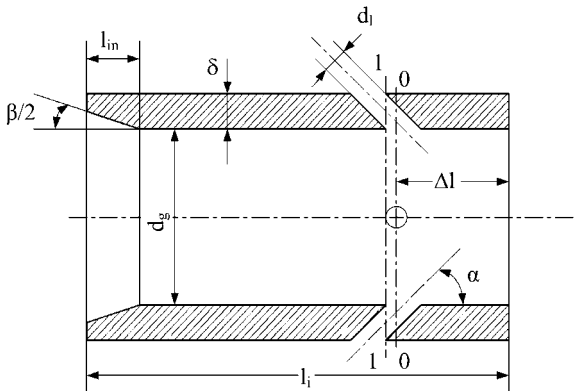

Fig. 27   Schematic diagram of gas-liquid injectors.

Liquid jet trajectory.   The analysis of the liquid trajectory in the gas flow is based on the results of experimental and theoretical studies of the jet shape in a cross flow. The gas flow in the passage tends to bend the injected liquid jet more severely as compared to the situation with an unbounded flow. The following expression is usually used for the external boundary of the jet:

$$\bar{x}_{ext} = 1.1\,\bar{y}^2 \rho_g U_g^2/\rho_l U_l^2 + \bar{y}\tan(90 - \alpha_j) \tag{34}$$

where $\bar{x}_{ext} = x_{ext}/d_l$ is the longitudinal coordinate of the external jet boundary reckoned from the 1-1 section, $\bar{y} = y/d_l$, the radial coordinate from the internal surface of the gas passage, and α_j the angle of the jet exhausted from the passage. If $\delta/d_l > 1.0$, the jet direction at the exit can be assumed to coincide with the passage direction, i.e., $\alpha_j = \alpha$. As expected, the momentum ratio of the gas to the liquid flow, $\rho_g U_g^2/\rho_l U_l^2$, and the injection angle α determine the jet trajectory.

Flow coefficient of gas passage.   A gas-liquid injector is usually designed using the results of cold-flow tests. The flow coefficient of the gas passage can be written in the following form:

$$\mu_g = \frac{1}{\sqrt{1 + \xi_{in}(1 - d_g^2/l_i^2) + \xi_{l,j}}} \tag{35}$$

where $\xi_{in}(1 - d_g^2/l_i^2)$ is the hydraulic-loss coefficient at the inlet to the gas passage (see Fig. 23). It depends on the ratio between the gas and liquid heads, the angle of the jet entering the flow, and the number and diameters of jets. Figure 28 plots $\xi_{l,j}$ vs $\rho_g U_g^2/\rho_l U_l^2$ and α for the case of four jets.
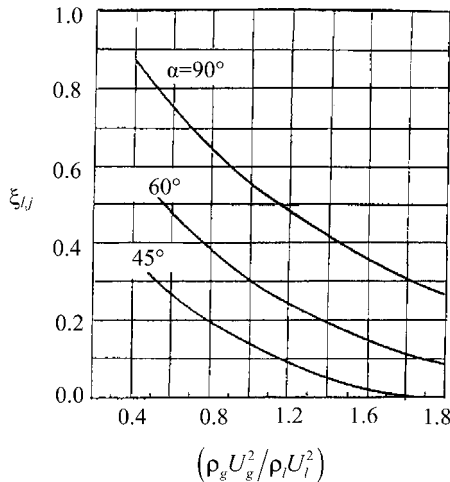

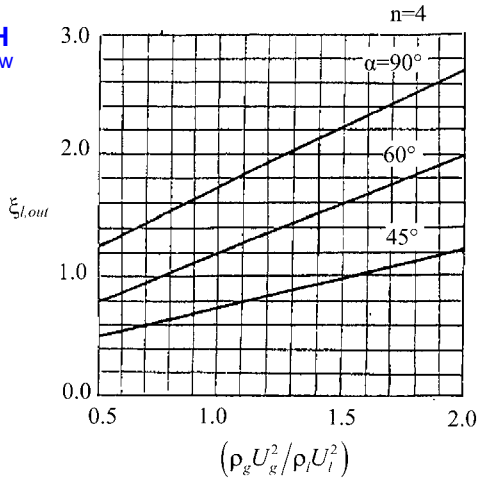Fig. 28   Effect of momentum ratio on μ_g for gas-liquid injectors.

Fig. 29   Effect of momentum ratio on μ_l for gas-liquid injectors.

Flow coefficient of liquid passage.   In calculating the flow coefficient for the liquid passage μ_l, an increase in the pressure loss due to tilted entry of the liquid into the cylindrical gas passage should be taken into consideration. Furthermore, μ_l is also influenced by the conditions outside the passage, which depend on the energy of the gas flow and the injection angle α. If we ignore these factors, μ_l becomes

$$\mu_l = \frac{1}{\sqrt{1 + \xi_{in} + \xi_{l.out}}} \tag{36}$$

The coefficient ξ_{in} represents the hydraulic loss at the inlet to the cylindrical tilting passage with sharp edges (see Fig. 25), and $\xi_{l.out}$ is the coefficient characterizing the additional losses when the tilted jet is introduced into the gas flow. Figure 29 shows the effects of the momentum ratio and injection angle on $\xi_{l.out}$, based on the data of cold-flow tests. In calculating μ_l, the length of the tilted passage is assumed to be greater than its diameter, i.e., $\delta > d_l$. If the gas injector wall is thinner, the effect of wall thickness on the flow coefficient should be taken into account.[17,19]

V.   Theory and Design of Liquid Monopropellant Swirl Injectors

Although the fundamentals of swirling flow dynamics were established more than 60 years ago by G. N. Abramovich[8] in 1944 and independently by Taylor[12] in 1947, the hydraulic characteristics of a liquid swirl injector remains a complicated problem since fluid properties and injector geometric parameters have pronounced and sometimes conflicting effects on injector characteristics. For example, the mass flow through a swirl injector increases with an increase in liquid viscosity, while the situation is reversed in jet injectors, despite the fact that the general trend of the two types of injectors is identical for ideal fluids.

Publications on the effect of injector geometric and operating parameters on spray characteristics often report contradictory results. Numerous and quite different empirical expressions[16] used to calculate the flow properties of swirl injectors do not allow evaluation of the effect of the primary parameters, and can only be applied to the specific configuration of concern or those similar to it.

A. Flow Characteristics of Ideal Swirl Injector

To gain a fundamental understanding of the flow development in a swirl injector and various underlying parameters, we first consider an ideal situation by ignoring the flow non-uniformity associated with the discrete tangential passages. Figure 30 shows a typical swirl injector consisting of a hollow casing (1), an axisymmetric vortex chamber (2), a nozzle (3), and tangential passages (4) connected upstream with the propellant feed system. Liquid propellant enters the vortex chamber at the velocity U_{in}, forms a circumferential swirling flow, exhausts at the axial velocity U_{an} through the nozzle, and finally establish a near-conic sheet in the mixture-formation zone. Ideally, the liquid sheet has the shape of a hyperboloid of revolution of one nappe. The spreading angle is determined by the ratio between the circumferential and axial components of the liquid velocity near the injector exit.

In such a swirl injector, the pressure all over the internal surface of the liquid vortex is equal to the pressure in the combustion chamber. The liquid potential energy in the form the pressure drop across the injector is fully converted to the kinetic energy. Thus, the liquid flow velocity on the surface becomes

$$U_{\Sigma} = \sqrt{\frac{2}{\rho}\Delta p_i} = \sqrt{U_u^2 + U_r^2 + U_a^2} \qquad (37)$$
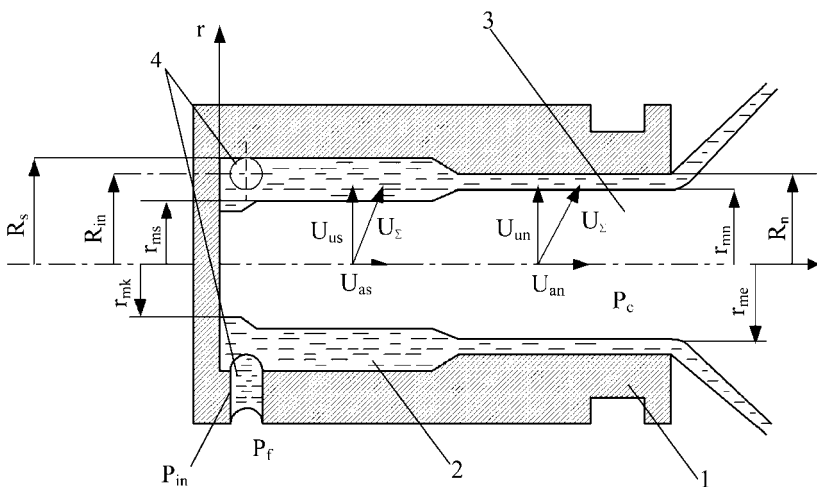

Fig. 30   Schematic diagram of liquid flow in swirl injector; 1-injector casing; 2-vortex chamber; 3-nozzle passage; 4-tangential passages.

On the injector wall $U_r = 0$, and

$$U_\Sigma = \sqrt{U_{us}^2 + U_{as}^2} = \sqrt{U_{un}^2 + U_{an}^2} = U_{uk} \tag{38}$$

The subscripts k, s, and n denote the conditions at the injector head end, vortex chamber, and nozzle, respectively. At the injector head end, $U_a = 0$. The circumferential component of the liquid velocity U_{uk} is maximum and the radius of the liquid-vortex surface, on the contrary, is minimum. In the vortex chamber, the axial velocity U_{as} is positive and the circumferential velocity U_{us} is smaller than U_{uk}, giving $r_{ms} > r_{mk}$. In the nozzle, the smaller liquid passage area leads to an increase of the axial velocity U_{an} and a decrease of U_{un}, giving $r_{mn} > r_{ms}$. Finally, at the nozzle exit, the centrifugal force arising from the swirling motion acts as a velocity head, leading to an additional increase of the axial velocity and subsequently an increase of the liquid-surface radius r_{me}. The swirling-liquid flow in the field of centrifugal force bears a resemblance to the liquid flow through a dam in the field of gravitational force of the Earth. According to N. E. Zhukovsky,[21] the longitudinal velocity along the dam cannot exceed the velocity of surface-wave propagation, much as the velocity of a gas flow in a pipe of constant cross section cannot exceed the sound velocity. The concept of a critical liquid flow in a swirl-injector nozzle results from the principle of maximum flow postulated by G. N. Abramovich[8] and later proved by L. A. Klyachko[2] in 1962. It serves as the basis of modern theories of swirl injectors. The whole theory of an ideal swirl injector is based on three principles, namely, Bernoulli's equation, conservation of mass energy, and conservation of angular momentum.

The swirl injector design involves 20 main parameters listed in Table 1. The variable r with subscript stands for the radius of the liquid film, and R with subscript the radial dimension of the injector.

All of these parameters can be related to each other through Bernoulli's equation and conservation of mass, energy, and angular momentum. The total velocity can be determined in terms of the pressure drop $(p_f - p_c)$ using Bernoulli's equation:

$$U_\Sigma = \sqrt{2(p_f - p_c)/\rho} \tag{39}$$

where p_f is the pressure in the propellant feed system for tangential channels and p_c the chamber pressure. The mass flow rate can be expressed in terms of the total velocity U_Σ and the nozzle area A_n as well as the mass flow coefficient:

$$\dot{m} = \mu A_n \sqrt{2\rho(p_f - p_c)} \tag{40}$$

The total velocity is the vectorial sum of its three components:

$$U_\Sigma = \sqrt{U_{un}^2 + U_{an}^2 + U_{rn}^2} \tag{41}$$

<div align="center">

Table 1   Parameters involved in swirl injector design

</div>

Parameter	Definition
$\dot{m}$	Mass flow rate
p_f	Pressure in propellant feed system
p_c	Combustion chamber pressure
p_{in}	Inlet pressure at tangential channel
α	Spray cone angle
μ	Mass flow coefficient
φ	Fractional area occupied by liquid in nozzle
h	Liquid film thickness
U_Σ	Total velocity
U_{un}	Swirl velocity in nozzle
U_{an}	Axial velocity in nozzle
U_{rn}	Radial velocity in nozzle
U_{uk}	Swirl velocity at head end of vortex chamber
U_{rk}	Radial velocity at head end of vortex chamber
U_{in}	Velocity at entrance of vortex chamber
r_{mk}	Radius of liquid film at head end of vortex chamber
r_{mn}	Radius of liquid film in nozzle
A_n	Area of nozzle
R_{in}	Radial location of center of tangential channel
A	Geometrical characteristic parameter

Application of Bernoulli's equation at the tangential entry gives

$$U_{in} = \sqrt{2(p_f - p_{in})/\rho} \tag{42}$$

where p_{in} is the tangential inlet pressure. It has been assumed in ideal injector theory that the radial of velocity in the liquid film is zero in the vortex chamber and nozzle:

$$U_{rk} = U_{rn} = 0 \tag{43}$$

According to the conservation of angular momentum, the azimuthal velocity satisfies the following relations:

$$U_{um}r_m = U_{uk}r_{mk} = U_{in}R_{in} = U_{rn}r_{mn} \tag{44}$$

Since U_a and U_r are zero at the liquid surface at the head end of the vortex chamber, the total velocity equals the circumferential velocity:

$$U_\Sigma = U_{uk} \tag{45}$$

Equation (44) implies that the swirl velocity becomes infinity as the radius approaches zero. Since the angular velocity cannot be infinite, a gas core must be present, and the liquid will not fully occupy the entire injector. We can thus define a parameter φ, known as the coefficient of passage fullness, that relates

the area filled by the liquid to the nozzle area:

$$\varphi = \frac{\pi(R_n^2 - r_{mn}^2)}{\pi R_n^2} = 1 - \frac{r_{mn}^2}{R_n^2} \tag{46}$$

where R_n is the radius of the nozzle and r_{mn} is the radius of liquid film in the nozzle. Similarly, a non-dimensional parameter μ, known as the mass flow coefficient, is defined that relates the actual flow rate to the maximum possible flow rate through the nozzle. The two parameters can also be related to each other.

$$\mu = \frac{\rho U_{an} A_n \varphi}{\rho U_\Sigma A_n} = \frac{U_{an} \varphi}{U_\Sigma}$$

where U_{an} is the axial velocity in the nozzle. Thus,

$$\mu = \varphi \sqrt{\frac{U_\Sigma^2 - U_{un}^2}{U_\Sigma^2}} = \varphi \sqrt{1 - \frac{r_{mk}^2}{r_{mn}^2}} \tag{47}$$

Various geometrical parameters can be correlated to form a non-dimensional geometrical characteristic parameter defined by

$$A = A_n R_{\text{in}}/A_{\text{in}} R_n \tag{48}$$

where R_n is the nozzle radius, R_{in} the radial location of the center of the inlet passage, and A_{in} is the total area of inlet passages. Finally, the spreading angle of the liquid sheet at the nozzle exit, α, can be expressed in terms of the velocity components:

$$\tan \alpha = U_{un}/U_{an} \tag{49}$$

Parameters such as $\dot{m}$, p_f, p_c, p_{in}, and α are design specifications that are chosen at the engine system design stage. Thus, there are in total 15 unknown parameters involved in the injector analysis. Since there are only 14 equations, Eqs. (39)–(49), an additional equation is required, which can be found using the principle of maximum flow or an alternative differential volume approach as shown next. Introducing $P_t = P_f - P_c$ for this derivation and equating the pressure and centrifugal forces on a liquid element of radius r with width dr, length $rd\Phi$, and unit thickness, we have

$$rd\Phi dP = dm \frac{U_u^2}{r} \tag{50}$$

where U_u is the circumferential velocity at radius r inside the liquid film, and $dm = \rho r dr d\Phi$. The conservation of angular momentum,

$$U_u = U_{um} r_m/r \tag{51}$$

leads to

$$dP = \rho U_{um}^2 r_m^2 \frac{dr}{r^3} \qquad (52)$$

where U_{um} is the circumferential velocity at the liquid film radius r_m. Integrating the preceding equation and applying $P = 0$ at $r = r_m$, we have

$$P = \frac{\rho}{2}(U_{um}^2 - U_u^2) \qquad (53)$$

From Bernoulli's equation,

$$\frac{\rho}{2}(U_a^2 + U_u^2) + P = P_t \qquad (54)$$

Substituting the value of P from Eq. (53) into Eq. (54), and rearranging the result, we have

$$U_a = \sqrt{\frac{2P_t}{\rho} - U_{um}^2} \qquad (55)$$

The conservation of angular momentum gives

$$U_{um} = \frac{U_{in} R_{in}}{r_m} \qquad (56)$$

The total volumetric flow rate can be expressed as the product of the inlet passage area and velocity U_{in}:

$$Q = n \pi r_{in}^2 U_{in} \qquad (57)$$

where n is the number of tangential inlet passages and r_{in} the radius of tangential inlet passage. Substituting the value U_{um} from Eq. (56) in Eq. (55) and replacing the value of U_{in} from Eq. (56), we obtain

$$U_a = \sqrt{\frac{2P_t}{\rho} - \frac{R_{in}^2 Q^2}{n^2 \pi^2 r_{in}^4 r_m^2}} \qquad (58)$$

The definition of the coefficient of passage fullness, φ, gives

$$Q = \varphi(\pi R_n^2 U_a) \qquad (59)$$

With the preceding three equations, we may eliminate U_a and substitute for the parameter A to obtain the following expression for the volumetric flow rate Q:

$$Q = \frac{1}{\sqrt{\dfrac{A^2}{1 - \varphi} + \dfrac{1}{\varphi^2}}} \pi R_n^2 \sqrt{\frac{2P_t}{\rho}} \qquad (60)$$

Since $\sqrt{2P_t/\rho}$ represents the total velocity, $\pi R_n^2\sqrt{2P_t/\rho}$ is the total volumetric flow rate possible through the nozzle. By substituting the definition of the flow coefficient μ, Eq. (60) can be rearranged as follows:

$$\mu = \frac{1}{\sqrt{\dfrac{A^2}{1-\varphi}+\dfrac{1}{\varphi^2}}} \tag{61}$$

The flow discharge coefficient depends on the injector geometric parameter A and the coefficient of passage fullness φ. If φ is decreased, then the decrease in the equivalent flow area is faster than the increase in the axial velocity, and so the mass flow rate decreases. Similarly, for an increase in φ, the decrease in the axial velocity is faster than the increase in the equivalent flow area, and so the mass flow rate decreases. Thus there exists an optimum maximum mass flow rate (or the discharge coefficient). Figure 31 shows the mass flow coefficient as a function of the φ for various values of the geometric characteristic A. A maximum value of μ for each value of A is observed, indicating the existence of the maximum flow rate for a given value of A. Application of the condition $d\mu/d\varphi = 0$ gives the optimum value of the discharge coefficient:

$$\mu = \varphi\sqrt{\frac{\varphi}{2-\varphi}} \tag{62}$$

Equation (62) is the final equation required to close the formulation for the injector analysis. The axial velocity in the cylindrical nozzle is

$$U_{an} = \frac{\mu}{\varphi}\sqrt{\frac{2}{\rho}(p_f - p_c)} \tag{63}$$
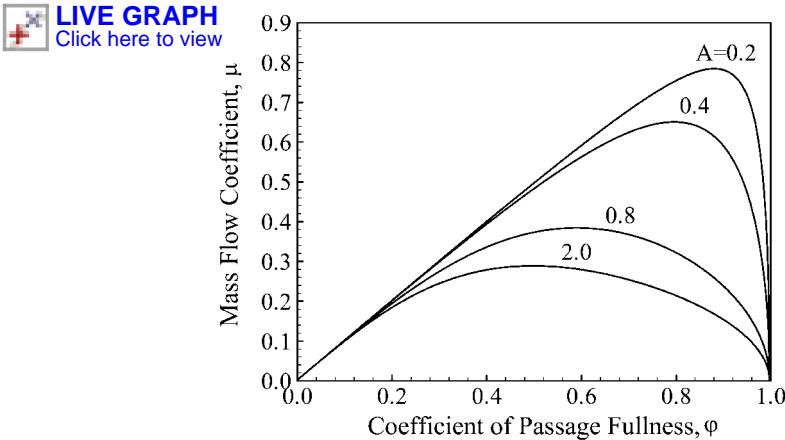
Fig. 31   Effect of coefficient of passage fullness on mass flow coefficient for various geometric characteristic parameters.

According to the flow continuity condition, the liquid mass flow rates in the nozzle and tangential passages are equated:

$$\mu A_n \sqrt{2\rho(p_f - p_c)} = \mu_t n \pi R_{\text{in}}^2 \sqrt{2\rho(p_f - p_{\text{in}})} \tag{64}$$

We now determine the azimuthal velocity U_{um} at some arbitrary point of the liquid vortex at the radius r_m. The conservation of angular momentum gives

$$U_{um} = \frac{R_{\text{in}}}{r_m} U_{\text{in}} = \frac{r_{mk}}{r_m} U_\Sigma = \frac{R_{\text{in}}}{r_m} \sqrt{\frac{2}{\rho}(p_f - p_{\text{in}})} \tag{65}$$

where U_Σ is the idealized total liquid velocity. Application of Bernoulli's theorem to the cylindrical part of the nozzle passage leads to

$$p_f = p_c + \frac{\rho}{2}(U_{un}^2 + U_{an}^2) \tag{66}$$

Substitution of Eqs. (63) and (65) into Eq. (66) gives

$$p_f - p_c = \frac{\mu^2}{\varphi^2}(p_f - p_c) + \frac{R_{\text{in}}^2}{r_{mn}^2}(p_f - p_{\text{in}}) \tag{67}$$

A simple manipulation yields

$$\frac{p_f - p_{\text{in}}}{p_f - p_c} = \frac{\Delta p_{\text{in}}}{\Delta p_i} = \frac{1 - \mu^2/\varphi^2}{(R_{\text{in}}/r_{mn})^2} \tag{68}$$

With the aid of the principle of maximum flow, $\mu = \sqrt{\varphi^3/(2 - \varphi)}$, and $r_{mn} = R_n\sqrt{1 - \varphi}$, Eq. (68) results in the ratio of the pressure drops across the tangential passage and the injector as a whole:

$$\frac{\Delta p_{\text{in}}}{\Delta p_i} = \frac{2(1 - \varphi)^2/(2 - \varphi)}{(R_{\text{in}}/R_n)^2} \tag{69}$$

The preceding equation is valid only for injectors having $R_{\text{in}}/R_n > 1$; otherwise, it may give a physically unrealistic solution with $\Delta p_{\text{in}}/\Delta p_i > 1$, which makes no sense. Indirectly, this means that for such injectors the principle of flow maximum does not hold.

We now normalize all of the radii with respect to R_n and all of the velocities with respect to U_Σ to express injector parameters in terms of three non-dimensional parameters φ, μ, and A. To simplify notation, all the non-dimensional quantities are expressed with a bar over them. Thus the radius of the liquid film at the head end of the vortex chamber becomes

$$\bar{r}_{mk} = \sqrt{2(1 - \varphi)^2/(2 - \varphi)} \equiv \sqrt{a}$$

This quantity will be hereinafter included in many expressions. It is convenient to use because of its sole dependence on the injector geometric characteristic parameter A. Figure 32 shows the effects of the geometric characteristic parameter, A on various commonly used injector parameters. The azimuthal velocities U_{un} and U_{ue} increase with A, whereas the axial velocities U_{an} and U_{ae} decrease with increasing A. The coefficient of passage fullness φ and the mass flow coefficient μ also show a decrease with an increase in A.

At the head of the vortex chamber, $U_a = 0$, and

$$\frac{\Delta p_{\text{in}}}{\Delta p_i} = \frac{U_{\text{in}}^2}{U_{uk}^2} = \left(\frac{r_{mk}}{R_{\text{in}}}\right)^2 = \frac{(r_{mk}/R_n)^2}{(R_{\text{in}}/R_n)^2} \tag{70}$$

With Eq. (70) in mind, the physical meaning of the parameter $a \equiv \bar{r}_{mk}^2$ is evident. The ratio of the liquid film radius at the head end to that in the nozzle becomes

$$\bar{r}_{mk}^2/\bar{r}_{mn}^2 = a/(1 - \varphi) = 2(1 - \varphi)/(2 - \varphi) \equiv b \tag{71}$$

Equations (70) and (71) are employed to derive the components of the steady-state velocity in the injector element. Applying the conservation of angular momentum, $\bar{U}_{un}\bar{r}_{mn} = \bar{U}_{\Sigma}\bar{r}_{mk}$, we obtain the circumferential velocity in the nozzle:

$$\bar{U}_{un} = \bar{r}_{mk}/\bar{r}_{mn} = \sqrt{2(1 - \varphi)/(2 - \varphi)} \tag{72}$$

The axial velocity in the nozzle becomes

$$\bar{U}_{an} = \sqrt{1 - \bar{U}_{un}^2} = \sqrt{1 - 2(1 - \varphi)/(2 - \varphi)} = \sqrt{\varphi/(2 - \varphi)} \tag{73}$$
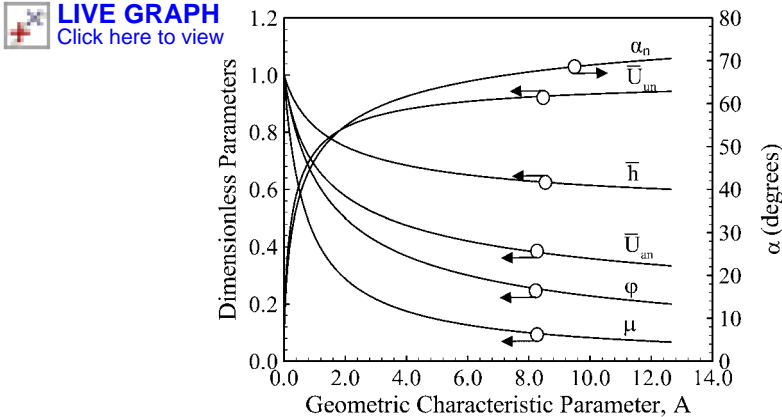

Fig. 32   Effects of geometric characteristic parameter A on other injector design and flow parameters.

Combining Eqs. (72) and (73) determines the spreading angle of the liquid sheet at the injector exit:

$$\alpha_n = \tan^{-1}(U_{un}/U_{an}) = \tan^{-1}(\bar{U}_{un}/\bar{U}_{an}) = \tan^{-1}\sqrt{2(1-\varphi)/\varphi} \qquad (74)$$

Owing to the effect of centrifugal force, the liquid surface radius at the nozzle exit r_{me} is larger than r_{mn}, and the circumferential velocity decreases as well.[2] According to Eq. (66), the circumferential velocity downstream of the nozzle exit is

$$\bar{U}_{ue} = r_{mk}/R_n = \sqrt{2(1-\varphi)^2/(2-\varphi)} = \sqrt{a} \qquad (75)$$

The axial velocity becomes

$$\bar{U}_{ae} = \sqrt{1-a} \qquad (76)$$

Combining Eqs. (75) and (76) gives the spreading angle of the liquid sheet downstream of the injector exit:

$$\alpha_e = \tan^{-1}\sqrt{a/(1-a)} \qquad (77)$$

It should be noted from Eq. (76) that the axial velocity at the nozzle exit,

$$U_{ae} = U_\Sigma\sqrt{1-a} = U_\Sigma\sqrt{(3-2\varphi)\varphi/(2-\varphi)} \qquad (78)$$

exceeds that in the nozzle section. The ratio of the two velocities depends solely on the coefficient of passage fullness φ:

$$\lambda_e = \bar{U}_{ae}/\bar{U}_{an} = \sqrt{(1-a)(2-\varphi)/\varphi} = \sqrt{3-2\varphi} \qquad (79)$$

In the limit of $\varphi \to 0$ (i.e., infinitesimally thin liquid film),

$$\bar{U}_{ae} = \sqrt{3}\,\bar{U}_{an} \qquad (80)$$

The liquid velocity exceeds the critical velocity at the nozzle exit. Hence, the nozzle throat is offset by some distance from the exit. The relation between r_{me} and injector parameters can be expressed by the following transcendental equation[2]:

$$\mu = \sqrt{1-\mu^2A^2} = \bar{r}_{me}\sqrt{\bar{r}_{me} - \mu^2A^2} - \mu^2A^2\ln\frac{1+\sqrt{1-\mu^2A^2}}{\bar{r}_{me} + \sqrt{\bar{r}_{me} - \mu^2A^2}} \qquad (81)$$

A more accurate evaluation of the liquid spreading angle α_e can be made by substituting r_{me} from Eq. (81) for a.

The velocity in the tangential passage, U_{in}, can be determined from Eq. (44):

$$\bar{U}_{in}\bar{R}_{in} = \bar{r}_{mk}$$

This implies

$$\bar{U}_{in} = \sqrt{a}/\bar{R}_{in} \tag{82}$$

We determine the velocity components on the liquid surface in the vortex chamber. In the root section of the vortex chamber, U_{am} is calculated from the condition of flow continuity:

$$\bar{U}_{am} = \bar{U}_{an}(\bar{R}_n^2 - \bar{r}_{mn}^2)/(\bar{R}_m^2 - \bar{r}_m^2) \tag{83}$$

Note that $\pi(\bar{R}_n^2 - \bar{r}_{mn}^2)$ is the flow area in the nozzle and $\pi(\bar{R}_m^2 - \bar{r}_m^2)$ is the flow area in the vortex chamber. Equation (83) can be written as

$$\bar{U}_{am} = \bar{U}_{an}\varphi/(\bar{R}_m^2 - \bar{r}_m^2) = \mu/(\bar{R}_m^2 - \bar{r}_m^2) \tag{84}$$

Applying the conservation of angular momentum, $U_m r_m = U_\Sigma r_{mk}$, and noting $U_{am}^2 + U_{um}^2 = U^2$ and Eq. (71), we obtain:

$$\bar{r}_m^2 = a/(1 - \bar{U}_{am}^2) \tag{85}$$

By substituting r_m from Eq. (85) into Eq. (84), U_{am} and r_m can be obtained by the successive approximation method.

B. Flow Characteristics of Real Swirl Injectors

The flow process in a real swirl injector can be described by taking into account viscous effects with the Navier-Stokes equations.[14] No analytical solutions are available for general cases, and the use of numerical calculations is inevitable.[26] In practice, the real conditions can be approximately taken into account by introducing the hydraulic loss coefficient, ξ_i, which characterizes the total-pressure loss in the injector, and the angular-momentum loss coefficient K:

$$p_f = p_c + \frac{\rho U_{un}^2}{2} + \frac{\rho U_{an}^2}{2} + \xi_i \frac{\rho U_{in}^2}{2}$$

Thus,

$$U_{an} = \sqrt{\frac{2}{\rho}\Delta p_i - \xi_i U_{in}^2 - U_{un}^2} \tag{86}$$

where $\Delta p_i = p_f - p_c$ is the pressure drop across the injector. The actual mass flow rate through the injector nozzle can be represented in the following form:

$$\dot{m}_i = \varphi\pi R_n^2 \rho U_{an} = \varphi\pi R_n^2 \sqrt{2\rho\Delta p_i - \xi_i \rho^2 U_{in}^2 - \rho^2 U_{un}^2} \tag{87}$$

where

$$U_{\text{in}} = \frac{\dot{m}_i}{n\pi r_{\text{in}}^2 \rho} \quad \text{and} \quad U_{un} = \frac{KR_{\text{in}}U_{\text{in}}}{r_{mn}}$$

where K represents the loss of angular momentum. Substitution of the definitions of the geometric parameter A and the coefficient of nozzle opening, $\bar{R}_{\text{in}} = R_{\text{in}}/R_n$, gives

$$U_{\text{in}} = \frac{\dot{m}_i A}{\pi R_n^2 \rho \bar{R}_{\text{in}}} \tag{88}$$

$$U_{un} = \frac{KR_{\text{in}}U_{\text{in}}}{R_n\sqrt{1-\varphi}} = \frac{KR_{\text{in}}\dot{m}_i}{R_n\sqrt{1-\varphi}\, n\pi r_{\text{in}}^2 \rho} = \frac{K\dot{m}_i}{\rho\pi R_n^2\sqrt{1-\varphi}}A \tag{89}$$

Substitution of Eqs. (88) and (89) into Eq. (87) and rearrangement of the result yields an explicit expression for the flow characteristic parameter A that accounts for viscous losses:

$$\dot{m}_i = \mu_i \pi R_n^2 \sqrt{2\rho\Delta p_i} \tag{90}$$

where the mass flow coefficient μ_i takes the form

$$\mu_i \equiv \frac{1}{\sqrt{\dfrac{1}{\varphi^2} + \dfrac{A^2 K^2}{1-\varphi} + \xi_i \dfrac{A^2}{\bar{R}_{\text{in}}^2}}} \tag{91}$$

As is evident, the flow coefficient depends on the flow area ratio, φ, combination of the geometric dimensions, A and R_{in}, hydraulic losses, ξ_i, and angular momentum losses, K. With the use of the principle of maximum flow,

$$AK = \frac{(1-\varphi)\sqrt{2}}{\varphi\sqrt{\varphi}} \tag{92}$$

we have

$$\mu = \frac{1}{\sqrt{\dfrac{2-\varphi}{\varphi^3} + \xi_i \dfrac{A^2}{R_{\text{in}}^2}}} \tag{93}$$

The spray-cone angle is determined from the ratio between the circumferential and total velocities in the nozzle exit section: $\sin\alpha = U_{un}/U_{\Sigma n}$. Application of Eqs. (88) and (90) gives

$$U_{un} = \frac{R_n}{r_{mn}}\mu_i AK \sqrt{\frac{2}{\rho}\Delta p_i} \tag{94}$$

and the total velocity becomes

$$U_{\Sigma n} = \sqrt{U_u^2 + U_a^2 + U_r^2 - \xi_i U_{in}^2} = \sqrt{1 - \xi_i \mu_i^2 \frac{A^2}{\bar{R}_{in}^2}} \sqrt{\frac{2}{\rho} \Delta p_i} \qquad (95)$$

Equations (94) and (95) lead to the following equation for the liquid-sheet spreading angle:

$$\sin \alpha = \frac{R_n}{r_{mn}} \mu_i A \frac{K}{\sqrt{1 - \xi_i \mu_i^2 \frac{A^2}{\bar{R}_{in}^2}}} \qquad (96)$$

Equation (96) suggests that the spreading angle is different for liquid particles located at various distances r from the axis ($\sin \alpha \sim 1/r$). In calculations, with some inaccuracy assumed, the spray cone angle α corresponding to the average radius is used:

$$r_{av} = \frac{R_n + r_{mn}}{2} = \frac{R_n}{2}\left(1 + \sqrt{1 - \varphi}\right) \qquad (97)$$

Thus,

$$\sin \alpha = \frac{2\mu_i A K}{(1 + \sqrt{1 - \varphi})\sqrt{1 - \xi_i \mu_i^2 \frac{A^2}{\bar{R}_{in}^2}}} \qquad (98)$$

For ideal liquid ($\xi_i = 0$ and $K = 1$), with the neglect of the radial component of the liquid velocity, the spray cone angle 2α and flow parameters μ and φ are determined by the injector geometric characteristics alone and can be calculated as a function of A.

C. Effect of Viscosity on Injector Operation

Propellant viscosity and the ensuing friction losses affect the injector characteristics in terms of μ, α, and φ. The momentum loss measured by the coefficient K is first considered. For simplicity, the hydraulic losses are neglected with $\xi_i = 0$. The injector performance can be conveniently evaluated by the equivalent-injector characteristic parameter A_{eq} from Eq. (92):

$$A_{eq} \equiv AK = \frac{(1 - \varphi_{eq})\sqrt{2}}{\varphi_{eq}\sqrt{\varphi_{eq}}}$$

Consequently,

$$\mu_{eq} = \frac{\varphi_{eq}\sqrt{\varphi_{eq}}}{\sqrt{2 - \varphi_{eq}}}; \quad \text{and} \quad \mu_i = \frac{\mu_{eq}}{\sqrt{1 + \xi_i \mu_{eq}^2 \frac{A^2}{\bar{R}_{in}^2}}} \qquad (99)$$
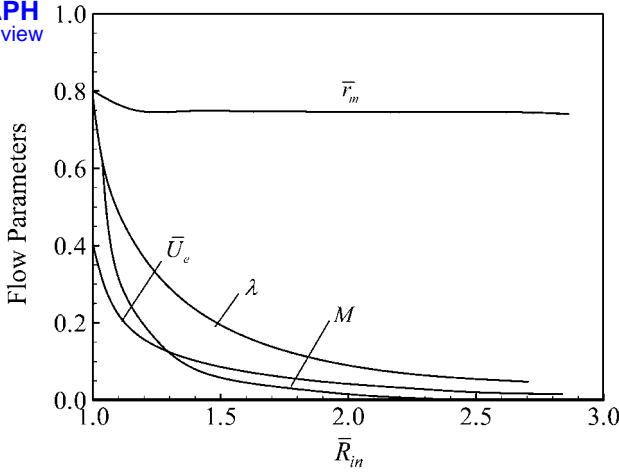
Fig. 33   Effect of nozzle opening on flow parameters of swirl-injector vortex chamber.

This method is convenient because the numerical relations obtained for an ideal injector and displayed graphically in Fig. 32 remain valid for the equivalent injector by replacing A with A_{eq}. Since $K < 1.0$ and $A_{eq} < A$ for the same injector under the effect of viscosity, it is evident from Fig. 33 that the momentum losses lead to increase of the mass flow (μ_{eq}) and passage fullness (φ_{eq}) coefficients and a decrease of the spray cone angle $2\alpha_{eq}$.

To evaluate A_{eq} for the suggested injector geometry ($A = R_{in}R_n/nr_{in}^2$) and to find real values of μ, α, and φ, the following expression can be used[23]:

$$A_{eq} = \frac{R_{in}R_n}{nr_{in}^2 + \dfrac{\lambda}{2}R_{in}(R_{in} - R_n)} \tag{100}$$

where

$$\lambda = 0.3164/(Re_{in})^{0.25} \quad \text{and} \quad Re_{in} = \frac{U_{in}r_{in}2\sqrt{n}}{\nu} = \frac{2\dot{m}_i}{\pi\sqrt{n}r_{in}\rho\nu} \tag{101}$$

Equation (100) characterizes the behavior of an open-type injector ($C = \bar{R}_{in} = 1.0$) with $R_{in} = R_n$, $A_{eq} \equiv A$. Unlike the momentum losses K, the total-pressure losses ξ_i decrease the flow coefficient. The main total-pressure losses occur in the inlet passages. For most designs, we can assume that

$$\xi_i = \xi_{in} + \lambda\frac{l_{in}}{d_{in}} \tag{102}$$

D.   Design Procedure

When designing an injector, the mass flow rate $\dot{m}_i$, pressure drop Δp_i, and propellant properties are usually known, and we need to evaluate the actual flow

coefficient μ_i and the injector dimensions. The problem is reduced to correlating the parameters in Eq. (99). The calculation proceeds as follows:

1) Prescribe the spray cone angle based on the injector operating conditions (usually between 90 and 120 deg, lower values may be used for special cases).[1] The geometric characteristic parameter A and the flow coefficient μ_i are then determined from the plots in Fig. 32.

2) Determine the nozzle radius using

$$R_n = 0.475 \sqrt{\frac{\dot{m}_i}{\mu \sqrt{\rho \Delta p_i}}} \tag{103}$$

3) Specify the number of inlet passages (usually between two and four) and the coefficient of injector opening, based on structural considerations. Then, the radius of the inlet passage is obtained:

$$r_{\text{in}} = \sqrt{\frac{R_{\text{in}} R_n}{nA}} \tag{104}$$

4) Revise the following injector parameters:
    a) length of the tangential passages, usually $l_{\text{in}} = (3-6)r_{\text{in}}$;
    b) nozzle length, $l_n = (0.5-2)R_n$, vortex-chamber length $(l_s > 2R_{\text{in}})$ and vortex chamber radius $(R_s = R_{\text{in}} + r_{\text{in}})$

5) Find the Reynolds number in the inlet passages using

$$Re_{\text{in}} = 0.637 \frac{\dot{m}_i}{\sqrt{n r_{\text{in}} \rho \nu}}$$

and the friction coefficient using $\lambda = 0.3164/(Re_{\text{in}})^{0.25}$.

6) Determine A_{eq} using Eq. (100), and find μ_{eq} and α_{eq} from the plots of Fig. 32.

7) Calculate the hydraulic-loss coefficient in the tangential passages using

$$\xi = \xi_{\text{in}} + \lambda \frac{l_{\text{in}}}{2 r_{\text{in}}}$$

The coefficient ξ_{in} is determined from the plots of Fig. 25 with allowance for the tilting angle of the tangential passage relative to the external surface of the vortex chamber, which can be calculated using the following formula:

$$\alpha = 90 \deg - \tan^{-1} \frac{R_s}{l_{\text{in}}} \tag{105}$$

8) Determine the actual flow coefficient μ_i using Eq. (99).

9) Calculate the nozzle radius using the new approximation

$$R_n = 0.475 \sqrt{\frac{\dot{m}_i}{\mu_i \sqrt{\rho \Delta p_i}}}$$

10) Calculate the geometric parameter A in the new approximation

$$A^{(1)} = \frac{R_{in}R_n^{(1)}}{nr_{in}^2}$$

11) Repeat steps 1–10 until the calculated injector parameters converge.

Another method of designing swirl injectors is also possible. It is based on the results of model experiments shown in Figs. 34 and 35. The advantage of this approach is its simplicity and adequate accuracy. The limited amount of experimental data is the major limitation. The design procedure is as follows:

1) Prescribe the spray cone angle and l_n/D_n from the plots in Fig. 34. Find the value of A, and then obtain $\mu_{exp} \equiv \mu_{in}$, using the plots in Fig. 34.
2) Calculate the nozzle radius using Eq. (103).
3) Prescribe the number of inlet passages and the coefficient of injector opening R_{in} based on structural considerations. Then, the radius of the inlet passage is obtained:

$$r_{in} = \sqrt{\frac{R_{in}R_n}{nA}}$$

4) Determine the Reynolds number Re_{in} in the inlet passages from Eq. (101), and use this result for design if $Re_{in} > 10^4$.
5) Determine the other injector parameters such as l_{in}, l_n, l_s, and R_s, find the relative liquid vortex radius $\bar{r}_m$ from the plots in Fig. 35, and then r_m from $r_m = \bar{r}_m R_n$.
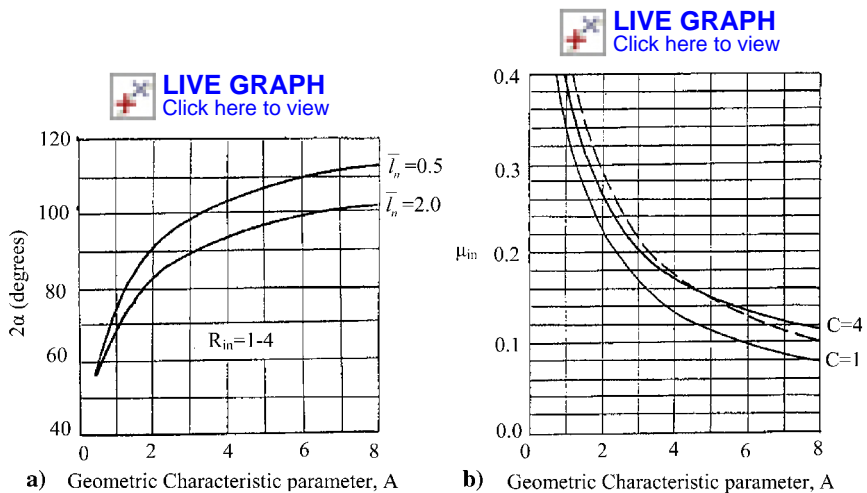

Fig. 34   Experimental plots of a) spray cone angle 2α and b) flow coefficient as functions of geometric parameter of swirl injector.
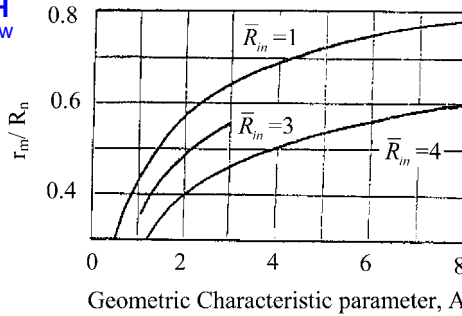
Fig. 35 **Experimental plot of relative liquid vortex radius in vortex chamber as function of geometric parameter of swirl injector.**

VI. Theory and Design of Liquid Bipropellant Swirl Injectors

In bipropellant injectors, the liquid-phase mixing occurs even before the liquid sheet starts disintegrating. Both designs with internal and external mixing have been implemented.

A. Injectors with External Mixing

Figure 36 shows three different configurations of injectors with external mixing. Two swirl injectors are structurally connected in such a way that the nozzle of stage 1 is located concentrically inside the nozzle of stage 2. The exit sections of both injectors are located at the same plane. Sometimes, to decrease the overall dimension of the injector, stage 2 or both stages are made completely open.

A basic design requirement for injectors with external mixing is that the spray-cone angle of stage 1 should be larger than its counterpart of stage 2, such that the fuel and oxidizer sheets intersect and mix outside the injector even before they start disintegrating into droplets. The injector designs can be further classified into two categories. If one of the nozzles is inside the other one, two injector designs are possible. In version 1, the nozzle of stage 1 is accommodated by the gas vortex of stage 2. Both injectors are hydraulically independent of each other and can be designed using the procedure described in Section II. In version 2, the nozzle of stage 1 is submerged in the liquid stream in stage 2. This design is usually associated with the quest for increased flow capacity of stage 1 without increasing the pressure drop Δp_i and decreasing the spray cone angle by increasing the nozzle dimension ($A_{n1} = \pi R_{n1}^2$). The operation of stage 2, in particular its flow coefficient μ_2, depends on the ratio $R = R_{n2}/R_1$ where R_{n2} is the radius of the nozzle of stage 2 and R_1 is the external radius of the nozzle of stage 1. Figures 37 and 38 show the theoretical results of the spray cone angle and flow coefficient of stage 2 as functions of $\Delta \bar{l}_n$ and A_2, respectively.

1. Design Procedure for Version 1

To initiate the injector design, the pressure drop Δp_i, mass flow rate $\dot{m}_i$, and propellant properties for each injector stage are prespecified. In addition, the following parameters are provided from structural considerations:
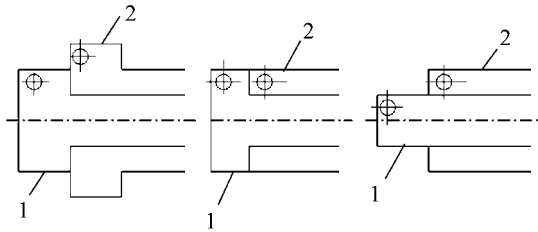
Fig. 36   Versions of bipropellant swirl injectors with external mixing.

1) $\bar{R}_{in1}$ and $\bar{R}_{in2}$ are the coefficients of nozzle opening;
2) $\bar{l}_{n1}$ and $\bar{l}_{n2}$ are the relative nozzle lengths $\bar{l}_n = l_n/2R_n$;
3) n_1 and n_2 are the number of inlet passages.

The design is based on the results of model experiments (see Section II) and is carried out in accordance with the following procedure:

1) Prescribe the spray cone angles $2\alpha_2$ and $2\alpha_1$, according to the empirical condition $2\alpha_1 - 2\alpha_2 = 10$ to 15 deg based on injector operating conditions. With these values and the correlation given in Fig. 34a, find the geometric characteristic parameters, A_1 and A_2. The flow coefficients of stages 1 and 2, μ_1 and μ_2, are then determined from Fig. 34b.
2) Calculate the nozzle radii R_{n1} and R_{n2} from Eq. (103), and determine the tangential-entry radii r_{in1} and r_{in2} from Eq. (104).
3) Determine the Reynolds numbers Re_{in1} and Re_{in2} using Eq. (101). The design is completed if $Re_{in} > 10^4$, and the injector dimensions and flow parameters are calculated.
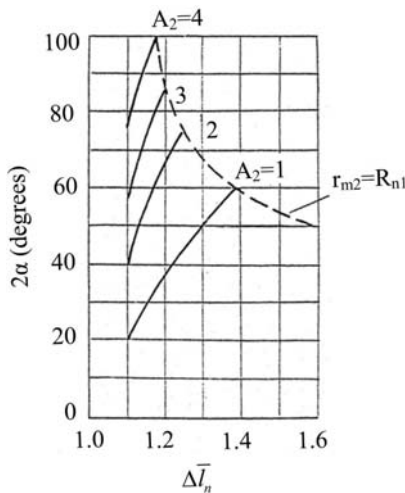

Fig. 37   Spray cone angle as function of relative radial spacing between nozzles in bipropellant swirl injectors.
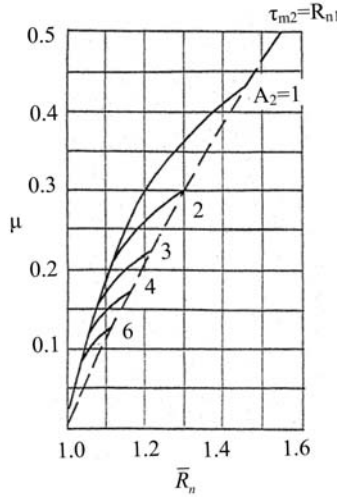
Fig. 38 Flow coefficient as function of relative radial spacing between nozzles in bipropellant swirl injectors.

There are cases that the initial requirements are not satisfied. For example, the nozzle of stage 1 is not accommodated inside the gas vortex of stage 2, a situation frequently observed when oxidizer is fed through stage 1. In this case, version 2 of the injector design should be chosen, with the nozzle of stage 1 submerged in the liquid stream in stage 2.

2. Calculation Procedure for Version 2

The initial injector requirements are the same as those in the previous version. With the spray cone angles $2\alpha_2$ and $2\alpha_1$ prescribed, the injector of stage 1 is designed following the same procedure for version 1. The calculation proceeds as follows:

1) Specify the thickness of the nozzle wall δ_w and determine the external radius of the nozzle of stage 1, $R_1 = R_{n1} + \delta_{w1}$.

2) Specify the spacing between the nozzles Δr (no less than 0.3 mm) and calculate the nozzle radius $R_{n2} = R_1 + \Delta r$ of stage 2.

3) Determine the geometric parameter A_2 from Fig. 37 and find μ_2 from Fig. 38.

4) Calculate the inlet-passage radius $r_{in2} = \sqrt{R_{in2}R_{n2}/n_2 A_2}$.

5) Determine the required pressure drop across stage 2 following the standard formula for the mass flow rate in terms of the injector pressure drop:

$$\Delta p_{i2}^{(1)} = 0.05 \frac{\dot{m}_{i2}^2}{\mu_2^2 \rho_2 R_{n2}^4} [N/m^2]$$

6) Repeat steps 1−5 using another R_1 until the calculated Δp_{i2} matches its prespecified value.

B. Injectors with Internal Mixing

Figure 39 shows three different versions of injectors with internal mixing. The inner injector (stage 1) is recessed from the exit of stage 2, to achieve stable and efficient mixing of propellants on the internal surface of the nozzle of stage 2. This part of the nozzle of stage 2 is referred to as the injector mixer, whose length can be varied to provide the desired propellant flow residence time in the mixer, τ_i. If τ_i is too long (e.g., 1.5–10 ms), burnouts and explosions may occur in injectors. Conversely, if τ_i is too short (e.g., less than 0.1 ms), poor mixing of the propellants may take place leading to degraded combustion efficiency. The optimal value of τ_i depends on propellant properties, injector flow rate, and several factors whose effects are still not clearly understood. Provisionally, $\tau_i = 0.1$ ms is recommended for hypergolic propellants, and $\tau_i = 0.2$ ms for non-hypergolic propellants with the total propellant flow rate $m_{i1} + m_{i2}$ in the range of 0.2–1.0 kg/s. The final τ_i value (and hence, the recess length Δl_n) is determined during the engine development.

The spray cone angle, when both stages operate simultaneously, depends on many factors. It is generally assumed that the total angle $2\alpha_2$ is 30–40 deg, smaller than the spray cone angle of an isolated stage 2 without the inclusion of stage 1. During the design of an injector, hydraulically independent operation of each stage should be provided, namely,

1) the gas-column radius of stage 2 should exceed the external radius of the nozzle of stage 1, with $r_{m2} - r_{m1} = 0.2$–0.3 mm;
2) the spray cone angle of stage 1 should be such that the propellant arrives at the mixer wall 2–3 mm downstream of the tangential entries of stage 2.

The preceding conditions prevent the ingress of propellant from one of the stages into the other.

To initiate the injector design, propellant properties, pressure drops, Δp_{i1} and Δp_{i2}, and mass flow rates, $\dot{m}_{i1}$ and $\dot{m}_{i2}$, for both stages should be prespecified as basic requirements. In addition, the following parameters should be given for each stage based on structural considerations:

1) $\bar{R}_{in1}$ and $\bar{R}_{in2}$: coefficients of nozzle opening; $\bar{R}_{in} = 3$ for closed stages and $\bar{R}_{in} = 0.7$–0.8 for open ones;
2) $\bar{l}_{n1}$ and $\bar{l}_{n2}$: relative nozzle lengths, $\bar{l}_{n1} = 1.0$;
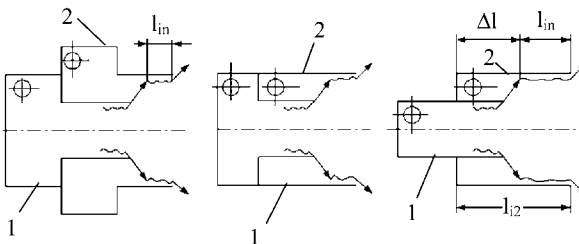3) n_1 and n_2: number of inlet passages (2–6);

Fig. 39   Versions of bipropellant swirl injectors with internal mixing.

4) $2\alpha_1$: spray cone angle of stage 1, 60–80 deg

The injector design proceeds in the following steps.

1. Design of Stage 1

1) From the experimental correlations given in Fig. 34, determine the non-dimensional parameter a, coefficient of passage fullness φ, geometric characteristic parameter A_1, and mass flow coefficient μ_1.

2) Calculate the nozzle radius R_{n1} from the relation

$$R_{n1} = 0.475\sqrt{\dot{m}_1/(\mu_1\sqrt{\rho_1\Delta p_{i1}})}$$

radius R_{in1} using $R_{in1} = \bar{R}_{in}R_{n1}$, and the radius of the inlet passages,

$$r_{in1} = \sqrt{R_{in1}R_{n1}/(n_1A_1)}$$

3) Determine the Reynolds number in the inlet passages from Eq. (101). If $Re > 10^4$, consider the design of stage 1 completed and calculate the other parameters of stage 1.

4) Calculate the length of the tangential passages using $l_{in1} = (3\text{–}4)\,r_{in1}$, the length of the nozzle using $l_{n1} = 2R_{n1}$, and the length of the vortex chamber using $l_{s1} = (2\text{–}3)\,R_{in1}$.

5) Calculate the external radius of the nozzle, $R_1 = R_{n1} + \delta_w$, where the nozzle wall thickness is $\delta_w = 0.2\text{–}0.8$ mm.

The relative vortex radius r_m is found from Fig. 35, and the vortex radius r_{m1} is calculated.

2. Design of Stage 2

1) Determine the permitted gas-vortex radius, $r_{m2} = R_1 + 0.3$ mm.

2) Assume $r_{m2} = R_{n2}$ to first approximation, and calculate μ using $\mu^{(I)} = 0.225\dot{m}_{i2}/(R_{n2})^2\sqrt{\rho_2\Delta p_{i2}}$, where the superscript (I) denotes the initially guessed value of the mass flow coefficient.

3) Determine A_2 from experimental correlations in Fig. 34, and then the relative vortex radius r_{m2} from Fig. 35.

4) Determine the nozzle radius $R_{n2}^{(II)} = r_{m2}/r_{m2}^{(1)}$ based on the known values of $r_{m2}^{(1)}$ and r_{m2}, and calculate $\mu_2^{(II)}$ using $\mu_2^{(II)} = 0.225\dot{m}_{i2}/(R_{n2}^{(II)})^2\sqrt{\rho_2\Delta p_{i2}}$ with the updated value of $R_{n2}^{(II)}$, where the superscript (II) denotes the iteration step. Repeat steps 3 and 4 until the calculated $R_{n2}^{(i)}$ converges, and update the values of A_2, R_{n2}, and r_{m2}.

5) Calculate R_{in2} with $R_{in2} = \bar{R}_{in2}R_{n2}$ and r_{in2} with $r_{in2} = \sqrt{R_{in2}R_{n2}/n_2A_2}$.

6) Determine Re_{in} from Eq. (101). If $Re_{in} > 10^4$, consider the design of stage 2 completed, and calculate the other parameters of stage 2. Determine the spray cone angle $2\alpha_2$ from Fig. 34 with stage 1 being idle and assume the total spray cone angle of the injector 2α to be $2\alpha_2 - 35$ deg. Using the prescribed value of $\tau_i = 0.1\text{–}0.2$ ms, calculate the length of propellant mixing using the
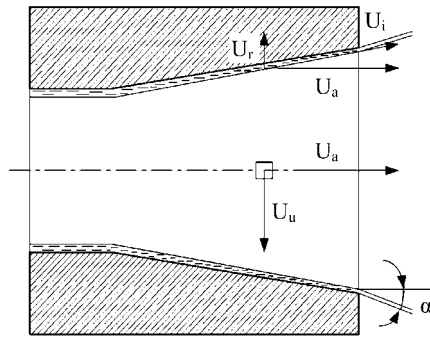
Fig. 40   Schematic diagram of liquid flow along swirl injector with divergent nozzle.

following equation:

$$l_{\text{mix}} = \sqrt{2}\tau_i \left(\frac{K_m \mu_2}{(K_m + 1)\varphi_2} \sqrt{\frac{\Delta p_{i2}}{\rho_2}} + \frac{\mu_1}{(K_m + 1)\varphi_1} \sqrt{\frac{\Delta p_{i1}}{\rho_1}} \right)$$

where K_m is the propellant ratio and φ_1 and φ_2 are the coefficients of stage passage fullness ($\varphi = 1 - \bar{r}_m^2$).

7) Calculate the nozzle length $l_{n2} = 2\bar{l}_{n2}R_{n2}$, compare it with l_{mix}, and finally obtain $l_{\text{mix}} + \Delta l_n = l_{n2}$. Determine the final values of τ_i and 2α during the experimental development.

VII.   Modulation of Liquid Spray Characteristics of Swirl Injectors

Theoretically, the spray of a swirl injector with an ideal liquid resembles a hyperboloid of revolution of one nappe. The spray cone angle is confined by the asymptotes of the hyperbolas bounding it and is determined solely by the geometric characteristic parameter A. For real injectors, as a result of viscous losses, the spray shape varies from a tulip-like to a near-conic configuration, depending on the pressure drop. In practice, there are often cases in which the spray cone angle needs to be changed without affecting the geometric parameter and mass flow of the injector. A notable example is the requirement for the spray of a coaxial bipropellant liquid injector to intersect in the mixture formation zone, especially when hypergolic propellants are used. Theoretically, it is impossible to vary the spray cone angle without changing A. Designers are thus forced to make the sheets intersect on the wall of the peripheral-injector nozzle, as described in Section VI. The potential disadvantages of such propellant mixing are:

1) nozzle erosion due to decreased distance between the combustion zone and the injector; and

2) ingress of one propellant into the vortex chamber of the other and ensuing explosions of the bipropellant mixture during engine restarts. The other important

requirement imposed on flow-controlled injectors is minimum changes in the spray cone angle with respect to variations of the geometric parameter.[1]

Methods of modulating the spray cone angle independently of the geometric parameter have been developed by Bazarov at the Moscow Aviation Institute. The techniques do not require any moving parts in injectors. According to classic theories of ideal swirl injectors,[2] the spray cone angle of an injector is unambiguously determined by its geometric characteristic A, which is related to the flow coefficient μ_i. However, as shown in Ref. 1, the flow coefficient μ_i and the spray cone angle can be changed independently. One can either act upon the liquid sheet in the injector nozzle once it has passed through the throat section where the liquid axial velocity U_a equals its surface wave velocity U_w, or use means leading to the violation of the principle of maximum flow.

Several methods may be used to control the spray cone angle independently of the liquid flow, as shown in Fig. 40. The simplest method is profiling of the post-throat section of a swirl injector nozzle. When the degree of nozzle opening increases, the circumferential velocity decreases, thereby leading to an increase in both the axial and radial components. The relationship between the liquid circumferential velocity and the nozzle radius is based on the conservation of angular momentum:

$$U_u r_i = U_\Sigma r_{mk} \qquad (106)$$

where r_i is the radius of the passage section of the injector nozzle; r_{mk} is the radial location of liquid film at the head end of the vortex chamber. The nozzle profile determines the ratio between the axial and radial velocities:

$$U_r/U_a = dr_i/dz \qquad (107)$$

where z is the coordinate along the nozzle length and dr_i/dz represents the slope at the nozzle.

According to gas-hydraulic analogy between the free-surface liquid flow and gas flow through a pipe proposed by N. E. Zhukovsky, liquid velocity is critical in the narrowest section and is equal to the velocity of disturbance (long waves) propagation over the surface. This conclusion refers not only to spillways, but also, as shown by L. A. Klyachko,[2] to other potential liquid flows with free-surface swirling motions in the field of gravitational forces in particular.

The inference about the impossibility of reaching a supercritical velocity,[2] however, does not hold for swirling liquid flows in the divergent part of the nozzle. It is reasonable to suggest that with the gas-hydraulic analogy proposed by N. E. Zhukovsky, the free-surface liquid flow may become supercritical in the divergent nozzle with its velocity exceeding the surface wave propagation speed.

Consider an ideal swirling liquid flow along an axisymmetric divergent nozzle (see Fig. 40). With all of the velocity components normalized by the total velocity of the liquid exhausted from the nozzle, U_Σ, and the geometric dimensions by R_n, Eqs. (41), (106), and (107) can be written in the dimensionless

form:

$$\bar{U}_a^2 + \bar{U}_u^2 + \bar{U}_r^2 = 1; \quad \bar{U}_u = \bar{r}_{mk}/\bar{r}_i; \quad \bar{U}_r/\bar{U}_a = d\bar{r}_i/d\bar{z} = q \tag{108}$$

where q is the tangent of the nozzle-profile angle in reference to the injector axis, and r_{mk} is the liquid-vortex radius at the head end of the vortex chamber. From the theory of ideal swirl injectors, the normalized circumferential velocity at the nozzle throat is

$$\bar{U}_{u,\text{th}} = \bar{r}_{mk} \tag{109}$$

where r_{mk} depends solely on the geometric characteristic parameter A and can be expressed in terms of the coefficient of passage fullness φ. With $r_i = f(z)$ available, the velocity components in each nozzle section can be calculated from Eq. (108), and hence the spray cone angle is obtained.

Substitution of $U_r = qU_a$ in Eq. (108), along with the use of Eq. (75) and the conservation of angular momentum, gives

$$\bar{U}_u^2 + \bar{U}_a^2 + q^2\bar{U}_a^2 = 1; \quad \bar{U}_a = \sqrt{(1 - a/\bar{r}_i^2)/(1 + q^2)} \tag{110}$$

The spray cone angle becomes

$$\tan \alpha = \sqrt{a(1 + q^2)/(\bar{r}_i^2 - a)} \tag{111}$$

The desired spray angle can thus be achieved by varying q. For a cylindrical nozzle exit $q = 0$ and

$$\tan \alpha = \sqrt{a/(\bar{r}_i^2 - a)} \tag{112}$$

For an axisymmetric divergent nozzle with $A = 2$, $a = 1/3$, $\bar{r}_i = 2$, and $\tan \alpha \approx 0.301$. The resultant spray cone angle becomes $\alpha = 16.7$ deg, which is 12 deg less than that for a cylindrical nozzle with $A = 2$.

The liquid velocity along the wall is

$$\bar{U}_L = \sqrt{\bar{U}_a^2 + \bar{U}_r^2} = \sqrt{1 - \bar{U}_u^2} \tag{113}$$

Substitution of $\bar{U}_u$ from Eq. (108) into Eq. (113) gives

$$\bar{U}_L = \sqrt{1 - a/\bar{r}_i^2} \tag{114}$$

The value of $\bar{U}_L$ in the divergent nozzle exit section ($\bar{r}_i > 1$) exceeds the velocity of wave propagation in the throat section given by $\bar{U}_w = \bar{U}_e = \sqrt{1 - a}$.

The ratio between the liquid velocity along the nozzle wall U_L and the velocity of wave propagation in the nozzle throat section U_{th}, Eq. (73), can be found in a

manner similar to that for gas flow, and is denoted as λ_i:

$$\lambda_i = U_L/U_{\text{th}} = \sqrt{(1 - a/\bar{r}_i^2)(2 - \varphi)/\varphi} \qquad (115)$$

Substitution of the a value in terms of φ, Eq. (75), for the cylindrical nozzle exit into Eq. (115) gives the expression for λ_i in the cylindrical nozzle with allowance for the Skobelkin effect described in Ref. 2:

$$\lambda_i = \sqrt{3 - 2\varphi} \qquad (116)$$

Since φ lies between zero and unity, λ_i is always greater than unity.

The liquid velocity U_L increases in the remaining length of the nozzle as r_i increases according to Eq. (115). As $r_i \to \infty$, $\lambda_{i.\,\text{max}} = \sqrt{(2 - \varphi)/\varphi}$. There exists a limiting λ_i value for each geometric characteristic parameter A that can be achieved by the liquid.

The coefficient of passage fullness at the exit of a profiled nozzle, $\varphi_{i.\text{exit}}$, can be determined as follows. Application of conservation of mass gives

$$\mu_i A_{\text{th}} U_\Sigma = \varphi_{i.\text{exit}} A_i U_a \qquad (117)$$

Substitution of U_a from Eq. (110) to Eq. (117) yields

$$\varphi_{i.\text{exit}} = \frac{\varphi\sqrt{\varphi}\sqrt{1 + q^2}}{\sqrt{2 - \varphi}\,\bar{A}_i\sqrt{1 - a/\bar{r}_i^2}}$$

For a cylindrical nozzle ($q = 0$ and $\bar{A}_i = 1$), the coefficient of passage fullness is obtained by considering for the Skobelkin effect:

$$\varphi_{i.\text{exit}} = \frac{\varphi\sqrt{\varphi}}{\sqrt{2 - \varphi}\sqrt{1 - 2(1 - \varphi)^2/(2 - \varphi)}} = \frac{\varphi}{\sqrt{3 - 2\varphi}} \qquad (118)$$

The liquid-vortex radius r_v in the profiled nozzle is readily calculated

$$\pi\varphi_{i,\text{exit}} r_i^2 = \pi(r_i^2 - r_v^2) \qquad (119)$$

and

$$\bar{r}_v = \bar{r}_i\sqrt{1 - \varphi_{i,\text{exit}}} \qquad (120)$$

where φ_i is the coefficient of passage fullness of the injector. Since $r_i - r_v = h$, with h being the liquid-layer thickness, we have

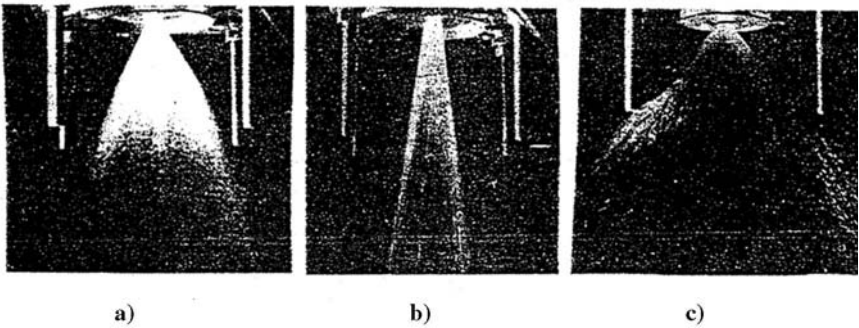$$\bar{h} = 1 - \sqrt{1 - \varphi_i} \qquad (121)$$

a)   b)   c)

Fig. 41 Liquid spray cone of swirl injector with $R_s = 7$ **mm,** $r_{in} = 1$ **mm,** $n = 2$**:
a) cylindrical nozzle with** $d_i = 2$ **mm; b) divergent nozzle with** $d_{i.th} = 2$ **mm and**
$d_{i.exit} = 6$ **mm; c) cylindrical nozzle with** $d_i = 6$ **mm.**

Equation (111) shows that a profiled divergent extension of a nozzle whose length is of the order of its diameter is an effective means to provide spray intersection in coaxial bipropellant injectors. Figure 41 shows photographs of swirl-injector sprays for various nozzle configurations. The divergent nozzle extension decreases the spray cone angle and the range of its variations. It does not ensure a constant spray cone angle. Furthermore, such a divergence piece increases frictional losses at the wall and, consequently, leads to deterioration of atomization quality.

A decrease in the flow velocity by increasing the injector area A_i causes a simultaneous decrease in the spray cone angle. On the other hand, a decrease in the flow velocity by increasing μ_i increases the spray cone angle. Thus, the spray cone angle can be fixed within a prescribed narrow region by approximately adjusting these two factors. Figure 42 schematically shows the liquid flow along a combined dual-orifice injector with its spray cone angle varied using a hydrolock. When fed to the chamber (3) through passages (5) and (6) and to the nozzle (2) from the manifold through the slot (11), the liquid is swirled and flows out from the nozzle edge as a hollow near-conic spray (12). The liquid flow running out through the slot is bent by the main swirling flow and forms a liquid bulkhead (13) in the nozzle, through which the main swirling flow exhausts in a manner similar to a profiled nozzle. With the throttle valve (10) open, the flow passage in the nozzle (2) is reduced, thereby decreasing the main liquid flow and the spray cone angle. With the throttle valve (8) closed, the flow decreases and the spray cone angle increases. Modulating the flow areas of throttle valves (8) and (10) makes it possible to vary either the spray cone angle or the flow rate, without affecting the other parameters. The previously described method of maintaining the prespecified spray cone angle can also be used in combination with a bypass injector. To do this, passage (6) is connected to the throttle valve (8) in line (4) and the liquid from the vortex chamber is throttled.

The passage area of the nozzle can be changed using other methods. For dual-orifice injectors, application of partition cowlings with nozzles between the
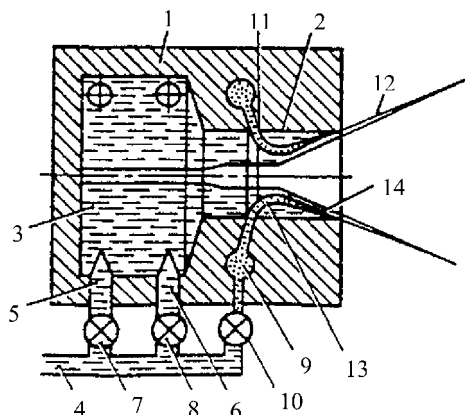
Fig. 42   Liquid flows in combined dual-orifice injector with its spray cone angle varied using a hydrolock; 1-casing; 2-nozzle; 3-vortex chamber; 4-feed line; 5, 6 tangential passages; 7, 8, 10 throttles; 9-ring collector; 11-ring slot; 12-liquid spray; 13-liquid bulkhead; 14-liquid film.

high- and low-flow parts of the vortex chamber is very effective. If the internal-nozzle diameter is smaller than the external-nozzle diameter, liquid exhaust from such an injector is close to that along a divergent extension piece. The possibility of controlling the spray cone angle by compressing the liquid flow in the area between the vortex chamber and the nozzle of the swirl injector is also considered. The classic theory of swirl injectors neglects the radial velocity component in the vortex chamber. However, as shown by A. M. Prakhov,[3] the presence of the radial velocity component in the area between the vortex chamber and nozzle is responsible for the failure of the principle of maximum flow, since the axial velocity in the nozzle is higher than the velocity of disturbance propagation along the liquid surface. In other words, a "supercritical" liquid flow appears with a corresponding decrease of the sheet thickness in the nozzle. The conditions of "supercritical flow" migrate downstream from the vortex chamber to the nozzle.

Both the axial and the radial velocity components in the transition area between the vortex chamber and the nozzle can be increased by introducing a central body whose diameter is larger than the diameter of the liquid-vortex free surface into the nozzle, or by means of axial contraction between the vortex chamber and nozzle. Although the former measure is undesirable because of increased losses in the kinetic energy of the liquid flow, it is often unavoidable in practice due to structural considerations in the case of coaxial arrangement of multiple-orifice injectors. On the other hand, axial contraction does not cause any increase in losses and is applicable to swirl injectors of any type.

Consider the liquid flow under the condition of axial contraction. Part of the pressure is consumed in the annular radial slot connecting the vortex chamber with the passages. The resultant decrease in the liquid flow velocity reduces the circumferential velocity of the liquid sheet velocity in the nozzle and the spray cone angle. By changing the cross-sectional areas of the tangential inlet

passages and the width of the radial slot, the prescribed value of the flow coefficient μ_i and a spray cone angle smaller than the one based on the principle of maximum flow can be obtained.

This contraction decreases the liquid velocity in the tangential passages and can be expressed as $U_{in}^* = \zeta U_{in0}$. In this case, r_{mk} decreases by a factor of ζ according to the conservation of angular momentum:

$$r_{mk}^* = \zeta r_{mk} \tag{122}$$

Physically, this decrease of r_{mk} is caused by the presence of the radial velocity U_r in the annular slot and can be determined from the conservation of energy,

$$\Delta p/\rho + U_r^2/2 + U_u^2/2 = \text{const} \tag{123}$$

and the mass continuity equation,

$$2\pi r l U_r = U_{in} A_{in} \tag{124}$$

The spray cone angle for ideal liquid is determined from the formula[14]

$$\alpha = 2 \tan^{-1} \sqrt{\bar{r}_{mk}^*/(1 - \bar{r}_{mk}^*)} \tag{125}$$

Substitution of r_{mk}^* from Eq. (122) into Eq. (125) gives

$$\alpha^* = 2 \tan^{-1} \sqrt{\zeta \bar{r}_{mk}/(1 - \zeta \bar{r}_{mk})} \tag{126}$$

Figure 43 shows schematically an experimental injector, and Fig. 44 presents the experimental data of the spray cone angle as a function of the slot widths h_1 and h_2. The flow testing results agree well with the calculations. Axial contraction is an effective method of modulating the spray cone angle without changing the injector geometric characteristic parameter A. The decrease in the flow rate due to the velocity drop in the inlet passages U_{in} can be compensated by increasing the passage flow area. Such a measure decreases the geometric characteristic parameter A, and thus provides an additional decrease of the spray cone angle because not only ζ but also $\bar{r}_{mk} = (1 - \varphi)\sqrt{2}/\sqrt{2 - \varphi}$ decrease in this case.
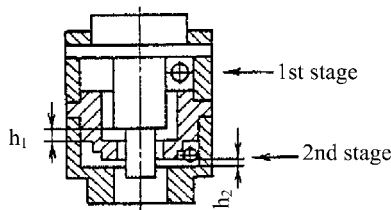

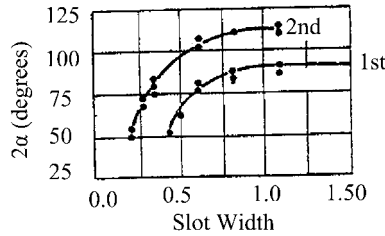**Fig. 43**   **Experimental swirl injector with axial contraction between vortex chamber and nozzle.**

Fig. 44 Effect of slot width on spray cone angle for an experimental swirl injector with axial contraction.

The spray cone angle of the injector with axial contraction can be determined from the formula

$$\tan^2 \alpha = \frac{1}{(1 + 1/\tan^2 \alpha_0)(1 + 1/\zeta^2) - 1} \tag{127}$$

where α_0 is the spray cone angle without flow contraction.

Figure 2 shows a bipropellant swirl injector [A.C. 792023 (USSR)] with an annular slot made in its peripheral region between the vortex chamber and the nozzle, to provide guaranteed intersection between sprays 1 and 2. This design is especially attractive when peripheral fuel delivery is used, and the sprays can hardly be intersected in space using conventional methods due to the lower propellant flows and greater geometric characteristic parameter of the peripheral injector. As discussed in earlier sections, to provide contact for hypergolic ignition, the central nozzle should be deepened into the peripheral one for propellants to mix at the edge of the external nozzle. Such a design leads to propellant ingress to the pre-injector cavity of the other propellant, and causes explosions when the engine start cyclogram is disrupted.

To reduce the effect of flow compression by either decreasing the flow rate or increasing the injector geometric characteristic parameter is a disadvantage of the preceding method of modulating the spray cone angle as applied to LREs. Therefore, spray flow compression in multimode injectors with fixed elements is applied only to provide intersection of sprays in a prescribed range of modes. In the process of thrust control, such injectors have a wider range of spray cone angle variations than conventional ones. For swirl injectors with moving elements, especially with moving screw conveyers, the radial clearance can be changed simultaneously with the tangential passages area, and thus, to achieve constant spray cone angle.

Consider the effect of liquid swirl U_u/U_a in the vortex chamber on the spray cone angle. According to the conservation of momentum, a change in U_u leads to a change in U_u/U_a. This can be achieved, for example, by turning the injection flow passage to the extent that the liquid swirl ceases completely and the swirl injector becomes a jet one. Consequently not only the spray cone angle is decreased but also the flow rate is increased in accordance with the change in the nozzle flow coefficient. In this design, with the spray cone angle controlled, the flow rate can be maintained fixed by correspondingly decreasing the inlet passage section area.[1]
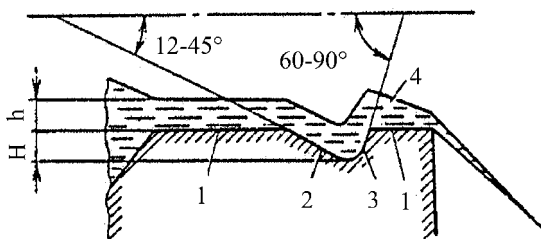
Fig. 45   Profiled nozzle of swirl injector with jump in liquid level.

Stabilization of the spray cone angle can be achieved by using dual-orifice injectors for each propellant. As for the flow rate and spray cone angle, each injector should operate independently and be designed to fulfill the prescribed requirements. In the transition mode, the spray cone angle remains unchanged and the atomization quality is ensured by intersecting the external throttled spray with the central spray operating under excess pressure drop. Stabilization of the spray cone angle can also be obtained by varying the degree of swirling through the use of low flow rate swirling passages with smaller swirling radii.

Consider the possibility of stabilizing the spray cone angle by introducing a liquid jump in the nozzle. Following the gas-hydraulic analogy of N. E. Zhukovsky,[21] we obtain a liquid flow with a jump of the liquid level in a swirl injector similar to the compression jump in a supersonic gas flow. As shown schematically in Fig. 45, a supercritical liquid flow should first be achieved by making a divergent section (2) in the nozzle (1) and a subsequent contraction (3). The liquid travels along the nozzle and forms a standing annular wave (4) whose radius is no less than r_{mk}. Because of flow anisotropy in the jump, the circumferential velocity component does not reach U_{uk}. During subsequent decrease of the liquid level and the flow exhaust from the nozzle to the mixing zone, the spray cone angle of a swirl injector with a profiled groove in the nozzle becomes smaller than its theoretical counterpart for the case without a jump. The effect of the groove decreases with the decreasing ratio between its depth H and the liquid sheet thickness h, and completely disappears with $H/h < 0.3$. This allows the use of a liquid jump in the nozzle to stabilize the spray cone angle of a swirl injector with variable flow coefficient μ_i and coefficient of passage fullness φ. In the mode of maximum flow, a groove with depth $H < 0.3h$ exerts little influence on the spray. As μ_i and φ decrease, the liquid sheet thickness h decreases, and the effect of groove on the spray increases. The increase of the spray cone angle associated with the decrease of μ_i is partially or completely counterbalanced.

VIII.   Design of Gas Swirl Injectors

A.   Design Procedure

A gas injector, shown schematically in Fig. 46, can be designed by determining its basic dimensions D_n, d_{in}, R_{in}, and n, on which the prescribed flow and spray properties are dependent. The design proceeds in the following steps:
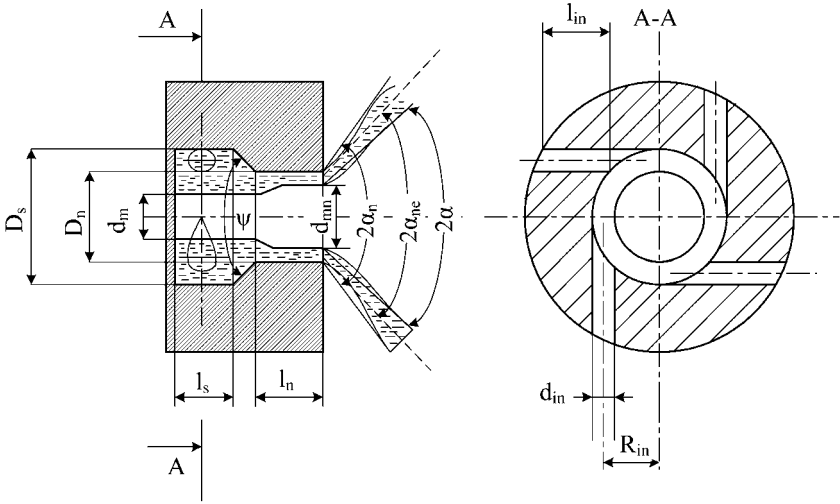
Fig. 46   Schematic diagram of gas swirl injector.

1) Choose the nozzle expansion ratio π_i, the geometric characteristic parameter A, and the degree of nozzle opening $\bar{R}_{in}$ to accommodate the specific features of the injector under consideration.

2) Determine the flow coefficient μ from Fig. 47. For intermediate $\bar{R}_{in}$ values in the range between 0.2 and 1, μ is calculated from the following formula:
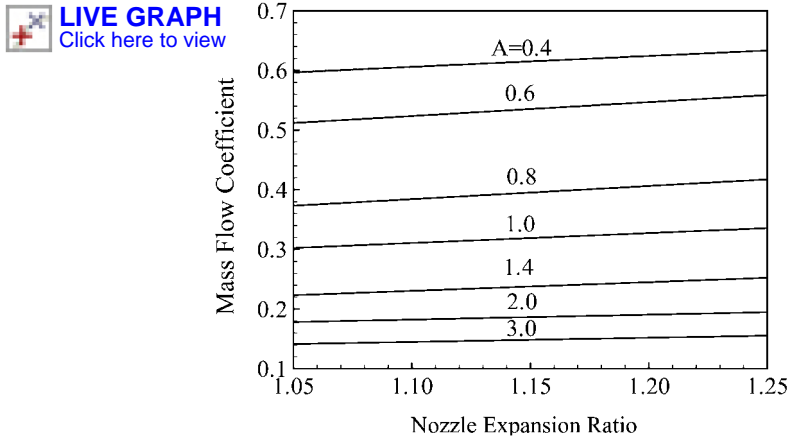
$$\mu = \mu_{ref}\bar{\mu} \qquad (128)$$

Fig. 47   Flow coefficient μ_{ref} vs A and nozzle expansion ratio π_i for $\bar{R}_{in} = 0.75$ of gas swirl injector.
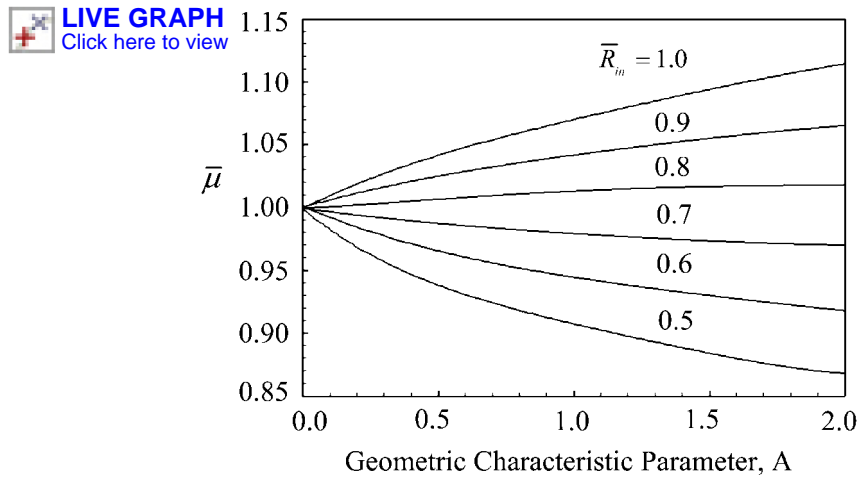
Fig. 48   Correction of flow coefficient based on the degree of nozzle opening.

where μ_{ref} is the initial flow coefficient for $\bar{R}_{\text{in}} = 0.75$ and $\bar{\mu}$ is a correction for the nozzle opening determined from Fig. 48. While making calculations, one must meet the following conditions under which the experimental data given by Figs. 47 and 48 were obtained: $Re_{\text{in}} > 3000$; $\bar{l}_{\text{in}} = 1–1.2$; $\bar{l}_n = 0.2–1$ and $\bar{l}_s = 0.2–0.3$.

3) Calculate the Reynolds number for the inlet passages Re_{in} using

$$Re_{\text{in}} = 1413 \frac{\mu d_n p_2 \varphi}{\mu_d \sqrt{RT_1}} \sqrt{\frac{A}{R_{\text{in}}}} \qquad (129)$$

where μ_d is the dynamic viscosity of the gas, $Pa \cdot s$.

4) Calculate the nozzle diameter in mm using

$$d_n = 0.948 \sqrt{\frac{\dot{m}\sqrt{RT_1}}{\mu p_2 \varphi}} \qquad (130)$$

where T_1 is the gas temperature at the inlet to the injector, K; p_2 is the gas pressure downstream of the injector, MPa; R is the gas constant, J/kg K; $\dot{m}$ is the mass flowrate through the injector, kg/s; and φ is calculated from the formula:

$$\varphi = \pi_\iota \sqrt{\frac{\aleph}{\aleph - 1}\left(\frac{1}{\pi_i^{\frac{2}{\aleph}}} - \frac{1}{\pi_i^{\frac{\aleph+1}{\aleph}}}\right)} \qquad (131)$$

where $\aleph$ is the polytropic exponent of gas expansion.

5) Calculate the gas flow rate $\dot{m}$ using the prescribed nozzle diameter,

$$\dot{m} = 1.11 \frac{d_n^2 \mu p_2 \varphi}{\sqrt{RT_1}} \tag{132}$$

6) Calculate the total gas velocity at the nozzle exit, U_Σ, in m/s using

$$U_\Sigma = 1.413 \frac{\mu \varphi \sqrt{RT_1}}{\left(1 - \bar{d}_m^2\right) \pi_i^{\frac{\aleph-1}{\aleph}} \cos \alpha_{\text{exit}}} \tag{133}$$

Calculate the axial velocity component using

$$U_a = U_\Sigma \cos \alpha_{\text{exit}} \tag{134}$$

and the tangential component using

$$U_u = U_\Sigma \sin \alpha_{\text{exit}} \tag{135}$$

7) Calculate the inlet passage diameter d_{in} in mm using

$$d_{\text{in}} = d_n \frac{R_{\text{in}}}{A n_{\text{in}}} \tag{136}$$

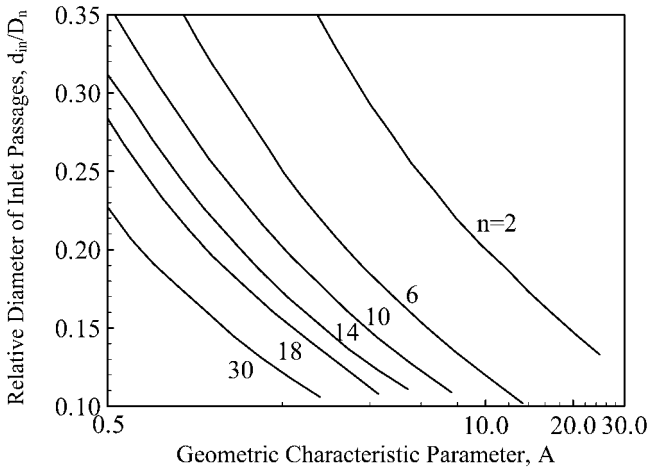Determine the inlet passage diameter for a fully open injector using Fig. 49.

Fig. 49 **Relative diameter of inlet passage d_{in}/D_n vs A and n for fully open injector $(D_s = D_n)$.**

8) Calculate the inlet radius R_{in} and the vortex-chamber diameter D_s using the following formulae:

$$R_{in} = \bar{R}_{in} \frac{D_n}{2} \qquad (137)$$

$$D_s = 2R_{in} + d_{in} \qquad (138)$$

B. Selection of Geometric Dimensions and Flow Parameters

This section summarizes the common practice used in the design of gas injectors in Russia:

1) The relative length of the inlet passages $\bar{l}_{in}$ is chosen between 1.0 and 1.5.
2) The relative length of the vortex chamber $\bar{l}_s = l_s/D_s$ is chosen between 0.1 and 0.3. If $\bar{l}_s$ is greater than 0.3, μ is calculated from the formula

$$\mu = \mu_1 + b\mu_2 \qquad (139)$$

where μ_1 can be found from Figs. 47 and 48 for prescribed values of A, $\bar{R}_{in}$ and π_i and μ_2 for $\pi_i = 1.05$. The parameter b is determined form the empirical formula

$$b = 0.0225A(\bar{R}_{in} - 0.3)(\bar{l}_s - 0.3) \qquad (140)$$

The formula is applicable for $A \le 3$, $\bar{R}_i \le 4$, and $\bar{l}_s \le 4$.
3) The number of inlet passages n is chosen based on the condition that the required coefficient of gas-distribution non-uniformity K is obtained from Figs. 50 and 51.
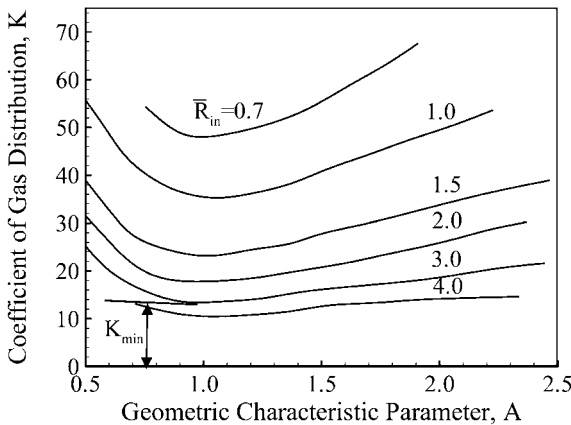4) The convergence angle at the nozzle entrance Ψ is chosen between 90 and 120 deg.

Fig. 50   Effect of geometric characteristic parameter A on coefficient of gas-distribution non-uniformity in mixing layer for different $\bar{R}_{in}$ ($n = 4$).
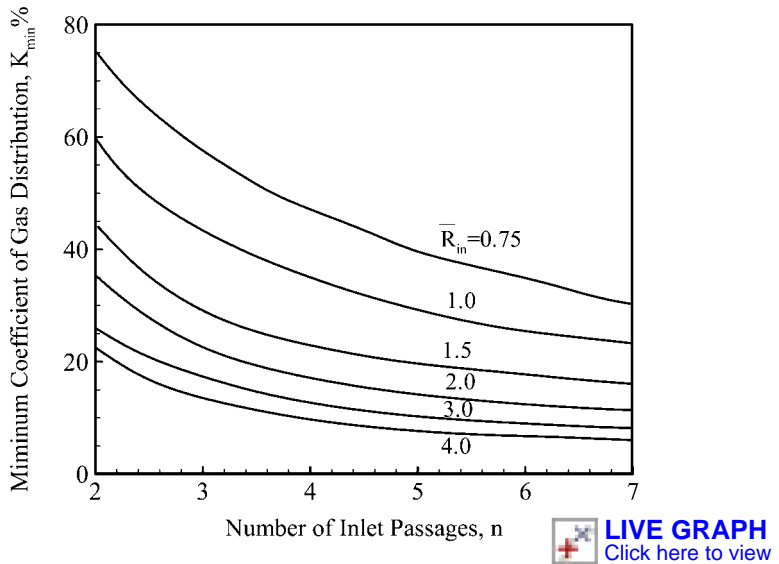
Fig. 51   Effect of number of inlet passages on minimum coefficient of gas-distribution non-uniformity in mixing layer.

5) With the relative nozzle length $\bar{l}_n$ between 1 and 10, the gas flow coefficient μ remains constant.

6) The tolerances for the basic dimensions are chosen according to the manufacturing specifications. The error for the injector flow coefficient should be less than 10% for $D_n < 10$ mm and 16% for $D_n > 10$ mm. The final geometric dimensions are determined in accordance with the results of injector flow tests.

7) The surface roughness should be $Rz < 40$ μm for the inlet passages, $Rz < 20$ μm for the vortex chamber, and $Rz < 2.2$ μm for the cylindrical and end surfaces of the nozzle. No burrs are permitted at the nozzle edge and in the inlet passages. The radius of the blunting chamber is 0.05–0.2 mm.

IX.   Dynamics of Liquid Rocket Injectors

A liquid rocket engine, as shown schematically in Fig. 52, contains various sources of intense pressure fluctuations caused by turbulent flows in the feed line, fluttering of pump wheel blades, vibrations of control valves, and unsteady motions in the combustion chamber and gas generator. As a consequence, the actual process of mixture formation in injector elements typically occurs in the presence of highly developed fluctuations, as the feedback coupling (loop 1 in Fig. 53) affects the processes occurring in the combustion chamber and forms a self-oscillating circuit.[23,27] All conceivable mechanisms of intrachamber instability are included here. Additionally, the chamber pressure fluctuation P'_c directly affects the liquid stage of the injector, L, forming another feedback
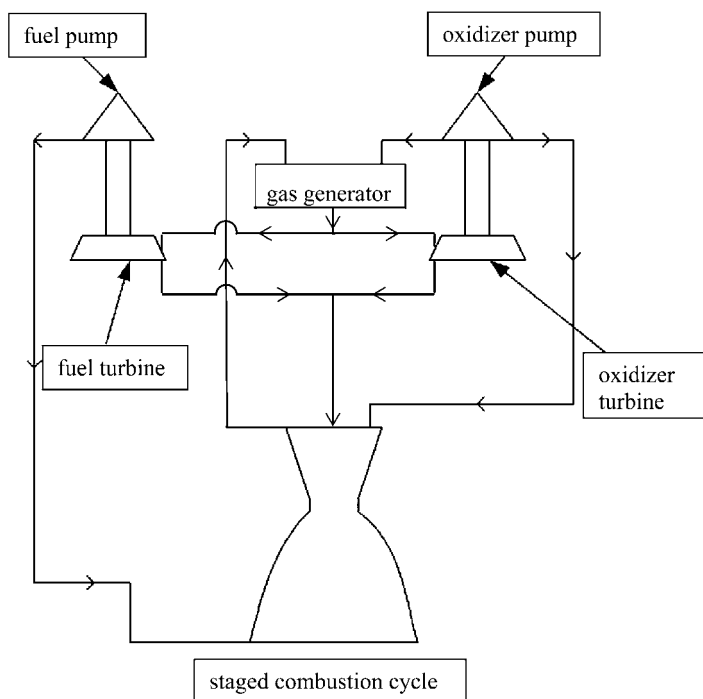
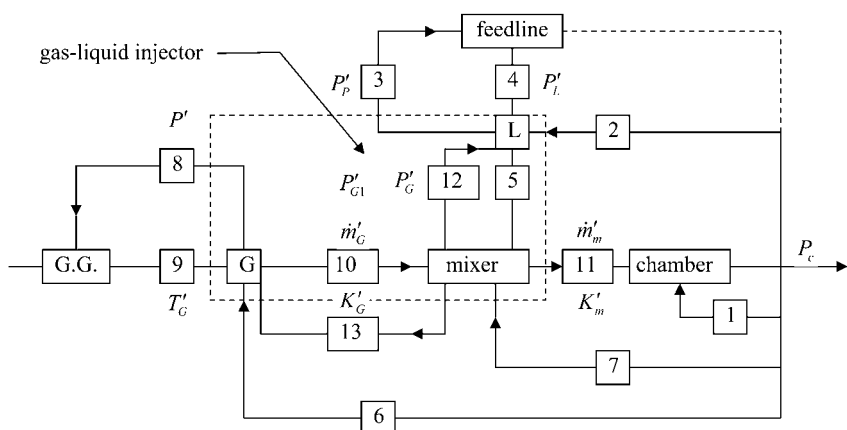Fig. 52   Schematic diagram of liquid rocket engine with staged combustion.

Fig. 53   Interactions of dynamic processes in liquid rocket engine with staged combustion.

coupling (loop 2). Acting as an oscillator in the feed system with the feedback coupling 3, the injector excites pressure fluctuations P'_L which then affect the injector response through the direct coupling 4. The ensuing fluctuation in pressure drop across the liquid injector, P'_L, causes liquid-flow fluctuations $\dot{m}'_L$ in the nozzle exit. In parallel, the chamber pressure fluctuations P'_c affect the gas stage of the injector, G, by means of the feedback coupling 6, and consequently, the gas generator (G.G.) through the feedback coupling 8. For a gas-liquid injector with internal mixing, the pressure fluctuations P'_c affect the mixer through the feedback coupling 7, and consequently, the liquid (12) and gas (13) stages of the injectors. The gas generator responds to the disturbances of the flow rate $\dot{m}'_G$, temperature T'_G, composition K'_G, exhaust velocity U'_G, and pressure P'_G of the generator gas which, when passing through the mixer, results in fluctuations of droplet mass and size distributions of the combustible mixture spray. The feedback couplings 12 and 13 can form their own self-oscillating circuits, causing fluctuations in the propellant flow at the injector exit as well as changes in the main mixture-formation parameters, including the atomized droplet-size distribution, spray angle, and uniformity of mixture composition.[14]

In LRE systems, injection is a key process since through it all feedback couplings of the combustion chamber with other engine components are realized. In addition to its main function of preparing a combustible mixture, an injector acts as a sensitive element that may generate and modify flow oscillations.[24] This section summarizes various important aspects of injector dynamics. The mechanisms of driving self-pulsations in both liquid and gas-liquid injectors are addressed systematically.

A. Linear Dynamics of Jet Injectors

For a short injector whose length is much less than the wavelength of oscillation, the equation of motion for inviscid liquid takes the form

$$\frac{d\tilde{U}}{dt} + \frac{\tilde{U}^2}{2L_i} = \frac{\tilde{P}_f - \tilde{P}_c}{\rho L_i} \equiv \frac{\Delta \tilde{P}}{\rho L_i} \tag{141}$$

where $\sim$ stands for the instantaneous quantity and L_i for the injector length. Each flow property may be decomposed into mean and fluctuating parts:

$$\Delta \tilde{P} = \Delta P + \Delta P' \quad \text{and} \quad \tilde{U} = U + U' \tag{142}$$

For time-harmonic oscillations,

$$\Delta P' = |\Delta P'| e^{i\omega t} \quad \text{and} \quad U' = |U'| e^{i\omega t} \tag{143}$$

Substitute Eq. (142) into Eq. (141) and linearize the result to get

$$\frac{dU'}{dt} + \frac{U}{L_i} U' = \frac{|\Delta P'|}{\rho L_i} e^{i\omega t} \tag{144}$$

The solution to the preceding equation is

$$U' = \frac{\Delta P'}{\rho U + i\omega\rho L_i} \tag{145}$$

A transfer function relating the fluctuating velocity U' and pressure drop $\Delta P'$ is obtained as follows:

$$\Pi_j = \frac{U'/U}{\Delta P'/\Delta P} \equiv \frac{\bar{U}'_j}{\Delta\bar{P}'_j} = \frac{1}{2}\cdot\frac{1 - i\omega L_i/U}{1 + (\omega L_i/U)^2} = \frac{1}{2}\cdot\frac{1 - iSh_j}{1 + Sh_j^2} \tag{146}$$

where the overbar denotes a dimensionless quantity. The Strouhal number of the jet injector, Sh_j, is defined as $Sh_j \equiv \omega L_i/U$.

Figure 54 shows the amplitude-phase diagram of the transfer function Π_j for a short jet injector. The normalized pressure-drop fluctuation $\Delta\bar{P}'_j$ is taken to be unity, and the phase angle between $\bar{U}'_j$ and $\Delta\bar{P}'_j$ is Φ_j. The locus is obtained by increasing the Strouhal number (or oscillation frequency) in Eq. (146). For practical injector dimensions and oscillation frequencies commonly observed in LREs, a jet injector can be considered as a single inertial element in which the amplitude of flow oscillation U' decreases smoothly as the Strouhal number increases, and the phase angle Φ_j increases asymptotically to $\pi/2$. The transfer functions Π_j for step-shaped and other shapes of jet passages can be calculated as a synthesis of several passages connected in series. In the case of long liquid injectors and coaxial gas-liquid injectors, resonance at multiple frequencies may occur when the injector length becomes comparable to the wavelength of the fluctuation. The influence of injector length should be taken into account
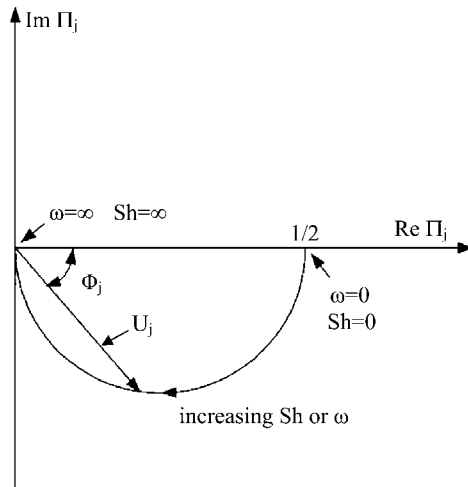

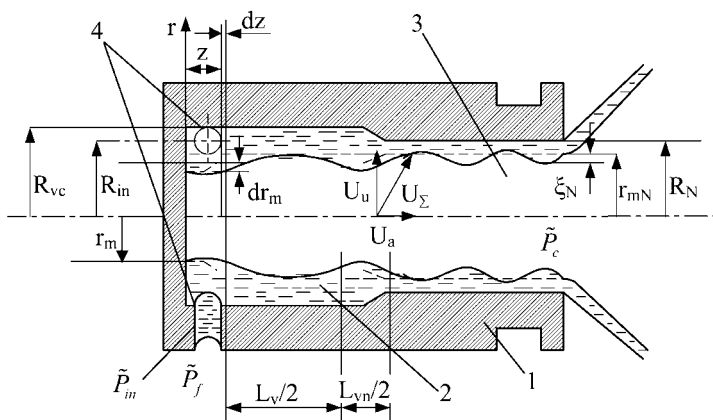Fig. 54   Amplitude-phase diagram of response function of a short jet injector.

Fig. 55   Schematic of liquid swirl injector; 1-casing; 2-vortex chamber; 3-nozzle; 4-tangential passage.

for cryogenic liquids since the sound speed is relatively low due to the existence of gas bubbles.

B.   Linear Dynamics of Swirl Injectors

Figure 55 shows schematically a swirl injector with liquid flow. The liquid is fed to the injector through tangential passages (station 4), and forms a liquid layer in the vortex chamber (station 2) with a free internal surface shown by the dashed line for the stationary case. The liquid is exhausted from the nozzle (station 3) in the form of a thin, near-conical sheet that then breaks up into fine droplets. Compared with a jet injector of the same flow rate, the flow passage of a swirl injector is much larger, and as such any manufacturing inaccuracy exerts a much weaker effect on its atomization characteristics. The resultant droplets are finer and have higher uniformity, thereby motivating the predominant application of swirl injectors in Russian LREs. From the dynamics standpoint, a swirl injector is a much more complicated element than a jet injector. The liquid residence time is longer than that of a jet injector; its axial velocity component U_a is smaller for the same pressure drop, and the speed of disturbance propagation is lower due to the existence of a central gas-filled cavity in the liquid vortex. A swirl injector contains an inertial element (i.e., tangential passage), an energy capacitor (i.e., vortex chamber partially filled with rotating fluid), and a transport element (i.e., nozzle). Each of these elements can be described with rather simple relationships.

The unsteady behavior of the tangential passage can be determined following the same analysis as that for a jet injector, Eq. (146). The dynamics of the liquid layer inside the vortex chamber and the nozzle can be modeled by means of a wave equation that takes into account the disturbance propagation in the liquid with centrifugal force. If we ignore the liquid-layer thickness and radial velocity,

and follow the approach given in Ref. 2, a wave equation characterizing the flow oscillation in the liquid layer is obtained:

$$\frac{\partial^2 \xi}{\partial t^2} = \frac{1}{r_m^4} U_{in}^2 R_{in}^2 \left(\frac{R_{vc}^2 - r_m^2}{2}\right) \frac{\partial^2 \xi}{\partial z^2} \tag{147}$$

Here ξ denotes the fluctuation of the liquid-layer thickness, and r_m the radius of the liquid surface. The surface-wave propagation speed U_w is

$$U_w = \sqrt{\left(\frac{U_{in}^2 R_{in}^2}{r_m^3}\right)\left(\frac{R_{vc}^2 - r_m^2}{2 r_m}\right)} = \frac{U_{in} R_{in}}{r_m^2} \sqrt{\frac{R_{vc}^2 - r_m^2}{2}} \tag{148}$$

The first parenthesized term in the square root represents the centrifugal acceleration, and the second parenthesized term the effective thickness of the liquid layer. The expression for the wave speed is analogous to that for shallow-water wave propagation. The solution to Eq. (147) for a semi-infinite vortex is

$$\xi = \Omega e^{i\omega(t - z/U_w)} \tag{149}$$

where Ω represents the amplitude of the liquid surface wave. For an axisymmetric rotating flow with a free interior surface, linearization of the equations of motion leads to a relationship between the fluctuations of the liquid surface and axial velocity:

$$\frac{\partial U_a'}{\partial t} = \frac{U_{in}^2 R_{in}^2}{r_m^3} \frac{\partial \xi}{\partial z} \tag{150}$$

The amplitude of the axial velocity fluctuation U_a' is

$$|U_a'| = \Omega U_{in}^2 R_{in}^2 / (U_w r_m^3) \tag{151}$$

In a non-dimensional form, the liquid surface-wave velocity inside the vortex chamber can be determined from Eq. (148):

$$(\bar{U}_w)_{vc} \equiv \frac{U_{w,vc}}{U_\Sigma} = \sqrt{\frac{1}{2}\left(\frac{\bar{R}_{vc}^2}{a} - 1\right)} \tag{152}$$

Here U_Σ is the liquid velocity at the head end of the vortex chamber. The non-dimensional parameters a and $\bar{R}_{vc}$ are defined respectively as

$$a \equiv \left(\frac{r_{mk}}{R_n}\right)^2 = A^2 \mu^2; \quad \bar{R}_{vc} \equiv \frac{R_{vc}}{R_n} \tag{153}$$

The subscript k denotes the head end of the vortex chamber, and A is the geometric characteristic parameter.

In accordance with the principle of maximum flow,[2] the axial velocity of the liquid flow inside the injector nozzle is the same as the surface wave speed, analogous to the gas flow in a choked nozzle. Thus,

$$(\bar{U}_w)_n = (\bar{U}_a)_n \equiv \frac{U_{an}}{U_\Sigma} = \sqrt{\frac{\varphi}{2 - \varphi}} \qquad (154)$$

where $\varphi \equiv A_L/A_n$ is the coefficient of passage fullness, representing the ratio of the cross-sectional area occupied by the liquid to that of the entire nozzle.

As the wave propagation speed varies in the injector, the unsteady liquid flow rate also changes with the flow. To quantify the dynamic characteristics of the vortex chamber subject to flow disturbances, a reflection coefficient of the surface wave at the nozzle entrance (or the exit of the vortex chamber), β, is defined according to the fluctuation of the liquid flow rate. A simple analysis based on mass conservation leads to the following relation between the flow-rate oscillations in the vortex chamber and the nozzle:

$$\frac{Q'_n}{Q'_{vc}} = \frac{U_{wn}}{U_{w,vc}} \cdot \frac{\Omega_n}{\Omega_{vc}} \cdot \frac{r_{mn}}{r_{m,vc}} \qquad (155)$$

After some straightforward manipulations, a reflection coefficient β characterizing the nozzle dynamics is obtained:

$$\beta = \frac{Q'_{vc} - Q'_n}{Q'_{vc}} = 1 - \frac{2\sqrt{\varphi}}{\sqrt{\bar{R}_{vc}^2 - a}} \qquad (156)$$

The amplitude of the surface wave in an infinitely long vortex chamber (i.e., no wave reflection) is

$$\bar{\Omega}_\infty \equiv \frac{\Omega_\infty}{r_{mk}} = \frac{1}{A\sqrt{2\left(\bar{R}_{in}^2 - a\right)}} \frac{U'_{in}}{U_{in}} \qquad (157)$$

For a vortex chamber with zero length, the surface-wave amplitude can be determined by the acoustic conductivity of its nozzle:

$$\bar{\Omega}_o = \frac{\bar{\Omega}_\infty \sqrt{\bar{R}_{in}^2 - a}}{2\sqrt{\varphi}} = \frac{\varphi \bar{R}_{in}}{4\sqrt{1 - \varphi}} \frac{U'_{in}}{U_{in}} \qquad (158)$$

which is much greater than $\bar{\Omega}_\infty$. For an intermediate case, the surface-wave amplitude depends on the reflection coefficients at the head end and the exit of the vortex chamber, as well as on liquid viscosity. The surface wave causes
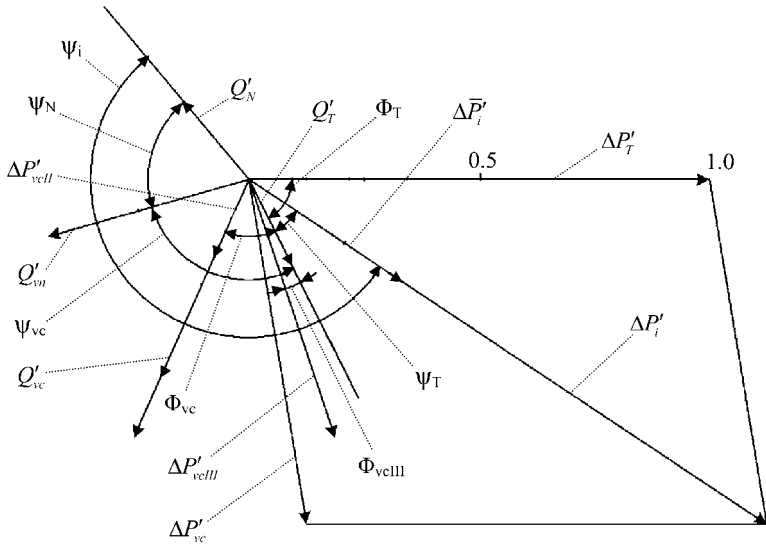
Fig. 56 Amplitude-phase diagram of response function of a swirl injector.

pulsations of the circumferential velocity U'_u in the radial direction according to the conservation of angular momentum ($U_u r = $ const) and consequently gives rise to pulsations of centrifugal pressure. The non-dimensional amplitude of centrifugal-pressure pulsations $\Delta \bar{P}'_{vc}$ (defined as the pressure difference between the tangential entry and the liquid free surface) caused by surface wave motions is not high and is equal to the non-dimensional amplitude of surface waves in the swirl chamber.

The main difference between a swirl and a jet injector as a dynamic element lies in the different mechanisms of disturbance propagation between the combustion chamber and the feed system. For conventional injector dimensions that are significantly smaller than disturbance wavelengths in the gas and liquid, pressure oscillations arising in the combustion chamber propagate through the liquid vortex layer almost instantaneously. This results in fluctuations of pressure drop across the tangential entries, $\Delta P'_T$, as shown in the amplitude-phase diagram in Fig. 56, where $\Delta P'_T$ is set to unity on the abscissa. Similar to a jet injector, these fluctuations lead to oscillations of the liquid flow rate, Q'_T, which subsequently produce surface waves in the vortex chamber propagating back and forth. Their amplitudes and phase angles ψ_{vcII} with respect to the pressure oscillations depend on the resonance properties of the liquid vortex in the injector, and can be determined by the reflection coefficients based on Eq. (156). When disturbances occur, part of these waves pass through the injector nozzle and cause fluctuations of the flow rate Q'_N and spray angle at the exit. Concurrently, the fluctuation Q'_T gives rise to oscillations of the circumferential velocity U'_u in the vortex chamber that propagate with the liquid flow and produce centrifugal-pressure fluctuations $\Delta P'_{vcIII}$ on the vortex chamber wall.
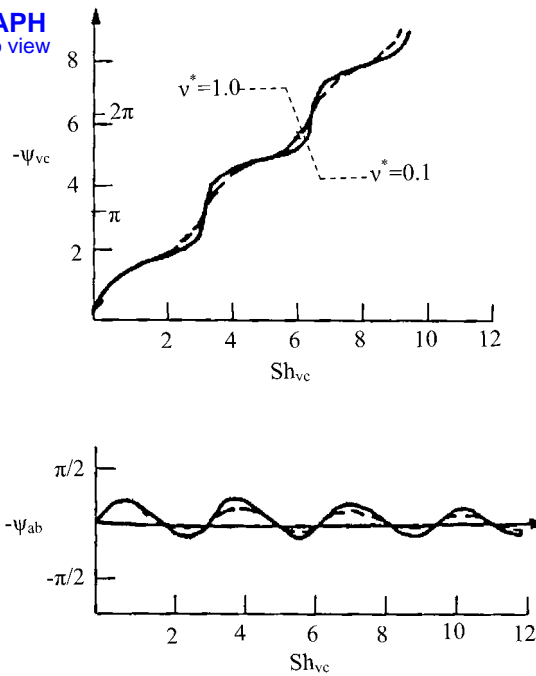
Fig. 57   Phase angle of pressure pulsation in vortex chamber as function of Strouhal number.

This secondary fluctuation $\Delta P'_{vcIII}$ can be vectorially summed with the original pressure-drop fluctuation in the liquid vortex $\Delta P'_{vcII}$ under the action of the surface wave to obtain the total pressure-drop fluctuation $\Delta P'_{vc}$. Finally, the vector sum of $\Delta P'_{vc}$ and $\Delta P'_T$ forms the dynamic pressure drop in the injector $\Delta P'_i$ relative to which the flow-rate fluctuation in the tangential entry is phase-shifted by an angle ψ_T. If the tangential-velocity disturbance is not damped by viscous losses, it will reach the injector nozzle exit considerably later than the surface wave. The resultant fluctuations of the flow rate and other properties must be determined by their vector sum.

Compared to the unsteady flow in the tangential inlet channel, the characteristic time of circumferential-velocity pulsations in the liquid vortex layer is much shorter, and as such any disturbance in the liquid layer is rapidly transmitted in the radial direction. Measurements of centrifugal-pressure pulsations at the outer wall of a typical vortex chamber at frequencies of hundreds of Hz reveal that the liquid vortex layer responds in a quasi-steady-state manner to radial disturbances. Their amplitudes are only a few percent lower than the quasi-stationary variations for given changes of the circumferential velocity. Figure 57 shows the phase angle between the pressure pulsations in the feed line and the vortex chamber, where ψ_{vc} is the phase difference between oscillations at the head end and exit of the vortex chamber, and ψ_{ab} between the
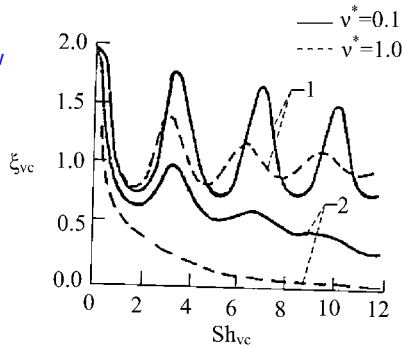
Fig. 58   Amplitude of liquid surface wave in vortex chamber as function of Strouhal number; 1-head end, 2-exit.

exit of the tangential entry and the liquid free surface at the vortex-chamber head end. The Strouhal number Sh_{vc} is defined as $\omega L_{vc}/U_w$. Two different liquids with dimensionless viscosities of $v^* = 0.1$ and 1.0 are considered here. For reference, $v^* = 0.08$ for water at room conditions. Figure 58 shows the amplitude of the liquid surface wave in the vortex chamber, where station 1 corresponds to the head end and 2 to the exit.

Theoretical and experimental studies on the effect of the velocity pulsations in the tangential entries U'_{in} on the liquid swirling flow suggest at least two different mechanisms of disturbance propagation in the vortex chamber. First, U'_{in} pulsations cause fluctuations of the liquid free surface r'_{mk} which then propagate at the speed U_w according to Eq. (148). Second, U'_{in} pulsations result in an energy disturbance in the form of circumferential velocity fluctuations that propagate throughout the entire liquid layer in both the radial and axial directions. Analogous energy waves in gaseous flows are observed and generally referred to as entropy waves.[24] When propagating along the axis of the swirler, the lengths of these waves decrease but the amplitudes grow in accordance with the conservation of angular momentum.

The pressure variation in the radial direction is obtained by integrating the centrifugal force across the liquid vortex layer:

$$\Delta \tilde{P}_{sc} = \rho \int_{R_{in}}^{r_m} \frac{\tilde{U}_u^2}{r}\,dr \qquad (159)$$

In dimensionless form, Eq. (159) becomes

$$\Delta \bar{P}'_{sc} = 2\rho U_{in} U'_{in} \int_1^{\sqrt{a}/\bar{R}_{in}} \frac{\arg \overline{U'_u}}{\bar{r}^3}\,d\bar{r} \qquad (160)$$

where $\arg \bar{U}'_u \equiv U'_u/U_{in}$ is the deviation from the stationary dependence of U_u per dimensionless radius $\bar{r}$. As an example, for an infinitely long vortex
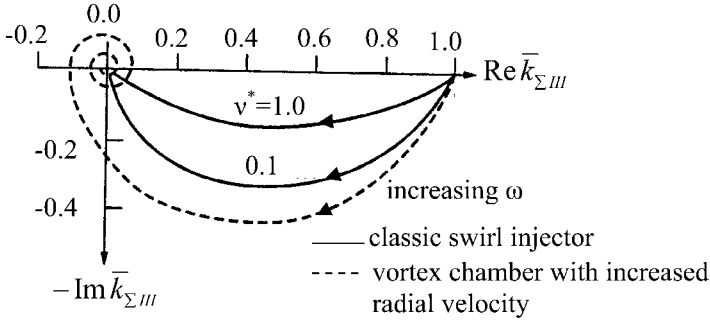
Fig. 59 Amplitude-phase diagram of amplification coefficient of a typical liquid vortex chamber.

chamber (i.e., no wave reflection from the nozzle), we have from Ref. 14

$$
\arg \bar{U}_u = \tan\left[\frac{\pi}{2} \cdot \frac{\bar{R}_{vc}(1-\bar{r})}{\bar{R}_{vc} - \sqrt{a}}\right] \cdot \exp\left[iw\left\{\tau - \frac{R_{in}}{U_\Sigma}\frac{\bar{R}_{vc}^2}{\mu}(1-\bar{r})\right\}\right] \qquad (161)
$$

Figure 59 shows the amplitude-phase diagram of the liquid swirler response to incoming pressure pulsations for different values of liquid viscosity. The subscript *III* stands for the results obtained from the third model. At zero frequency, the amplification coefficient k (defined as $k \equiv U'_{in}/\Delta P'_{sc}$) has its stationary value of unity. The coefficient decreases rapidly with increasing frequency, but the phase angle grows from 0 to $\pi/2$. Thus, the swirling flow movement is stable if the amplification coefficient is placed in the fourth quadrant of this complex plane.

For small disturbances, surface and entropy (or energy) waves behave independently and the net effect can be represented by their vectorial sum. At high frequencies, the entropy wave and its influence on centrifugal pressure can be ignored due to the high inertia of the liquid vortex layer. In contrast, the influences of surface waves become negligible at low frequencies because of the rapid decrease of their amplitudes. Entropy waves prevail in this situation. Calculations have shown that centrifugal-pressure pulsations resulting from circumferential velocity fluctuations may exist for several periods of pulsation, but at the same time surface waves may propagate throughout the liquid almost instantaneously with their high wave speed. This effect, known as the memory effect of a swirling flow, may suppress these fluctuations if they are out of phase.

The overall response function of a swirl injector Π_{sw} can be obtained in terms of the transfer characteristics of each individual element of the injector. The transfer function between the fluctuating velocity in the tangential inlet passage and the pressure drop $\Delta P'_T$ across the inlet is defined as

$$
\Pi_T = \frac{U'_{in}/U_{in}}{\Delta P'_T/\Delta P_T} = \frac{Q'_T/Q_T}{\Delta P'_T/\Delta P_T} \qquad (162)
$$

The centrifugal-pressure pulsations caused by liquid surface wave motions and circumferential velocity fluctuations can be characterized by the following transfer functions, respectively:

$$\Pi_{vcII} = \frac{\Delta P'_{vcII}/\Delta P_T}{2U'_{in}/U_{in}} = \frac{\Delta P'_{vcII}/\Delta P_T}{2Q'_T/Q_T} \tag{163}$$

$$\Pi_{vcIII} = \frac{\Delta P'_{vcIII}/\Delta P_T}{2U'_{in}/U_{in}} = \frac{\Delta P'_{vcIII}/\Delta P_T}{2Q'_T/Q_T} \tag{164}$$

Note that all of the variables in the preceding equations are complex to account for the phase differences between the various processes of concern. The fluctuation of the total pressure drop across the entire injector $\Delta P'_i$ is the vector sum of $\Delta P'_T$ and P'_{vc}, with the latter being $P'_{vcII} + P'_{vcIII}$. Thus,

$$\Delta P'_i = \Delta P'_T + \Delta P'_{vc} = \Delta P'_T + \Delta P'_{vcII} + \Delta P'_{vcIII} \tag{165}$$

Substitution of Eqs. (162–164) into (165) and rearrangement of the result give rise to the transfer function between Q'_T and $\Delta P'_i$:

$$\Pi_{in} = \frac{Q'_T/Q_T}{\Delta P'_i/\Delta P_i} = \frac{\Pi_T}{1 + 2\,(\Pi_{vcII} + \Pi_{vcIII})\Pi_T}\left(\frac{\Delta P_i}{\Delta P_T}\right) \tag{166}$$

The fluctuating flow rate at the exit of the vortex chamber (or the entrance of nozzle) Q'_{vc} can be expressed as

$$\frac{Q'_{vc}}{Q_{vc}} = \Pi_{vc}\frac{Q'_T}{Q_T} \tag{167}$$

Similarly, the fluctuating flow rate at the nozzle exit becomes

$$\frac{Q'_n}{Q_n} = \Pi_n\frac{Q'_{vc}}{Q_{vc}} \tag{168}$$

Since the mean flow rate through all elements of the injector is identical,

$$Q_T = Q_{vc} = Q_n \tag{169}$$

Substituting from Eqs. (167) and (168) and using Eq. (166), we obtain the mass transfer function for the entire injector.

The overall response function of a swirl injector Π_{sw} can be obtained by combining Eqs. (166–169)

$$\Pi_{sw} = \frac{\bar{Q}'_n}{\Delta\bar{P}'_i} = \frac{\Delta P_i}{\Delta P_T}\cdot\frac{\Pi_T\Pi_n\Pi_{vc}}{2\Pi_T\Pi_{vc} + 1} \tag{170}$$
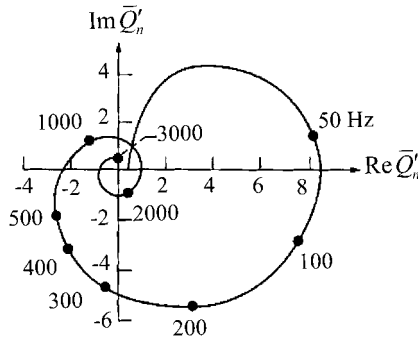
Fig. 60　Amplitude-phase diagram of response function of a typical liquid swirl injector.

Here $\Delta P_i (\equiv P_f - P_c)$ denotes the pressure drop across the entire injector. The pressure drop ratio can also be expressed in terms of the geometrical parameters of the injector. The intricate dynamics in a swirl injector produce complicated amplitude-phase characteristics of its overall response function, as shown in Fig. 60 where $\Delta \bar{P}'_i$ is set to unity for simplicity. This diagram allows one, under practical design limitations, to obtain any desired pulsation characteristic by either suppressing or amplifying flow oscillations. Thus, it becomes possible to control the engine combustion dynamics by changing the injector dynamics alone without modifying the other parts of the combustion device.

Acknowledgments

References

[1]Mikhailov, V. V., and Bazarov, V. G., *Throttlable Liquid Rocket Engines*, Mashinostroenie Pub., Moscow, Russia, 1985.

[2]Dityakin, Y. F., Klyachko, L. A., and Jagodkin, *Atomization of Liquids*, Mashinostroenie Pub., Moscow, Russia, 1977.

[3]Pazhi, D. G., and Prakhov, A. M., *Liquid Atomizers*, Khimiya, Moscow, Russia, 1979.

[4]Rollbuhler, H. J., "Experimental Investigation of Reaction Control, Storable Bipropellant Thrusters," NASA TND 4416, 1976.

[5]"Space Shuttle Orbital Maneuvering Subsystem Rocket Engine Design Features," Aerojet Liquid Rocket Co., Rept. N6673:271, PRA/SA, Rockwell, July 1976.

[6]Elverum, G., Jr., Staudhammer, P., Miller, J., Hoffman, A., and Rockow, R., "The Descent Engine for the Lunar Module," AIAA Paper 1967-521, 1967.

[7]Bazarov, V. G., *Dynamics of Liquid Injectors*, Mashinostroenie Pub., Moscow, Russia, 1979.

[8]Abrarnovich, G. N., *Applied Gas Dynamics*, Nauka, Moscow, Russia, 1976.

[9]Khavkin, Y. I., *Swirl Injectors*, Mashinostroenie Pub., Moscow, Russia, 1976.

[10]Andreev, A. V., Bazarov, V. G., Marchukov, E. Y., and Zhdariov, V. I., "Conditions of Hydrodynamic Instability Occurrence in Liquid Swirl Injectors," *Energetika*, 1985, pp. 6–10.

[11]Lyul'ka, L. A., and Bazarov, V. G., "Investigations of the Self-Oscillation Mode of Liquid Sheets in a Coaxial Air Flow," *Aviatsionnaya Tekhnika*, No. 3, 1978, pp. 19–24.

[12]Taylor, G., "The Mechanism of Swirl Atomizers," *Proceedings of 7th International Congress for Applied Mechanics*, Vol. 2, London, 1948.

[13]*Liquid Rocket Engine Injectors*, NASA SP-8089, 1976.

[14]Andreev, A. V., Bazarov, V. G., Dushkin, A. L., Ggrigoriev, S. S., and Lul'ka, L. A., *Dynamics of Gas-Liquid Injectors*, Mashinostroenie Pub., Moscow, Russia, 1991.

[15]Bazarov, V. G., "Injectors for Three-Propellant Liquid Rocket Engine with Smooth Thrust Variation," IAF-95-S.1.03, *Proceedings of 46th International Astronautical Congress*, Oslo, Norway, 1995.

[16]Baywel, L., and Orzechovski, Z., *Liquid Atomization*, Taylor & Francis, Washington, DC, 1993.

[17]Bazarov, V. G., "The Effect of Injector Characteristics on Combustion Efficiency and Stability," IAF Paper 92-0645, *Proceedings of 43rd Space Conference*, Washington, DC, 1991.

[18]Dressler, L., and Jackson, T., "Acoustically Driven Liquid Sheet Breakup," *Proceedings of 4th ILASS American Conference*, Hartford, CT, Vol. 4, 1990, pp. 132–141.

[19]Idelchik, I. E., *Handbook on Hydraulic Resistances*, Mashinostroenie Pub., Moscow, Russia, 1975.

[20]Kudriavtzev, V. M., *Basics of Theory and Design of Liquid Rocket Engines*, 4th ed., Visshaya Shkola, Moscow, Russia, 1993.

[21]Zhukovski, N. E., *Hydraulics*, Vol. 7, ONTI-NKTP, 1937 (in Russian).

[22]Bazarov, V. G., "Self-Pulsations in Coaxial Injectors with Central Swirl Liquid Stage," AIAA Paper 1995-2358, 1995.

[23]Bazarov, V. G., *Fluid Injectors Dynamics*, Mashinostroenie Pub., Moscow, Russia, 1979.

[24]Glickman, B. F., *Dynamics of Pneumo-hydraulic Liquid Rocket Engine Systems*, Mashinostroenie Pub., Moscow, Russia, 1983.

[25]Ditiakin, Y., Kliatchko, L., Novikov, B., and Yagodicin, V., *Atomization of Liquids*, 3rd ed., Mashinostroenie Pub., Moscow, Russia, 1987.

[26]Zong, N., and Yang, V., "Dynamics of Simplex Swirl Injectors for Cryogenic Propellants at Supercritical Conditions," AIAA Paper 2004-1332, 2004.

[27]Yang, V., and Bazarov, V., "Propellant Rocket Engine Injector Dynamics," *Journal of Propulsion and Power*, Vol. 14, No. 5, 1998, pp. 797–806.